THE MOLECULAR PHOTOPHYCICS OF CHLOROPHYLL

A STUDY OF ITS TRIPLET STATE

Dit proefschrift met stellingen van

JOHAN FREDERIK KLEIBEUKER

doctorandus in de chemie, geboren te Groningen op 19 februari 1948, is goed-gekeurd door de promotor dr. T.J. Schaafsma, hoogleraar in de moleculaire fysica.

De Rector Magnificus van de Landbouwhogeschool,

J.P.H. van der Want

Wageningen, 15 april 1977

J.F. KLEIBEUKER

The molecular photophysics of chlorophyll

A STUDY OF ITS TRIPLET STATE

proefschrift

ter verkrijging van de graad
van doctor in de landbouwwetenschappen,
op gezag van de Rector Magnificus,
dr.ir. J.P.H. van der Want,
hoogleraar in de virologie,
in het openbaar te verdedigen
op vrijdag 3 juni 1977
des namiddags te vier uur in de aula
van de Landbouwhogeschool te Wageningen

Stellingen

1

Een verdere integratie van de moleculaire fysica in het onderwijs en onder-
zoek aan de Landbouwhogeschool zal een positieve invloed hebben op de toe-
passing van fysische technieken bij het landbouwkundigonderzoek.

2

De toepassing van het excitonformalisme op de triplettoestand van chlorofyl-
aggregaten is alleen toegestaan, indien de effecten van de donor-acceptor-
interacties in de beschouwingen worden betrokken, zoals dit ook is gedaan
door Shipman et al. bij de beschrijving van de absorptie-spectra van deze
molecuulaggregaten.

> R.H. Clarke, R.E. Connors, H.A. Frank, J.C. Hoch, Chem. Phys. Lett.,
> 45, 523 (1977).
> L.L. Shipman, T.M. Cotton, J.R. Norris, J.J. Katz, J. Am. Chem.
> Soc., 98, 8222 (1976).

3

In het door Huang et al. opgestelde model voor de nulveldsplitsing van de
baan-ontaarde triplettoestand van metalloporfyrines en ftalocyanines wordt
ten onrechte verondersteld, dat de spin-spininteractie in alle gevallen
klein is t.o.v. de spin-baankoppeling.

> T.H. Huang, K.E. Rieckhoff, E.M. Voigt, E.R. Menzel, Chem. Phys.,
> 19, 25 (1977).

4

Het van elkaar aftrekken van spinlabel-ESR-spectra, gemeten voor loodrechte
en parallele oriëntatie van een gedeeltelijk georiënteerd monster t.o.v.
het magneetveld, zoals is toegepast door Chao et al., leidt niet tot een
meer doorzichtige analyse van de meetresultaten.

> Y.Y.H. Chao, A. Holtzer, Biochemistry, 14, 2164 (1975).

5

De aanname van Shida et al., dat de grondtoestand van het mononegatieve
anion van coroneen en van trifenyleen niet ontaard is, is niet in overeen-
stemming met experimentele resultaten, verkregen uit MCD metingen.

> T. Shida, S. Iwatw, J. Am. Chem. Soc., 95, 3473 (1973).
> P.J. Zandstra, D.J. Scholtens, R.E. Koning, J. Chem. Phys., 57
> 3821 (1972).

6

Het verwaarlozen van het effect van de kristalveldsplitsing op de ligging van de energieniveaus in de laagste kwartettoestand van koper-octaethylporfine en een niet bewezen aanname omtrent het karakter van de kwartet-sub-niveaus leiden Shatwell et al. op een dwaalspoor bij de interpretatie van de magnetisch geïnduceerde circulaire polarisatie van de emissie van CuOEP.

R.A. Shatwell, R. Gale, A.J. McCaffery, K. Sichel, J.Am. Chem. Soc., 97, 7015 (1975).

7

De verklaringen, gegeven door Gafni et al. en door Brochon et al., voor het niet-exponentiële verval van de pyridine-nucleotide fluorescentie, zoals die wordt gevonden voor het vrije coenzym in visceuze oplossing en voor het eiwit-gebonden coenzym, houden niet voldoende rekening met oplosmiddel-reoriëntatie effecten.

A. Gafni, L. Brand, Biochemistry, 15, 3165 (1976).
J.C. Brochon, Ph. Wahl, J.M. Jallon, M. Iwatsubo, Biochemistry, 15, 3259 (1976).

8

In een droge herfst kan een korte strenge vorstperiode de warmtestroom van de aarde naar de atmosfeer gedurende langere tijd doen verminderen.

9

Detectiegrenzen van ion-selectieve elektroden dienen betrekking te hebben op de totale concentratie van het betreffende ion en niet op de vrije ionen-concentratie.

Documentatie van Philips: Ion selective solid-state electrode for sulfide and silver, type 1S 550 S/Ag.
Documentatie van Orion: Guide to specific ion electrodes and instrumentation.

10

Het principiële verschil in de betekenis van het woord *trapezium* in het "Amerikaans-Engels" en in het "Oxford-Engels" kan gemakkelijk leiden tot begripsverwarring.

The Concise Oxford Dictionary.
Webster's New International Dictionary.

Proefschrift van J.F. Kleibeuker.
Wageningen, mei 1977.

aan Meishelien
aan mijn ouders

Voorwoord

Vijf jaar geleden, toen ik naar Wageningen kwam, was fotosynthese voor mij een volledig onbekend proces en was chlorophyll een wat groot uitgevallen molecuul. Zonder de medewerking van de vakgroep Plantenfysiologisch Onderzoek bij mijn eerste kennismaking met de fotosynthese en de kennis van mijn promotor m.b.t. de basis structuur van de fotosynthetische pigmenten was het onderzoek, zoals beschreven in dit proefschrift, voor mij niet mogelijk geweest.

Het onderzoek, dat is uitgevoerd op het Laboratorium voor Moleculaire Fysica te Wageningen, was alleen mogelijk dankzij de medewerking van velen binnen en buiten deze afdeling. De vele experimenten werden mogelijk gemaakt door het voorbereidend werk van Henny van Beek, Willem van Berkel, de heer Jansen, Adrie de Jager, Simon Maasland, Jillert Santema en Henny Zoutendijk, waarvoor ik aan allen mijn oprechte dank wil uitspreken.

Bij de experimenten en de daarop volgende discussies heb ik altijd veel steun gehad aan de belangstelling van alle medewerkers van de vakgroep Moleculaire Fysica. De medewerking van Roelof Platenkamp, Piet Geerse en Arie Sonneveld is onontbeerlijk geweest voor de afronding van het onderzoek.

In het bijzonder wil ik Tjeerd Schaafsma bedanken. Hij interesseerde mij voor de fotosynthese, motiveerde mij voor het triplet onderzoek en was te allen tijde bereid mij met raad en daad ter zijde te staan. De vele discussies met jou, Tjeerd, zijn de grondslag van het onderzoek, dat met het schrijven van dit proefschrift is afgerond.

Ten slotte wil ik mijn waardering uitspreken voor de wijze waarop Janny Siebring, de heer Hoogeveen en de medewerksters van de afdeling Tekstverwerking hebben meegewerkt aan het tot stand komen van dit manuscript. Ik ben de North-Holland Publishing Company erkentelijk voor de toestemming twee in Chemical Physics Letters gepubliceerde artikelen in dit proefschrift te mogen opnemen.

Contents

9

List of abbreviations

AO	atomic orbital
Bchl	bacteriochlorophyll $\underline{a}$
Bph	bacteriopheophytin $\underline{a}$
Chl $\underline{a}$	chlorophyll $\underline{a}$
Chl $\underline{b}$	chlorophyll $\underline{b}$
CI	configuration interaction
CNDO	complete neglect of differential overlap
ESP	electron spin polarization
ESR	electron spin resonance
FC	Franck-Condon
FDMR	fluorescence detected magnetic resonance
FE	free electron
HOMO	highest occupied molecular orbital
IEH	iterative extended Hückel
ISC	intersystem crossing
LCAO	linear combination of atomic orbitals
LUMO	lowest unoccupied molecular orbital
(Mg)TBP	(magnesium) tetrabenzoporphin
MO	molecular orbital
MTHF	2-methyltetrahydrofuran
Ph $\underline{a}$	pheophytin $\underline{a}$
Ph $\underline{b}$	pheophytin $\underline{b}$
PMMA	polymethylmethacrylate
PPP	Pople, Pariser and Parr
Py	pyridine ligand
SCF	self consistent field
SLR	spin lattice relaxation
SOC	spin orbit coupling
tol/pyr	toluene-pyridine mixture (9:1)
TPP	tetraphenylporphin
TPC	tetraphenylchlorin
ZFS	zero field splitting

1 General introduction

The process in which light energy is converted into chemical energy by plants, algae and bacteria is called *photosynthesis*. The photosynthesis can be divided in three kinds of processes, which are essentially different: (i) absorption of light, transport of excitation energy and induction of a charge separation using the excitation energy, together forming the so-called primary events;
(ii) transport of charge along a chain of different intermediate compounds;
(iii) conversion of the electro-chemical energy, stored in the separated charges, into chemical energy.
In this thesis we will limit ourselves to the processes described under (i); recent reviews covering the other processes can be found elsewhere |1|.

The photosynthetic pigments, especially the chlorophylls, being the subject of this investigation, are essential for the primary photosynthetic events. In view of their role, the various pigment systems are divided in three classes:
(i) light harvesting (bulk, antenna) pigments, responsible for the absorption of light;
(ii) pigments which are able to channel excitation energy from the light harvesting pigments to the reaction center;
(iii) reaction center pigments, participating in the first step of charge separation.
In plants and algae chlorophyll a (Chl a) is the most important pigment in all three classes, whereas chlorophyll b (Chl b) participates mainly in the process of light harvesting. In photosynthetic bacteria, probably bacteriochlorophyll a (Bchl) is the most important pigment; in green bacteria chlorobium chlorophyll provides the light harvesting facility. Since the differentiation of pigments in view of their role is not only a result of differences in molecular structure, it has to be attributed to different surroundings. The environmental effects can be understood by considering the molecular structure as given in fig. 1.
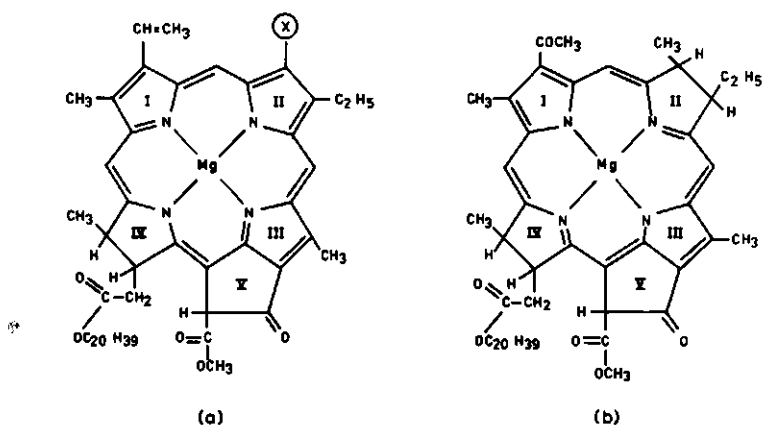
Fig. 1 (a) Molecular structure of chlorophylls; X ≡ CH₃ for Chl a,
X ≡ CHO for Chl b.
(b) Molecular structure of bacteriochlorophyll a.

The main skeleton of the chlorophylls is a porphyrin-like ring
system. In Chl a and Chl b one pyrrole ring is hydrogenated (ring IV) and in
Bchl ring IV and ring II are hydrogenated. All chlorophylls contain a Mg^{2+}-
ion in the center of the ring, which can be replaced by two protons, result-
ing in the corresponding pheophytins. The π-electrons are delocalized over
the tetrapyrrole macrocycle, except the hydrogenated bonds. Also carbonyl
groups can participate in this delocalization, e.g. the ring V keto group in
all chlorophylls, the aldehyde group in ring II in Chl b and the acetyl group
in ring I in Bchl. The π-electron distribution is responsible for many
relevant molecular properties, such as the lowest excitation energies and the
ionisation potentials. This distribution can be affected by interactions with
the surroundings through hydrogen bonding with carbonyl groups and ligation
of Mg^{2+}. Furthermore, the presence of electron donating groups such as the
carbonyl groups, and an electron accepting group, the Mg^{2+}-ion, in one
molecule provides the possibility to form dimers and oligomers.

The role and the surroundings of chlorophylls *in-vivo* |2|, as well
as the possible structure of aggregates *in-vitro* |3| have been studied
extensively. In this investigation, we have aimed at a deeper insight into
the electronic structure of monomeric chlorophylls in solution, especially
w.r.t. the lowest excited states. Absorption and fluorescence spectra of the
different chlorophylls, being related to the lowest excited singlet states of

14

these compounds, have been collected by Goedheer |4|. In a recent review, Weiss has correlated these spectra with quantum chemical calculations |5|.

Another excited state of interest for studies of the electronic structure is the lowest excited triplet state T_0. The main difference between T_0 and the lowest excited singlet state S_1 is the presence of a total spin angular momentum $S = 1$ in T_0, whereas for S_1, $S = 0$. Two consequences of these different S-values should be noted: (i) the triplet state is metastable and (ii) magnetic resonance measurements provide the possibility to study the electron distribution in T_0 |6|. When we started this investigation only little was known about the lowest excited triplet state of the chlorophylls. Triplet state lifetimes had been deduced from triplet-triplet absorption spectroscopy |7| and some triplet ESR studies had been reported, considering only the so-called $\Delta m = 2$ transitions |8|. The first $\Delta m = 1$ triplet ESR spectrum of a chlorophyll was reported by Lhoste |9|. This author measured the triplet ESR spectrum for Chl b in ethanol, using modulated optical excitation and phase-sensitive detection.

Interest in chlorophyll triplet states strongly increased when Dutton and Leigh |10| reported a $\Delta m = 1$ triplet ESR spectrum of Bchl in bacterial reaction centers, which could not be accounted for by theory existing at that time. Parallel to more extensive studies of the *in-vivo* triplet states in bacteria |11|, chloroplasts |12| and algae |13|, results have been reported on the triplet state of various chlorophylls *in-vitro*. Clarke et al. |14| used fluorescence detected zero-field magnetic resonance for the measurement of the zero-field splitting (ZFS) and the triplet state kinetics of Chl a, Chl b and the related Zn-compounds |15|, as well as of Bchl |11|. Thurnauer et al. |16| deduced the ZFS parameters of a series of chlorophylls by ESR, using modulated optical excitation and phase sensitive detection. Similar measurements have been reported by Levanon et al. |17|. Recently the energy levels of the lowest excited triplet state of Chl a and b as well as the related pheophytins in various solvents have been determined by Krasnovskii |18| using phosphorescence.

The basic skeleton of the photosynthetic pigments, the porphin ring, has been studied extensively |19|. As has been shown by Weiss |5|, the knowledge of the electronic structure of porphyrins is very important for successfull studies of chlorophyll, since the introduction of side groups, as well as the hydrogenation of pyrrole rings can be accounted for as relatively small perturbations on the electronic structure of the porphyrin ring. In view of these considerations we have studied in addition to photosynthetic pigments,

the spectroscopic properties of Mg-tetrabenzoporphin (MgTBP), which has the advantage of being a stable compound with D_{4h} symmetry. In Chapter 5 it will be discussed that in some respects MgTBP is a good model compound for Chl a.

Apart from a scientific curiosity for the properties of triplet states of such complex compounds as the chlorophylls, the triplet state study of chlorophylls was initiated having three aims in mind:
(i) to find an answer to the question whether the triplet state is an essential intermediate in photosynthesis;
(ii) to characterize the triplet state of various chlorophylls and the effects of surroundings on the triplet state properties, to be able to use the triplet state as a natural internal label, probing the *in-vivo* surroundings of the photosynthetic pigments;
(iii) to check current quantum chemical calculations on the electronic structure of chlorophylls by comparison of theoretical results with the experimental triplet state parameters.

Although the first question is the most interesting one for biologists, this investigation does not yield an outcome. Recently Parson et al. |20| have proposed a mechanism for the primary steps in bacterial photosynthesis in which the triplet state does not participate in the charge separation when the pathway for electron transport is unblocked. Several studies have provided indications that the triplet state can act as a "sink", draining excess excitation energy from the photosynthetic unit by coupling to carotenoid triplets |21|.

The parameters, characterizing a triplet state and the techniques for their measurement are discussed in Chapters 2 and 3. The main features of the electronic structure of porphyrin like molecules is briefly reviewed in Chapter 4, emphasizing Gouterman's 4-orbital model |22|, which is used throughout this investigation for the explanation of the effect of molecular structure on the lowest excited singlet and triplet states. The results of the investigations on MgTBP are presented in Chapters 5 and 6, whereas the data obtained for photosynthetic pigments are reported and discussed in Chapters 7-10. Since one of the possible interactions between the chlorophylls and its surroundings is the ligation of Mg^{2+}, pheophytins lacking Mg^{2+} have been included in the investigation (Chapter 9).

Special attention is given to the interaction of the pigment molecules with the surroundings. The effects of ligation on the spectroscopic properties of chlorophylls is related to those found for MgTBP (Chapter 5).

Hydrogen bonding is discussed in Chapters 9 and 10 by comparing its effect with that of introduction of an aldehyde group as in Chl b.

REFERENCES

1. Bioenergetics of photosynthesis, ed. Govindjee, New York, 1975.
2. W.W. Parson, R.J. Cogdell, Biochem.Biophys.Acta, 416, 105 (1975).
3. A.D. Trifunac, J.J. Katz, J.Am.Chem.Soc., 96, 5233 (1974).
4. J.C. Goedheer, in "The chlorophylls", eds. L.P. Vernon, G.R. Seely, New York, 1966.
5. C. Weiss, J.Mol.Spectrosc., 44, 37 (1972).
6. S.P. McGlynn, T. Azumi, M. Kinoshita, "The molecular spectroscopy of the triplet state", Englewood Cliffs, N.J., 1969.
7. G.R. Seely, in "The chlorophylls", eds. L.P. Vernon, G.R. Seely, New York, 1966.
8. G.T. Rikhireva, L.A. Sibel'dina, Z.P. Gribova, B.S. Marinov, L.P. Kayushin, A.A. Krasnovskii, Dokl.Akad. Nauk. SSSR, 181, 1485 (1968).
9. J.M. Lhoste, Studia Biophysica, 12, 135 (1968).
10. P.L. Dutton, J.S. Leigh, M. Seibert, Biochem.Biophys.Res.Commun., 46, 406 (1972).
11. R.H. Clarke, R.E. Connors, H.A. Frank, Biochem.Biophys.Res.Commun., 71, 671 (1976).
12. A.J. Hoff, J.H. van der Waals, Biochem.Biophys.Acta, 412, 615 (1976).
13. S.J. van der Bent, T.J. Schaafsma, J.C. Goedheer, Biochem.Biophys.Res. Commun., 71, 1147 (1976).
14. R.H. Clarke, R.H. Hofeldt, J.Chem.Phys., 61. 4582 (1974).
15. R.H. Clarke, R.E. Connors, T.J. Schaafsma, J.F. Kleibeuker, R.J. Platenkamp, J.Am.Chem.Soc., 98, 3674 (1976).
16. M.C. Thurnauer, J.J. Katz, J.R. Norris, Proc.Nat.Acad.Sci. USA, 72, 3270 (1975).
17. H. Levanon, A. Scherz, Chem.Phys.Lett., 31, 119 (1975).
18. A.A. Krasnovskii Jr., N.N. Lebedev, F.F. Litvin, Dokl.Akad.Nauk SSSR, 216, 1406 (1974).
19. M. Gouterman, in "Excited states of matter", ed. C.W. Shoppee, 1973.
20. W.W. Parson, R.K. Clayton, R.J. Cogdell, Biochem.Biophys.Acta, 387, 265 (1975).
21. R.J. Cogdell, W.W. Parson, M.A. Kerr, Biochem.Biophys.Acta, 430, 83 (1976)
22. M. Gouterman, J.Mol.Spectrosc., 6, 138 (1961).

2 Static triplet state parameters

2.1 INTRODUCTION

The wavefunction of an electron in an atom can be characterized by four quantum numbers; three of them (n, 1, m) define the spatial distribution of the electrons, whereas m_s defines the spin state. To interpret splittings in atomic line spectra, Uhlenbeck and Goudsmit [1] introduced the concept of spin: for electrons, having spin angular momentum quantum number $S = \frac{1}{2}$, the spin functions $|\alpha\rangle$ and $|\beta\rangle$ describe two states with $m_s = +\frac{1}{2}, -\frac{1}{2}$, respectively. In an external magnetic field these two states have different energies, since the spinning electron has a magnetic moment $\vec{\mu} = g\beta\vec{S}$ (where $g \sim 2.0$, is a dimensionless constant, called the electron g-value, $\beta = 9.27 \times 10^{-28}$ J/Gauss is the Bohr magneton and $\vec{S}$ is the spin angular momentum), which can be oriented in two ways w.r.t. the external magnetic field [2].

The existence of an electron spin is crucial for understanding the electron distribution in atoms and molecules because of Pauli's rule [3]. In addition, the electron spin provides another means to study this electron distribution in free radicals and triplet states by electron spin resonance (ESR). The energy difference between the two spin states depends on the effective magnetic field at the site of the electron and is related to the local surroundings of the electrons [2].

After a brief introduction to spin functions and spin operators, we will discuss the physical concept of the triplet state and the parameters characterizing this state. The second part of this chapter is devoted to experimental techniques to measure these parameters.

2.2 THEORY

2.2.1 Electron spin, its functions and operators

The one electron spin functions $|\alpha\rangle$ and $|\beta\rangle$ are eigenfunctions of the one electron spin operators $\underline{S}^2$ and $\underline{S}_z$ [2].

$$\underline{S}^2 |m_S\rangle = S(S+1)\hbar^2 |m_S\rangle = \tfrac{3}{4}\hbar^2 |m_S\rangle ,$$

$$\underline{S}_z |m_S\rangle = m_S \hbar |m_S\rangle = \pm \tfrac{1}{2}\hbar |m_S\rangle ,$$

where $|m_S\rangle$ denotes the spin function, S and m_S are the aforementioned quantum numbers. The operators $\underline{S}^2$ and $\underline{S}_z$ are related to the spin angular momentum operator $\underline{S}$, $\underline{S}^2 = \underline{S}.\underline{S}$, $\underline{S} = \underline{S}_x + \underline{S}_y + \underline{S}_z$.
The energy E of an electron with spin $S = \tfrac{1}{2}$ in an external magnetic field $\vec{H}//z$ is given by the Schrödinger equation for the spin function:

$$g\beta \, H_z \, \underline{S}_z \, |m_S\rangle = E \, |m_S\rangle$$

with $E_{\alpha,\beta} = \pm \tfrac{1}{2} g\beta H_z$. Defining the step operators $\underline{S}^+ = \underline{S}_x + i \underline{S}_y$, $\underline{S}^- = \underline{S}_x - i \underline{S}_y$
it can be shown that

$$\langle \alpha | \underline{S}^+ | \beta \rangle = \langle \beta | \underline{S}^- | \alpha \rangle = \hbar .$$

Because of these non-zero matrix elements a radiofrequent electromagnetic radiation field (rf field), with its magnetic field component $\vec{H}_1$ *perpendicular* to the external field $\vec{H}$ can induce transitions between the spin states, if the frequency fits the energy difference. This can be seen when considering the time dependent perturbation hamiltonian, resulting from the rf field,

$$\mathcal{H}^1 = g\beta H_1 . \underline{S} \tag{1}$$

If e.g. $H_1//x$, then

$$\langle \alpha | \mathcal{H}^1 | \beta \rangle = g\beta H_1^x \langle \alpha | \underline{S}_x | \beta \rangle = g\beta H_1^x \langle \alpha | \underline{S}^+ + \underline{S}^- | \beta \rangle \neq 0$$

demonstrating that $\mathcal{H}^1$ causes transitions between the spin states $|\alpha\rangle$ and $|\beta\rangle$.
When more electrons are considered, the total spin angular momentum operator $\underline{S}$ is given by $\underline{S} = \sum_i \underline{S}_i$, and the total spin function χ is given by $\chi = \prod_i \chi_i$, where $\underline{S}_i$ and χ_i are the spin operator and the spin function for electron $\underline{i}$. With two electrons, the possible spin functions are $|\alpha(1)\beta(2)\rangle$, $|\alpha(2)\beta(1)\rangle$, $|\alpha(1)\alpha(2)\rangle$, $|\beta(1)\beta(2)\rangle$. Because of the indistinguishability of electrons the total spin function has to be symmetric or anti-symmetric w.r.t. electron permutations [3] :

$$\chi^S = \frac{1}{\sqrt{2}} \left(|\alpha(1) \ \beta(2) \rangle - |\alpha(2) \ \beta(1) \rangle \right) \tag{2}$$

$$\chi^T = \left\{ \begin{array}{l} |\alpha(1) \ \alpha(2) \rangle \\ \frac{1}{\sqrt{2}} \left(|\alpha(1) \ \beta(2) \rangle + |\alpha(2) \ \beta(1) \rangle \right) \\ |\beta(1) \ \beta(2) \rangle \end{array} \right. \tag{3}$$

For the antisymmetric spin function χ^S one finds

$$\underline{S}^2 \, \chi^S = 0.$$

This corresponds to a spin quantum number $S = 0$. Since the multiplicity of this state, given by $(2S+1)$, equals one, this state is called a *singlet* state. For all three symmetric spin functions one finds

$$\underline{S}^2 \, \chi^T = 2 \, \hbar,$$

corresponding to a spin quantum number $S = 1$ and a multiplicity $(2S+1) = 3$: these three states together form the *triplet* state. Using the eigenvalues, m_S, of the triplet state spin functions w.r.t. the operator $\underline{S}_z$, these functions are normally denoted as

$$|+1 \rangle \equiv |\alpha(1) \ \alpha(2) \rangle \,, \quad |-1 \rangle \equiv |\beta(1) \ \beta(2) \rangle \ \ \text{and}$$

$$|0 \rangle \equiv \frac{1}{\sqrt{2}} \left(|\alpha(1) \ \beta(2) \rangle - |\alpha(2) \ \beta(1) \rangle \right).$$

A time dependent perturbation hamiltonian, related to the magnetic field component of an rf field, as given in eqn. (1), can induce the transitions $|+1 \rangle \leftrightarrow |0 \rangle$ and $|-1 \rangle \leftrightarrow |0 \rangle$, because the matrix elements $\langle +1 | \underline{S}^+ | 0 \rangle$, $\langle 0 | \underline{S}^- | +1 \rangle$, $\langle -1 | \underline{S}^- | 0 \rangle$, and $\langle 0 | \underline{S}^+ | -1 \rangle$ are non-zero; these transitions follow the selection rule $\Delta m_S = 1$.

The aforementioned triplet spin functions are only good functions in a sufficiently strong external magnetic field, when spin-spin interactions can be neglected. The full spin hamiltonian is given by

$$\mathcal{K} = g\beta \vec{H} \, (\underline{S}_1 + \underline{S}_2) + g^2 \beta^2 \left\{ \frac{\underline{S}_1 \cdot \underline{S}_2}{r^3} - \frac{3(\underline{S}_1 \cdot \vec{r})(\underline{S}_2 \cdot \vec{r})}{r^5} \right\} \tag{4}$$

$\vec{H}$ is the external magnetic field; $\underline{S}_1$ and $\underline{S}_2$ define the two one electron spin

20

angular momentum operators and $\vec{r}$ is the vector connecting the positions of the two electrons. When $\vec{H} = 0$, the hamiltonian given in eqn. (4), reduces to the spin-spin interaction hamiltonian $\mathcal{H}_{ss}$. This hamiltonian can be cast into the form

$$\mathcal{H}_{ss} = -X\underline{S}_x^2 - Y\underline{S}_y^2 - Z\underline{S}_z^2$$

where X, Y and Z are the expectation values of the $\vec{r}$ dependent operators,

$$\underline{X} = g^2\beta^2 \left(\frac{r^2 - 3x^2}{r^5} \right) , \quad \underline{Y} = g^2\beta^2 \left(\frac{r^2 - 3y^2}{r^5} \right) , \quad \underline{Z} = g^2\beta^2 \left(\frac{r^2 - 3z^2}{r^5} \right) \quad (5)$$

(x, y and z are the components of $\vec{r}$ along the three mutual perpendicular principal axes of the zerofield splitting tensor), using the orbital part of the triplet electronic wavefunctions. $\underline{S}_x$, $\underline{S}_y$ and $\underline{S}_z$ are the *total* (two electron) spin operators. The spin functions

$$|\tau_x\rangle = \frac{1}{\sqrt{2}} \left(|\beta(1)\ \beta(2)\rangle - |\alpha(1)\alpha(2)\rangle \right) \tag{6a}$$

$$|\tau_y\rangle = \frac{i}{\sqrt{2}} \left(|\beta(1)\ \beta(2)\rangle + |\alpha(1)\alpha(2)\rangle \right) \tag{6b}$$

$$|\tau_z\rangle = \frac{1}{\sqrt{2}} \left(|\alpha(1)\ \beta(2)\rangle + |\alpha(2)\beta(1)\rangle \right) \tag{6c}$$

are eigenfunctions of $\mathcal{H}_{ss}$ with the eigenvalues X, Y and Z respectively. Because $X + Y + Z = 0$, the relative energy levels of the three spin states can be defined by the zerofield splitting (ZFS) parameters

$$D = \tfrac{1}{2}(X + Y) - Z, \quad E = -\tfrac{1}{2}(X - Y) \tag{7}$$

The spin functions $|\tau_x\rangle$, $|\tau_y\rangle$, and $|\tau_z\rangle$ all have the eigenvalue $2\hbar$ for total spin operator $\underline{S}^2$. Furthermore, it follows from the transformation properties of angular momentum,

$$\underline{S}_z |\tau_x\rangle = i |\tau_y\rangle \qquad\qquad \underline{S}_z^2 |\tau_x\rangle = \hbar^2 |\tau_x\rangle$$

$$\underline{S}_z |\tau_y\rangle = -i |\tau_x\rangle \qquad\qquad \underline{S}_z^2 |\tau_y\rangle = \hbar^2 |\tau_y\rangle$$

$$\underline{S}_z |\tau_z\rangle = 0 \qquad\qquad \underline{S}_z^2 |\tau_z\rangle = 0$$

From this, it can be concluded that $|\tau_x\rangle$ and $|\tau_y\rangle$ are no eigen functions of $\underline{S}_z$; so, for these functions m_s is not a good quantum number. From the relations $\underline{S}_x |\tau_x\rangle = \underline{S}_y |\tau_y\rangle = \underline{S}_z |\tau_z\rangle = 0$, it can be concluded that the spin moves in a plane perpendicular to the x, y and z axes for $|\tau_x\rangle$, $|\tau_y\rangle$ and $|\tau_z\rangle$, respectively. The magnetic field component of a rf field can again induce transitions between the triplet spin states, following the perturbation hamiltonian given in eqn. (1). The non-zero matrix elements are now, however, $\langle \tau_z |\underline{S}_x |\tau_y\rangle$, $\langle \tau_y |\underline{S}_z|\tau_x\rangle$ and $\langle \tau_x |\underline{S}_y |\tau_z\rangle$.

High-field spin functions are related to the zero-field spin functions by:

$$|+1\rangle = \frac{1}{\sqrt{2}} (|\tau_x\rangle + i|\tau_y\rangle) \tag{8a}$$

$$|0\rangle = |\tau_z\rangle \tag{8b}$$

$$|-1\rangle = \frac{1}{\sqrt{2}} (|\tau_x\rangle - i|\tau_y\rangle) \tag{8c}$$

when the external magnetic field is along the z-axis of the ZFS tensor. The aforementioned selection rule $\Delta m_s = 1$ only holds when $|+1\rangle$, $|0\rangle$, and $|-1\rangle$ are the exact functions, i.e. in an infinitely strong field; in the inter-mediate case, when $\mathcal{H}_{ss}$ may not be neglected w.r.t. $g\beta\vec{H}.\underline{S}$ (eqn.4), $|+1\rangle$, $|0\rangle$, and $|-1\rangle$ are approximate functions and $\Delta m_s = 2$ transitions are also allowed. In fig. 1 the effect of an external magnetic field on the energy levels of the three spin states for $\vec{H}//x$, $\vec{H}//y$ and $\vec{H}//z$ is presented.

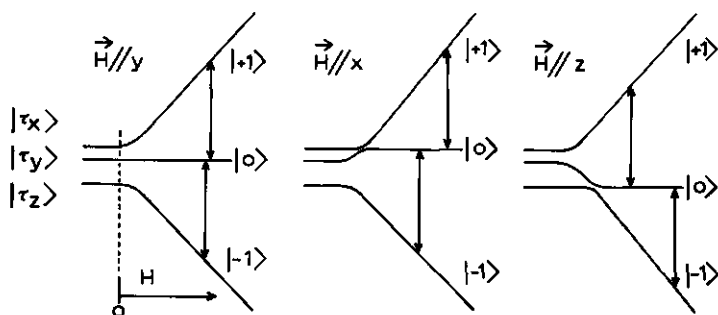Fig. 1. Magnetic field dependence of the energy levels of the three triplet states for the three canonical orientations H//x,y,z, where x,y,z are the principal axes of the ZFS tensor. $|\tau_x\rangle$, $|\tau_y\rangle$, and $|\tau_z\rangle$ are the zero-field states; $|+1\rangle$, $|0\rangle$ and $|-1\rangle$ are the high-field spin states. Arrows indicate resonance field positions for constant rf-frequency.

2.2.2 The physical concept of the triplet state.

The total wavefunction ψ, describing the spatial distribution
of the electrons as well as their spin state, can be written as a product
of a function ϕ, only dependent on the spatial electronic coordinates and a
spin function χ, $\psi = \phi \cdot \chi$. Due to Pauli's rule [3], ϕ or χ has to be anti-
symmetric w.r.t. electron permutation, the other being symmetric. Since in
the following we consider only the ground state and the lowest excited states
obtained by one electron promotions, the discussion will be confined to a
two electron - two orbital problem, using the MO approximation [3]. In the
ground state, both electrons occupy the lowest MO (molecular orbital) ϕ_a,
resulting in a symmetric function $\phi^0(1, 2) = \phi_a(1) \cdot \phi_a(2)$, to be combined
with the antisymmetric spinfunction χ^S given in eqn. (2): the ground state
is a singlet state. For the excited state, with one electron in both MO's
(ϕ_a and ϕ_b), two spatial wavefunctions are possible: a symmetric one,

$$\phi^{1S}(1,2) = \frac{1}{\sqrt{2}} (\phi_a(1) \phi_b(2) + \phi_a(2) \phi_b(1))$$

to be combined with χ^S resulting in a singlet state, and an antisymmetric one

$$\phi^{1A}(1,2) = \frac{1}{\sqrt{2}} (\phi_a(1)\phi_b(2) - \phi_a(2)\phi_b(1)),$$

to be combined with one of the χ^T's (eqns. 3 or 8a-c) resulting in a triplet
state. Therefore, we can conclude that the singlet and triplet excited states,
occupying the same MO's not only differ in their spin function but also in
spatial wavefunction ϕ. Taking into account the electric interaction between
the two electrons (the magnetic interactions between the spins may be neglec-
ted), the energy difference between the two excited states is found to be [4]

$$\Delta E = 2 K = 2 \iint \phi_a^*(1) \phi_b^*(2) \frac{e^2}{r^2} \phi_a(2) \phi_b(1) \, d\tau_1 \, d\tau_2 \tag{9}$$

whereas the triplet state has the lower energy.

A second aspect to be considered when discussing triplet states
is a direct consequence of the spin function. Because of the selection rule
$\Delta S = 0$, optical transitions between singlet and triplet states are forbidden
in first order. The set of all singlet states and the set of all triplet
states of a molecule can be considered as two separate manifolds, which can
be coupled by spin-orbit coupling (SOC). Since the intersystem crossing (ISC)
between singlet and triplet states is much slower than transitions within
each of the manifolds, the lowest excited triplet state T_0 is a metastable

23

state with a lifetime $\tau_{T_o} \sim 10^2 - 10^{-3}$ sec., as contrasted with the lifetime of the lowest excited singlet state $\tau_{S_1} \sim 10^{-7} - 10^{-10}$ sec.

2.2.3 *Definition of static triplet state parameters*

In fig. 2 the energy levels relevant for triplet state spectroscopy are depicted. The static parameters characterizing a triplet state are:

a) E_{T_o}, energy level of the mean of the three triplet spin states w.r.t. the ground state S_o and $\Delta E(S_o - T_o)$, the energy level of T_o w.r.t. the lowest excited singlet state S_1.

b) D and E, the ZFS parameters defining the energy separation between the three triplet spin states, resulting from spin-spin interaction.
As can be derived from (6) and (7)

$$D = \tfrac{3}{4} g^2\beta^2 \langle \frac{r^2 - 3z^2}{r^5} \rangle \; , \tag{10a}$$

$$E = \tfrac{3}{4} g^2\beta^2 \langle \frac{y^2 - x^2}{r^5} \rangle \; , \tag{10b}$$

where $\langle \; \rangle$ denotes that the expectation value, using the orbital part of the wavefunction, has to be calculated by integration over the space; r is the distance between the unpaired spins; x, y and z its components along the principal axes of the ZFS tensor.
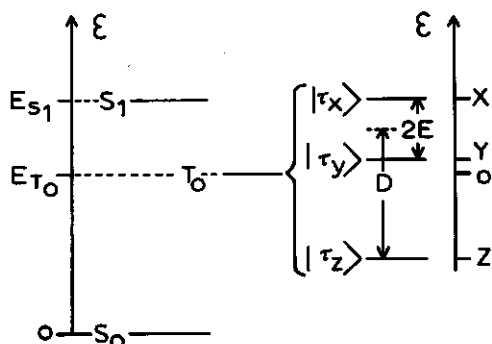
Fig. 2. Energy level diagram representing the energy level of the lowest excited triplet state T_o w.r.t. the lowest excited singlet state S_1, and the ground state S_o (left hand side of the diagram) and the zero-field splittings between the three triplet spin states $|\tau_x\rangle$, $|\tau_y\rangle$, and $|\tau_z\rangle$ (right hand side of the diagram). Note that the two vertical scales (energy ε) are different. For definition of X, Y, Z, D, and E see text.

2.2.4 *The triplet state parameters in relation to the electronic structure*

As shown in the last sections, the static triplet state parameters E_{T_0}, D and E are fully determined by the orbital part of the total wavefunction. In this section the effects of molecular structure on these parameters will briefly be discussed.

In the MO approximation two factors determine the triplet state energy level E_T. Firstly the energy difference, ΔE_{a-b}, between the MO's, occupied by the two unpaired electrons; secondly, the exchange integral K, given in eqn. (9), so that $E_{T_0} = \Delta E_{a-b} - K$ and $E_{S_1} = \Delta E_{a-b} + K$, where E_{S_1}

is the energy of the lowest excited singlet state. The simplest model describing the electronic wavefunctions is that of a particle in a box [3], especially when the electrons are delocalized over the molecule or at least over a part of the molecule as in the case of the $\pi\pi^*$ states considered in this study. This model predicts a decrease of ΔE_{a-b}, when the molecule, and consequently the size of the box is increased. The factor $1/r_{12}$ in the exchange intergral (eqn. 9) predicts also a decrease of K when the size of the molecule, or more specifically the extent of the MO's occupied by the unpaired electrons, is increased. The predicted decrease of $E_{S_1} - E_{T_0} = 2$ K is confirmed by experimental results for a series of aromatic hydrocarbons [4] When the symmetry of the molecule is changed or hetero-atoms (N, O) are introduced, more refined calculations are necessary to correlate theoretical and experimental results. In chapter 4 we will give an outline of some approximations used in the calculations on porphyrins.

The ZFS parameters D and E also depend on the interelectronic distance r_{12}, as is shown in eqns. (10a) and (10b). In addition, D and E depend on the *shape* of the electron distribution, as can be concluded from the x, y and z dependence. For a spherical electron distribution D and E both equal zero; molecules with at least a 3-fold axis of symmetry have E = 0 [4].

The ZFS tensor of planar aromatic hydrocarbons and porphyrins has its z-axis parallel to the normal to the molecular plane [5]; then eqn. (10a) reduces to

$$D = \tfrac{3}{4} g^2 \beta^2 \langle \frac{1}{r^3} \rangle,$$

since $\langle r^2 \rangle \gg \langle z^2 \rangle$ for planar molecules. Therefore, one expects for this

type of molecules a decrease of D when the extent of delocalization of the unpaired electrons is increased. Experimental results, however, indicate that effects of a change of shape of the electron distribution on D, due to changed electron wavefunctions, can dominate the effect of reducing the electron delocalization (see e.g. chapter 9).

The ZFS parameter E has been often referred to as a measure of the deviation from 3-fold or higher symmetry. Even a qualitative consideration of the effect of molecular geometry on this parameter is very difficult, since the value of E strongly depends on the orientation of the ZFS tensor axes w.r.t. the in-plane molecular axes of a planar molecule with two non-equivalent in-plane axes, such as is often occurring in porphyrins. For this reason, whereas E-values have been measured for several compounds, we will limit our discussions to the effects of size and shape of the π-electron distribution on the ZFS parameter D.

2.3 METHODS OF MEASUREMENT

In the following sections we describe the different techniques for measurement of triplet state parameters relevant for this study. In 2.3.1 we give a brief discussion of phosphorescence spectroscopy, whereas in 2.3.2 and 2.3.3 zero-field and high-field magnetic resonance are considered.

2.3.1 Optical transitions

Because of the optical selection rule $\Delta S = 0$ [3], absorption spectroscopy is not an appropiate technique to measure the energy level of the triplet state, as is normally done for singlet states. Although the decay $T_0 \to S_0$ is also strictly forbidden, the relative long lifetime of the triplet state makes detection of related emission (phosphorescence) possible.

The difficulties, related to the measurement of phosphorescence, which is weak w.r.t. fluorescence ($S_1 \to S_0$ emission) can be overcome using the differences between the two kinds of luminescence:

a) $E_{T_0} < E_{S_1}$, so that it is possible to discriminate on wavelength scale between the two kinds of luminescence by using optical filters or monochromators.

b) $\tau_{T_0} > \tau_{S_1}$, so that it is possible to discriminate by the time scale of the two emissions, using out-of-phase chopping of the exciting light and the emitted light.

Both principles have been used in the home-built phosphorimeter and have been described before [6].

2.3.2 *Microwave transitions*

2.3.2.1 Zero-field magnetic resonance

Without an external field the spin functions of the three triplet states are given by $|\tau_x\rangle$, $|\tau_y\rangle$, and $|\tau_z\rangle$ (eqns. 6a-c). Microwave radiation with the appropiate frequency (ν = 100 MHz - 2 GHz for porphyrins) can induce transitions between these states, as discussed in section 2.2.1.

The absence of sensitive detectors for the direct measurement of small microwave absorptions favours the use of indirect detection. It has been previously shown that transitions between two of the three triplet spin states can induce a change in the phosphorescence [7] and/or fluorescence [8] intensity. Especially the latter method has created the possibility to measure the ZFS parameters for the photosynthetic pigments, without an external field, in spite of the very weak phosphorescence of these compounds. To use these techniques, however, it is necessary that the rate of spin-lattice relaxation (SLR), inducing Boltzman equilibrium between the spin states, is small. This condition can be fulfilled only when the experiments are carried out at very low temperature (T = 1-10 K). At higher temperatures it is necessary to use an alternative technique, high field electron spin resonance (ESR).

2.3.2.2 High field magnetic resonance

In an external magnetic field the spin functions $|\tau_x\rangle$, $|\tau_y\rangle$, and $|\tau_z\rangle$ are no longer the eigenfunctions of the spin-hamiltonian, given in eqn. (4). When the zero-field splitting can be neglected w.r.t. the external field, i.e. when $g\beta H \gg X, Y, Z$, and H//z an appropriate description of the spin is given by the high-field spin functions $|+1\rangle$, $|0\rangle$ and $|-1\rangle$ defined in eqns. (3) and (8a-c). As discussed in section 2.2.1, transitions between spin states $|+1\rangle$ and $|0\rangle$ and between $|0\rangle$ and $|-1\rangle$ (Δm_s = 1) can be induced by an rf field, circularly polarized in the plane perpendicular to the external magnetic field [2]. In the intermediate case, when X, Y, and Z cannot be neglected, in addition to the Δm = 1 transitions, the so-called Δm = 2 transition $|+1\rangle \leftrightarrow |-1\rangle$ is also allowed, resulting in a half-field signal.

Resonance conditions, at which transitions can be induced, can be realized in two ways:

a) variation of the frequency of the rf field at constant magnetic field;

b) variation of the external magnetic field with a constant rf frequency. Because of experimental difficulties with method (a) (see e.g. section 2.3.2.1), in practice only method (b) is used [9]. Thus, an electron spin resonance (ESR) spectrum is obtained by sweeping the magnetic field, while keeping the rf frequency constant. For a *single* molecule in its triplet state, this results in three transitions (one $\Delta m = 2$ transition and two $\Delta m = 1$ transitions) at different magnetic fields. As long as all molecules have the same orientation, as can be realized in a single crystal, only these three transitions will be found. When, however, the molecules are randomly oriented, transitions will take place over a *range* of magnetic field strength values. Since all samples considered in this study contain randomly oriented molecules, this problem will be discussed in more detail.

To find the resonance conditions as a function of the orientation of the magnetic field w.r.t. the molecular frame, firstly the eigenvalues of the hamiltonian, given by eqn. (4) have to be calculated. With spin functions diagonalizing the spin-spin interaction hamiltonian, the hamiltonian matrix becomes

$$
\langle \tau_i | \mathcal{H} | \tau_j \rangle =
\begin{vmatrix}
X & -ig\beta H \cos\theta & ig\beta H \sin\theta\ \sin\phi \\
-ig\beta H \cos\theta & Y & ig\beta H \sin\theta\ \cos\phi \\
-ig\beta H \sin\theta\ \sin\phi & -ig\beta H \sin\theta\ \cos\phi & Z
\end{vmatrix}
$$

where the magnetic field is decomposed in its components along the ZFS tensor axes,

$$
\vec{H} = H
\begin{vmatrix}
\sin\theta\ \cos\phi \\
\sin\theta\ \sin\phi \\
\cos\theta
\end{vmatrix}
\quad ;
$$

θ is the angle between $\vec{H}$ and the z-axis, ϕ the angle between the component of $\vec{H}$ in the x-y plane and the x-axis. The principal values $E_{1,2,3}$ of this hamiltonian matrix are given by

28

$$E^3 - E \{g^2\beta^2H^2 - (XY + YZ + XZ)\} + g^2\beta^2H^2 (X \sin^2\theta \cos^2\phi$$

$$+ Y \sin^2\theta \sin^2\phi + Z \cos^2\theta) - XYZ = 0 \qquad (11)$$

The resonance conditions are fulfilled when the difference between two roots of eqn. (11) equals δ = $h\nu$, where h is Planck's constant and ν the rf frequency. This condition leads to the resonance equation:

$$g^2\beta^2H^2 \{X \sin^2\theta \cos^2\phi + Y \sin^2\theta \sin^2\phi + Z \cos^2\theta\} =$$

$$= XYZ - 3^{-3/2} \{(\delta^2 + XY + XZ + YZ) - g^2\beta^2H^2\} \times \{-\delta^2 - 4(XY + YZ + XZ) +$$

$$+ 4 g^2\beta^2H^2 \}^{\frac{1}{2}} \qquad (12)$$

Fig. 3a represents the dependence of resonance field values on the orientation of the magnetic field. It should be noted that for each field orientation three resonance conditions occur. To get the absorption spectrum as a function of magnetic field for an ensemble of randomly oriented molecules, the spectra of molecules with all possible orientations have to be superimposed. When the magnetic field dependence of the transition probability is neglected, this results in a spectrum as shown in fig. 3b; fig. 3c gives the first derivative of this absorption spectrum, the form in which ESR spectra are normally presented. It can be shown [4] that the mathematical discontinuities in the $\Delta m = 1$ part of the absorption spectrum, and consequently the observable peaks in the first derivative spectrum, occur at field position where the resonance conditions are fulfilled for molecules with one of their ZFS tensor axes oriented along the magnetic field: for $H^{\pm}_i$, $\bar{H}//i$ with i = x,y,z; H//x,y,z are the so-called canonical orientations. These field positions are given by the equations,

$$(g\beta H^{\pm}_x)^2 = (h\nu \pm D \mp E) (h\nu \pm 2E), \qquad (13a)$$

$$(g\beta H^{\pm}_y)^2 = (h\nu \pm D \pm E) (h\nu \mp 2E), \qquad (13b)$$

$$(g\beta H^{\pm}_z)^2 = (h\nu \pm D)^2 \mp E^2, \qquad (13c)$$

where $h\nu$ is the rf energy and D and E are the ZFS parameters.
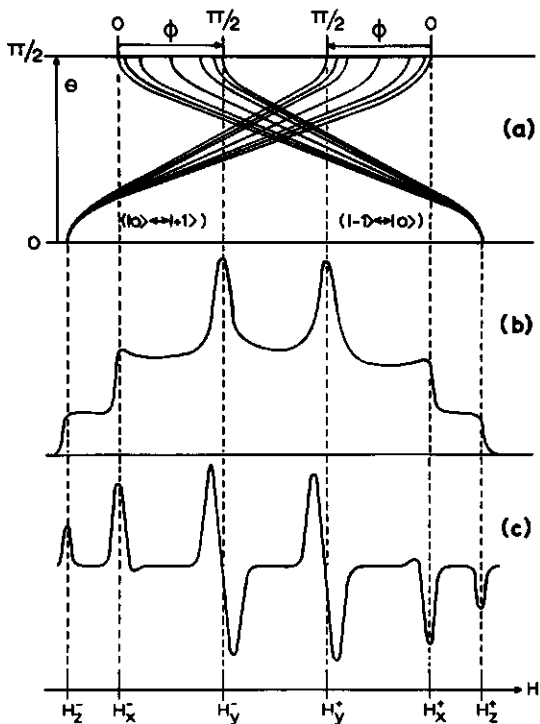
Fig. 3. $\Delta m = 1$ triplet ESR spectrum of an ensemble of randomly oriented molecules. (a) Relation between resonance field value H and orientation of the external magnetic field w.r.t. ZFS tensor axes x, y, and z; θ denotes the angle between $\vec{H}$ and the z-axes, ϕ the angle between the component of $\vec{H}$ in the x-y plane with the x-axis. Fully drawn lines represent the dependence of H on θ at a fixed value of ϕ. (b) ESR absorption spectrum derived from (a) by summation of absorption profiles for all possible orientations. (c) First derivative spectrum of (b), corresponding to experimental presentation. For (b) and (c) the transition probability is taken to be independent of H; in addition, Boltzman equilibrium between the spin levels is assumed.

When $|g\beta H| \gg |D|, |E|$, eqns. (12a-c) can be reduced to

$$g\beta \ (H_z^+ - H_z^-) = 2|D|, \tag{14a}$$

$$g\beta \ (H_x^+ - H_x^-) = |D| + 3|E|, \tag{14b}$$

$$g\beta \ (H_y^+ - H_y^-) = |D| - 3|E|. \tag{14c}$$

Eqns. (14a-c) are used to extract the values of the ZFS parameters from the triplet ESR spectra measured in this investigation.

2.4 REFERENCES

1.   G.E. Uhlenbeck, S. Goudsmit, Naturwiss., 13, 953 (1925)
2.   A. Carrington, A.D. McLachlan, Introduction to magnetic resonance,
     New York, 1967.
3.   H. Eyring, J. Walter, G.E. Kimball, Quantum Chemistry, New York, 1944.
4.   S.P. McGlynn, T. Azumi, M. Kinoshita, Molecular spectroscopy of the
     triplet state, Englewoods Cliffs N.J., 1969.
5.   W.G. van Dorp, M. Soma, J.A. Kooter, J.H. van der Waals, Mol. Phys.,
     28, 1551 (1974).
6.   J.D. Winefordner, P.A. St. John, Anal. Chem., 42, 639 (1970).
7.   J. Schmidt, J.H. van der Waals, Chem. Phys. Lett., 2, 640 (1968).
8.   C.B. Harris, R.J. Hoover, J. Chem. Phys., 56, 2199 (1972).
9.   C.P. Poole, Electron spin resonance, New York, 1967.

3 Kinetic triplet state parameters

3.1 INTRODUCTION

One of the most striking properties of the lowest excited triplet state T_0 is its relatively long lifetime: $\tau \sim 10^{-3} - 10^2$ sec.. From optical studies (phosphorescence and triplet-triplet absorption) it has been found that τ depends on the molecular structure and the medium in which the molecules are incorporated [1, 2]. Such optical studies, however, only yield information on the mean decay constant $K_T \equiv 1/3 \sum_i k_i$, where $i = x, y, z$ and k_i are the decay constants for the three triplet spin states $|\tau_x\rangle$, $|\tau_y\rangle$, and $|\tau_z\rangle$. Using magnetic resonance techniques it is possible to measure the decay constants k_i and the relative populating rates P_i for each of the three spin states separately; the relevant parameters are presented in fig. 1 and fig. 2. Apart from the populating and depopulating process, transitions between the three spin levels induced by spin lattice relaxation (SLR) are of importance for the kinetics of the triplet state. In this chapter we will give a theoretical introduction to the mechanisms, which play a rôle in the populating and depopulating processes. In the second part experimental techniques and methods for analysing the data will be discussed.

3.2 THEORY

3.2.1 Intersystem crossing processes

Transitions between the singlet and triplet manifolds (intersystem crossing, ISC) can be induced by spin-orbit coupling (SOC). The spin-spin interaction, discussed in section 2.2.1, only mixes spin states with the same quantum number S, but with different quantum number m_s; spin-orbit interactions can mix states with different spin multiplicity, as for example singlet and triplet states and therefore is operative in radiative as well as non-radiative transitions between singlet and triplet states. In the following we will discuss the main features of spin-orbit interactions; furthermore the

SOC matrix elements for the three spin levels of the lowest excited triplet state will be considered and their relation to ISC rates for the various spin levels will be mentioned.

The spin quantum numbers S and m_s are only good quantum numbers, when the electron, bearing the spin, is absolutely free and possesses no orbital angular momentum. For electrons having both spin- and orbital angular momentum, only the total angular momentum $\vec{J} = \vec{L} + \vec{S}$ is quantified [3]. If, however, the coupling between spin and orbital angular momentum is weak, the spin description may be retained; the effect of SOC can be included by a small admixture of states with other spin multiplicities. The effect of SOC on the hamiltonian can be understood, considering the energy resulting from the motion of a magnetic moment in an electric field. Usually, only the interaction of an electron spin S(i) with the average field, depending on the position and velocity of electron i, is retained. This results in a SOC hamiltonian

$$\mathcal{H}_{SO} = \sum_K \gamma_K \sum_i \underline{\ell}_K(i) \cdot \underline{S}(i),$$

where $\underline{S}(i)$ is the spin angular momentum operator and $\underline{\ell}_K(i)$ the orbital angular momentum operator of electron i w.r.t. nucleus K. The summation over the nuclei K, instead of integration over full space is permitted because of the strong dependence of γ_K on the distance r_{iK} between electron i and nucleus K: $\gamma_K(:)r_{iK}^{-4}$ [4]; γ_K is defined as the atomic SOC constant for nucleus K. The single nucleus (atomic) SOC hamiltonian can be written as [5]

$$\mathcal{H}_{SO} = \gamma \sum_i \underline{\ell}(i) \cdot \underline{S}(i) = \gamma \sum_i (\underline{\ell}_x(i) \cdot \underline{S}_x(i) + \underline{\ell}_y(i) \cdot \underline{S}_y(i) + \underline{\ell}_z(i) \cdot \underline{S}_z(i)).$$

It has been shown [5] that the x-component of this SOC hamiltonian,

$$\mathcal{H}_{SO}^x = \gamma \sum_i \underline{\ell}_z(i) \cdot \underline{S}_x(i)$$

can couple a triplet state with spin function $|\tau_x\rangle$ with a singlet state, whereas the orbital part of this operator $(\underline{\ell}_x(i))$ *simultaneously* can couple the atomic orbitals $2p_z$ and $2p_y$. Analogously $\mathcal{H}_{SO}^y$ and $\mathcal{H}_{SO}^z$ couple singlet states with the triplet spin states $|\tau_y\rangle$ and $|\tau_z\rangle$, together with a coupling of $2p_z$ and $2p_x$, and $2p_x$ and $2p_y$, respectively.

Considering the matrix elements of $\mathcal{H}_{SO}$ between the lowest excited

33

triplet state and singlet states, $\langle S_n | \mathcal{H}_{SO} | T_0 \rangle$, it should be noted that only single electron promotions have to be taken into account. Since only effects of $\mathcal{H}_{SO}$ on the two unpaired electrons are important [6], the wave function of these electrons has to be considered for the calculation of the matrix elements. All molecules to be discussed in this study have a $\pi\pi^*$ lowest excited triplet state, so that the molecular orbitals occupied by the two unpaired electrons in T_0 only contain $2p_z$ atomic orbitals. Retaining only one electron-one center integrals, as proposed by Metz [7], the spin states $|\tau_x \rangle$ and $|\tau_y \rangle$ can be coupled with singlet states; the one center SOC operator $\mathcal{H}_{SO}^z$ couples only $2p_x$ and $2p_y$ atomic orbitals.

Singlet states, coupled to the triplet spin states $|\tau_x \rangle$ and $|\tau_y \rangle$ by $\mathcal{H}_{SO}^x$ and $\mathcal{H}_{SO}^y$, respectively, must contain $2p_y$ and $2p_x$ orbitals. This requirement is met by $\sigma\pi^*$, $\pi\sigma^*$ and $n\pi^*$ excited singlet states. It has been shown by Antheunis [8] and Metz [9] that the mixing of these states with T_0 is mainly responsible for the triplet populating and depopulating processes for aromatics and aza-aromatics. Non-zero populating and depopulating rates for the spin state $|\tau_z \rangle$ can be attributed to SOC with singlet $\pi\pi^*$ states, retaining the small multicenter integrals [8] or to second order effects: Taking into account SOC between singlet *and* triplet $\sigma\pi^*$, $\pi\sigma^*$ and/or $n\pi^*$ states, also $\mathcal{H}_{SO}^z$ results in non-zero one electron-one center integrals [8].

Which singlet states can couple with the lowest excited triplet state can be deduced from group theoretical arguments. When, for example, the lowest excited triplet state of a molecule with D_{2h} symmetry, has orbital symmetry B_{2u}, the symmetries of the total wave functions T_{0x}, T_{0y} and T_{0z} ($T_{0x} = T_0 \cdot | \tau_x \rangle$, etc.) are given by B_{1u} for T_{0x}, A_u for T_{0y}, and B_{3u} for T_{0z}. The symmetry of each of the total wave functions is the product of the symmetries of the orbital- and corresponding spin functions. Since $\mathcal{H}_{SO}$ is totally symmetric, the matrix elements $\langle S_n | \mathcal{H}_{SO} | T_0 \rangle$ are non-zero only for coupling of T_{0x} with a B_{1u} singlet state and similarly, for coupling of T_{0y} and T_{0z} with A_u and B_{3u} singlet states. A_u and B_{1u} are antisymmetric w.r.t. reflection at the plane z=0 and so arise from $\pi\sigma^*$, $\sigma\pi^*$ or $n\pi^*$ excitations; B_{3u} states, which are symmetric w.r.t. that plane, arise from $\pi\pi^*$ excitations, in agreement with the discussion given before.

In view of the study of the decay rates of some photosynthetic pigments, we discuss in Chapter 9 the effects of electronic structure on ISC processes. For the moment the main conclusion from the foregoing

discussion is that the populating and depopulating rates for the three spin levels are predicted to be generally different, because of different coupling of these levels to the singlet manifold. It should be noted that the same SOC matrix elements occur in the relations for the populating and depopulating processes of the triplet state [8], so that one expects roughly the same ratios between the three depopulating rate constants $(k_x:k_y:k_z)$ and between the three populating rates $(P_x:P_y:P_z)$ of the triplet state. This is, because the P_i's and k_i's are both proportional to the square of the SOC matrix elements [8],

$$P_i, \; k_i (:) \; |\langle S_n |\mathcal{H}_{SO}| T_{0i} \rangle|^2.$$

3.2.2 *Relaxation*

A third process of importance for the kinetics of a triplet state is the spin-lattice relaxation (SLR), inducing transitions between the three spin levels. At least three mechanisms have been proposed for the coupling, between phonons of the matrix, in which the molecule is embedded, and the spin states. For paramagnetic ions, it has been shown that the relaxation occurs predominantly via the van Vleck SOC mechanism [10], in which phonon modulation of the crystal field affects the orbital motion and consequently the SOC of the unpaired electrons. The SLR in the triplet state of aromatics has been attributed to a modulation of the spin-spin interaction or the hyperfine interaction between the unpaired spins and nuclei in the molecule [10, 11]. To decide which of these mechanisms is operative, the SLR has to be measured at different temperatures and effects of side groups or isotope substitution have to be determined [10]. In this study the measurements of the kinetics have been carried out at one temperature and an accurate determination of the relaxation rates was not possible. Some features, however, deserve attention and comment: (1) The relaxation between the zero-field spin levels $|\tau_x\rangle$, $|\tau_y\rangle$, and $|\tau_z\rangle$ differs for each of the possible transitions [12]. (2) With an external field the relaxation rates depend on the orientation of the magnetic field w.r.t. the axes of the ZFS tensor [11, 13]. (3) In zero-field as well as in high-field the relaxation is strongly temperature-dependent [11, 12].

3.2.3 Definitions of zero-field kinetic parameters

The *population* of a state is defined as the number of molecules in that state; N_0 is the population of S_0, N_1 of S_1, N_x of T_{0x}, N_y of T_{0y}, and N_z of T_{0z}. The *populating rate* P_i is defined as the number of molecules entering the state T_{0i} per second ($i = x, y, z$). The *populating rate constant* p_i is the ratio of P_i and the population of the level from where the molecules, entering T_{0i}, originate. The transitions $S_n \rightarrow S_1$ and $T_n \rightarrow T_0$ are much faster than the ISC rates ($\sim 10^{12}$ vs $\lesssim 10^7$ sec.$^{-1}$). Therefore all three triplet spin states are assumed to be populated from S_1. For the molecules to be discussed in this investigation, this assumption has been proven to be correct: optical excitation into S_2 results in the same ratio of populating rates as excitation into S_1. Thus, the populating rate constants are given by $p_i = P_i/N_1$ ($i = x, y, z$). With the methods used in this study N_1 cannot be determined; only the ratio $P_x : P_y : P_z = p_x : p_y : p_z$ can be measured.

The *depopulating rates* K_i are defined as the number of molecules leaving a state per second, and the depopulating rate constants k_i are defined by $k_i = K_i/N_i$. As will be shown below, our experimental methods yield directly the absolute values for k_i.

In the case that $|\tau_x\rangle$ has a higher energy than $|\tau_y\rangle$, w_{xy} is defined as the SLR rate constant for the transition $|\tau_x\rangle \rightarrow |\tau_y\rangle$. Relaxation is a thermal process resulting in a Boltzman equilibrium between populations of the spin states, when the P_i's and k_i's can be neglected w.r.t. the SLR rate constants. Consequently, the SLR rate constant for the transition $|\tau_x\rangle \leftarrow |\tau_y\rangle$, w_{yx}, is given by

$$w_{yx} = e^{-\Delta E/kT}.w_{xy} \equiv \alpha\, w_{xy},$$

where ΔE is the energy separation between the two spin states $|\tau_x\rangle$ and $|\tau_y\rangle$. The other relaxation rate constants are defined in a similar way. In fig. 1 the zero-field kinetic parameters for a triplet state are depicted.

3.2.4 Relation between high-field and zero-field kinetic parameters

In a strong external magnetic field $\vec{H}$ (i.e. $g\beta H \gg X, Y, Z$ in eqn. (4) in Chapter 2) $|\tau_x\rangle$, $|\tau_y\rangle$, and $|\tau_z\rangle$ are no good functions for the spin states. With $\vec{H} \parallel z$ the functions are given by $|+1\rangle = 1/\sqrt{2}\,(|\tau_x\rangle + i|\tau_y\rangle)$,

$|0\rangle = |\tau_z\rangle$, and $|-1\rangle = \frac{1}{\sqrt{2}}(|\tau_x\rangle - i|\tau_y\rangle)$ (see section 2.2.1). The SOC matrix elements discussed in section 3.2.1 are the only spin state dependent factors of the populating and depopulating rate constants [8] so that,

$$P_{+1}, \ k_{+1} \ (:) \ \tfrac{1}{2}|\langle S_n|\mathcal{H}_{SO}|T_{0x}\rangle + i\langle S_n|\mathcal{H}_{SO}|T_{0y}\rangle|^2 \tag{1}$$

where P_{+1} and k_{+1} are the populating rate and depopulating rate constant for the spin state $|+1\rangle$. From eqn. (1) it is easily derived that

$$k_{+1} = \tfrac{1}{2}(k_x + k_y), \quad P_{+1} = \tfrac{1}{2}(P_x + P_y) \tag{2}$$

Furthermore, for the other rate constants one finds,

$$k_{-1} = k_{+1}, \ P_{-1} = P_{+1}, \quad k_0 = k_z \text{ and } P_0 = P_z \tag{3}$$

When $\vec{H}//x$ or $H//y$ similar relations hold. The zero-field spin state related to the axis, which is parallel with $\vec{H}$, remains pure, whereas the other two zero-field spin states are mixed, resulting in the $|+1\rangle$ and $|-1\rangle$ high-field spin states.

Whereas the relations between the zero-field k's and P's and their high-field counterparts are in first order independent of the strength of the magnetic field [14] - as long as $g\beta H \gg X, Y, Z$ -, the SLR is expected to be strongly dependent on the magnitude of $\vec{H}$, because of its dependence on the energy separation between the spin states. Because there is no theory for the dependence of the SLR on molecular structure, related spin states, and the energy gap between the spin states, it is not possible to deduce a relation between zero-field SLR rate constants and those at high-field.

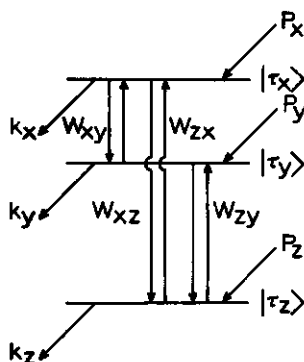The high-field kinetic parameters for a triplet state are de-

Fig. 1 Zero-field triplet state kinetics. k_i and P_i denote the depopulating rate constant and the populating rate of the spin level $|\tau_i\rangle$ (i = x,y,z). W_{ij} is the SLR rate constant for the transition $|\tau_i\rangle \rightarrow |\tau_j\rangle$.
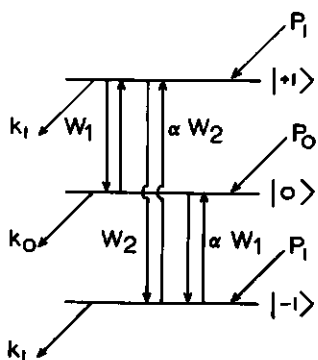
Fig. 2 High-field triplet state kinetics. k_1 and P_1 are the depopulating rate constant and populating rate for the spin levels $|+1\rangle$ and $|-1\rangle$, k_0 and P_0 for the spin level $|0\rangle$. W_1 is the SLR rate constant for transitions $|+1\rangle \rightarrow |0\rangle$ and $|0\rangle \rightarrow |-1\rangle$, W_2 for $|+1\rangle \rightarrow |-1\rangle$, α is the Boltzman factor $(1 - \exp(\Delta E/kT))$ (see text).

picted in fig. 2. The ratio between the relaxation rate constants for up and down transitions is again given by the Boltzman factor $\alpha = \exp(-\Delta E/kT)$, assuming that the relaxation between $|+1\rangle$ and $|0\rangle$ and between $|-1\rangle$ and $|0\rangle$ is equal, independent of the difference in energy separation between $|+1\rangle$ and $|0\rangle$ and between $|-1\rangle$ and $|0\rangle$.

3.3 OPTICAL ELECTRON SPIN POLARIZATION

3.3.1 *Signs and magnitudes of triplet ESR peaks*

In Chapter 2 only the positions of the peaks in a $\Delta m=1$ triplet ESR spectrum have been considered. As long as, under continuous optical excitations, Boltzman equilibrium between the three spin levels exists, the population difference between the levels $|+1\rangle$ and $|0\rangle$ and between $|0\rangle$ and $|-1\rangle$ is equal and a rf field will induce more transitions $|+1\rangle \leftarrow |0\rangle$ and $|0\rangle \leftarrow |-1\rangle$ than in reverse direction, because of the larger population of $|0\rangle$ w.r.t. $|+1\rangle$ and of $|-1\rangle$ w.r.t. $|0\rangle$, respectively, resulting in a nearly equal net absorption of energy for both transitions. A spectrum obeying these conditions is called a *normal* triplet ESR spectrum and is shown in fig. 3c, Chapter 2.

In the absence of Boltzman equilibrium, the sign and amplitude of the peaks depend on the relative population of the spin levels and thus on the kinetic parameters. In the following we will firstly discuss the case that the SLR may be neglected w.r.t. the populating and depopulating rates; next, we will consider the intermediate case, when SLR may no longer be neglected, but is not fast enough to induce a Boltzman equilibrium between

38

the spin states.

3.3.2 Electron spin polarization patterns

When SLR can be fully neglected, the population of the spin states for $\vec{H}//z$ are given by

$$N_{+1} = N_{-1} = \frac{P_{+1}}{k_{+1}} = \frac{P_x + P_y}{k_x + k_y} \text{ and } N_0 = \frac{P_0}{k_0} = \frac{P_z}{k_z}$$

(see section 3.2.3). If, for example, $N_0 > N_{+1}$, transitions induced between

$|0\rangle$ and $|+1\rangle$ will result in absorption of energy and the transitions $|-1\rangle \leftrightarrow$ $|0\rangle$ will result in emission. In the following, absorptive and emissive character of transitions will be denoted by the symbols A and E, respectively. Because the $Z^{\pm}$ peaks in a $\Delta m = 1$ triplet ESR spectrum of an ensemble of randomly oriented molecules are associated with the transitions of molecules with $\vec{H}//z$ (see Chapter 2), from the sign of these peaks the relative population of $|0\rangle$ and $|\pm 1\rangle$ can be deduced:

if Z^- is A and Z^+ is E, then $N_0 > N_{\pm 1}$ $(\vec{H}//z)$;

if Z^- is E and Z^+ is A, then $N_{\pm 1} > N_0$ $(\vec{H}//z)$.

Noting that for $\vec{H}//z$ H_z^- is related to the transitions $|+1\rangle \leftrightarrow |0\rangle$ and for $\vec{H}//x, y$ H_x^- and H_y^- correspond to the transitions $|0\rangle \leftrightarrow |-1\rangle$ (see fig. 2, Chapter 2), it can be shown that the following relations hold for $\vec{H}//x$ or $\vec{H}//y$:

if X^-, Y^- is A and X^+, Y^+ is E, then $N_0 < N_{\pm 1}$;

if X^-, Y^- is E and X^+, Y^+ is A, then $N_{+1} < N_0$.

It should be noted that the peaks H_i^- and H_i^+, related to molecules with $\vec{H}//i$ (i = x, y, z) always have an opposite character (i.e. A vs. E) and equal magnitude, as long as SLR may be neglected.

The relative populations of $|0\rangle$ and $|+1\rangle$ for the three canonical orientations are not independent of each other. As a result, not all electron spin polarization (ESP) patterns (a pattern in which the character

Table I   Possible ESP patterns, when mono-molecular kinetic processes, as defined in sections 3.2.3,4, are active only, and the corresponding relative spin state populations. $H_i^{\mp}$ denotes the peak position and E and A correspond to emissive and absorptive character of the peaks; N_i is the population of the zero-field spin state $|\tau_i\rangle$.

H_z^-	H_x^-	H_y^-	H_y^+	H_x^+	H_z^+	relative spin state populations
E	E	E	A	A	A	$N_x, N_y > N_z$
A	A	A	E	E	E	$N_x, N_y < N_z$
A	A	E	A	E	E	$N_y, N_z > N_x$
E	E	A	E	A	A	$N_y, N_z < N_x$
E	A	E	A	E	A	$N_x, N_z < N_y$
A	E	A	E	A	E	$N_x, N_z > N_y$

of the six peaks in a $\Delta m = 1$ triplet ESR spectrum are denoted by A or E) are possible. In table 1 the permitted ESP patterns are denoted; it can be shown that there are twelve other possibilities when for one of the orientations $N_0 = N_{+1}$, resulting in zero amplitude for the corresponding peaks. If the kinetic mechanisms defined in section 3.2.3 are the only ones, which are operative, the patterns E A A E E A and A E E A A E are forbidden, as will be proven   in Appendix B.

3.3.3   Electron spin polarization ratio

In the intermediate case, when SLR is not fast enough to induce Boltzman equilibrium, but the SLR rates may not be neglected w.r.t. the populating and depopulating rates, the population of the three triplet spin levels in the high-field limit is governed by the following equations,

$$\frac{dN_{+1}}{dt} = P_1 + N_{+1}(-k_1 - W_1 - W_2) + N_0\,\alpha W_1 + N_{-1}\,2\alpha W_2, \tag{4a}$$

$$\frac{dN_0}{dt} = P_0 + N_{+1}W_1 + N_0(-k_0 - \alpha W_1 - W_1) + \dot{N}_{-1}\,\alpha W_1, \tag{4b}$$

$$\frac{dN_{-1}}{dt} = P_1 + N_{+1}W_2 + N_0 W_1 + N_{-1}(-k_1 - \alpha W_1 - \alpha W_2). \tag{4c}$$

The kinetic constants, P_i, k_i and W are defined in section 3.2.2, fig. 2. The

40

steady state condition, obtained under continuous illumination, is given by

$$\frac{dN_{+1}}{dt} = \frac{dN_0}{dt} = \frac{dN_{-1}}{dt} = 0 \tag{5}$$

The amplitudes of the peaks for one of the three canonical orientations are related to the spin level populations for this orientation by

$$S^+ \ (:) \ N_0 - N_{+1}, \quad S^- \ (:) \ N_{-1} - N_0 \tag{6}$$

Introduction of eqns. (5) and (6) in eqns. (4a-c) yield a simple relation for the ESP ratio R:

$$R \equiv \frac{S^+ - S^-}{S^+ + S^-} = \frac{P_0 k_1 - P_1 k_0}{\delta W(P_0 + 2P_1)} \quad , \tag{7}$$

where $\delta = 1 - \alpha = 1 - \exp(-\Delta E/kT) \sim \Delta E/kT$. Furthermore, it is assumed that $W = W_1 = W_2$; in the derivation of eqn. (7) δ^2 has been neglected w.r.t. δ and $k_{0,1}$ has been neglected w.r.t. W. It should be noted that the same result is obtained when the relations for $\Delta N_+ = N_0 - N_{+1}$ and $\Delta N_- = N_{-1} - N_0$, deduced by Winscom [15] are used to calculate R. It follows from this derivation that it is not necessary to set $W_1 = W_2$, since W_2 is eliminated from the relation when $k_{+1} = k_{-1} \equiv k_1$ and $P_{+1} = P_{-1} \equiv P_1$ [15] .

In Chapters 7 and 8 the use of eqn. (7) to the $\Delta m = 1$ triplet ESR spectra will be discussed. Here we will give some comments. ESP will occur only when populating and/or depopulating processes are anisotropic ($k_0 \neq k_1$, $P_0 \neq P_1$). As discussed in section 3.2.1 the ratio between the three populating rates and between the three depopulating rate constants is expected to be nearly equal, so that $(P_0 k_1 - P_1 k_0)/(P_0 + 2P_1) \ll K_T$. Thus non-zero ESP ratios will occur only if $\delta W < K_T$. δ and W are temperature dependent; whereas δ (:) $1/T$, the temperature dependence of W is assumed to be given by W (:) $T^5 - T^9$ [11] , so that with increasing temperature δW will increase. ESP can be obtained at relatively high temperatures (T > 100 K) when K_T is relatively fast (as for Bchl, $K_T \sim 2000 \ \text{sec}^{-1}$) or when W is relatively slow as for polymer matrices (see Chapter 8).

Finally we note that, when no full ESP occurs, the ESP pattern can be deduced from the relative amplitudes, $S(H_i^{\pm})$, of corresponding peaks. Under conditions that all peaks are absorptive but R ≠ 0, the peaks which are

emissive when SLR can be neglected, will be smaller than the corresponding intrinsically absorptive peaks (i.e. peaks which remain absorptive under all conditions) : if $S(H_i^-) > S(H_i^+)$, the transitions at H_i^- and H_i^+ are intrinsically A and E, respectively. The reverse is true when $S(H_i^+) > S(H_i^-)$.

3.4 TIME DEPENDENT HIGH-FIELD ELECTRON SPIN RESONANCE

3.4.1. *Principles*

Many studies on the kinetics of the triplet state have been performed by optically detected zero-field magnetic resonance at 1.2 - 4.2 K [16]. Although this technique has great advantage above the high-field technique to be discussed in this section, in some cases time dependent high-field ESR is a more appropriate technique. For example, when the relaxation rates cannot be neglected even at the lowest possible temperature, such as has been found in glassy samples or biological material, or when for technical reasons measurement at 1.2 ~ 4.2 K is not possible. Furthermore, with high-field ESR it is possible to measure the temperature dependence of the various kinetic constants over a large temperature range.

The following part provides a brief introduction to time dependent ESR. In the next sections the methods for analysing the signals will be discussed. For samples with randomly oriented molecules, the six peaks in the $\Delta m = 1$ triplet ESR spectrum correspond to transitions of molecules with one of the canonical orientations (see Chapter 2). The time dependence of the population of the triplet spin levels for molecules with $\vec{H}//x$, $\vec{H}//y$ or $\vec{H}//z$ can be determined by measuring the time-dependent amplitude of the ESR peak, $S(t)$, at $H = H_x^\pm$, $H_y^\pm$ or $H_z^\pm$, using square-wave amplitude modulation of the exciting light creating triplet population. We consider in particular the behaviour of $S(t)$ immediately after the exciting light is turned on or off. In this manner we obtain the time-dependence of $\Delta N_+ = N_0 - N_{+1}$ and $\Delta N_- = N_{-1} - N_0$ for each of the three canonical orientations after starting and stopping the populating process of the triplet state. We denote the time-dependent behaviour of the ESR peaks as *transients*. Fig. 3 presents some transients for Chl a in MTHF at 100 K.
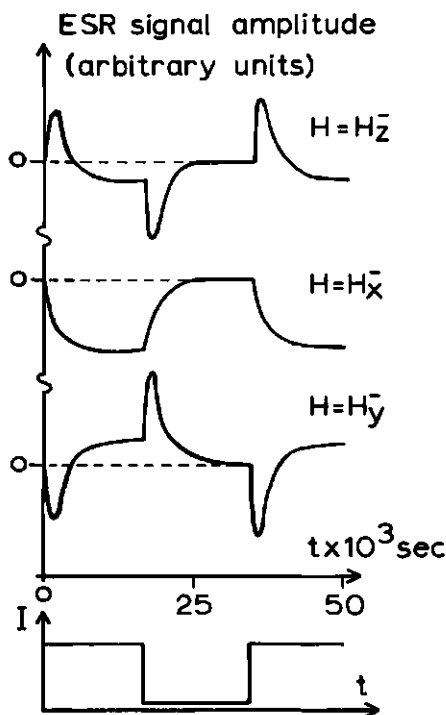
ESR signal amplitude
(arbitrary units)

$H = H_z^-$

$H = H_x^-$

$H = H_y^-$

$t \times 10^3$ sec

25   50

I

t

Fig. 3 Transients at $H = H_z^-$, H_x^- and H_y^- in the $\Delta m = 1$ triplet ESR spectrum of Chl a in MTHF at 100 K. The lower part of the figure represents the time dependence of the intensity (I) of the exciting light. Experimental conditions: microwave frequency 9.1 GHz, microwave power 2 mW, field modulation frequency 100 KHz, field modulation amplitude 16 Gauss, spectrometer RC-time 0.3 msec.

3.4.2   Mathematical analysis

The first mathematical analysis of the transient behaviour of $\Delta m = 1$ triplet ESR transitions of molecules with canonical orientations was given by Schwoerer and Sixl [14]. These authors started with three kinetic equations, comparable to eqns. (4a-c). While their analysis could account for the experimental results in a qualitative way, a good description of the kinetics of the triplet state can be given only, if the differential equation for the population of the singlet states is taken into account, as was done by Levanon and Vega [17]. Since the equilibrium distribution within the singlet manifold is established on a much shorter time scale than between the singlet and triplet manifolds, all singlet levels can be taken as a single state with total population N_S.

Using the approximation $P_{+1} = P_{-1} \equiv P_1$, $k_{+1} = k_{-1} \equiv k_1$, $W_1 = W_2$, and $k_{0,1} \ll W_1$, Levanon and Vega [17] have found that

$$S_{1i}(t) = S_{11}^i (1 - e^{-\lambda_-^i \cdot t}) + S_{12}^i (1 - e^{-\lambda_+^i \cdot t}) \tag{8a}$$

43

$$S_{2i}(t) = S_{21}^i (1 - e^{-\lambda_-\cdot t}) + S_{22}^i (1 - e^{-\lambda_+^i\cdot t}) \tag{8b}$$

for transients after switching light on; for light off (8a) and (8b) have to be modified by replacing $(1 - \exp(-\lambda_-.t))$ and $(1 - \exp(-\lambda_+.t))$ by $\exp(-\lambda_-.t)$ and $\exp(-\lambda_+.t)$. In eqns. (8a, b) S_{1i} and S_{2i} denote the time dependent $\Delta m = 1$ triplet ESR signals, corresponding to the transitions $|0\rangle \leftrightarrow |-1\rangle$ and $|+1\rangle \leftrightarrow |0\rangle$, respectively, for molecules with $\vec{H}//i$ (i = x, y, z). The time-independent constants are given by

$$S_{11}^i = \frac{C_i}{\lambda_-} [\frac{h\nu_E}{3k_BT} - \frac{k_1^i - k_0^i}{9W^i}] \quad , \tag{9a}$$

$$S_{21}^i = \frac{C_i}{\lambda_-} [\frac{h\nu_E}{3k_BT} + \frac{k_1^i - k_0^i}{9W^i}] \quad , \tag{9b}$$

$$S_{12}^i = -S_{22}^i = \frac{C_i}{\lambda_+^i} [\frac{P_1^i - P_0^i}{2P_1 + P_0} + \frac{k_1^i - k_0^i}{9W^i}] \quad , \tag{9c}$$

whereas the decay constants are defined by

$$\lambda_- = K_T, \quad \lambda_+^i = K_T + 3W^i. \tag{10}$$

In eqns. (9a-c) C_i is a constant dependent on the light intensity, the mean ISC rate and the orientation of the molecules w.r.t. $\vec{H}$; ν_E is the rf frequency, h is Planck's constant and k_B is Boltzman's constant; $k_{1,0}^i$, $P_{1,0}^i$ and W^i are the high-field kinetic triplet state parameters for $\vec{H}//i$. Eqns. (9a-c) can be rearranged, yielding

$$k_1^i - k_0^i = \frac{S_{21}^i - S_{11}^i}{S_{11}^i + S_{21}^i} \cdot \frac{h\nu_E}{3k_BT} \cdot 9W^i \quad , \tag{11a}$$

$$\frac{P_1^i - P_0^i}{2P_1 + P_0} = \frac{S_{12}^i}{S_{11}^i + S_{21}^i} \cdot \frac{2h\nu_E}{3k_BT} \cdot \frac{K_T + 3W^i}{K_T} - \frac{S_{21}^i - S_{11}^i}{S_{11}^i + S_{21}^i} \cdot \frac{h\nu_E}{3k_BT} \cdot \tag{11b}$$

In principle the values for W^i and K_T can be derived from the decay constants λ_- and λ_+, so that combination of eqns. (11a, b) for each of the canonical

44

orientations with eqns. (2) and (3), defining the relations between high-field and zero-field kinetic triplet state parameters, yields the zero-field kinetic parameters k_x, k_y and k_z and $P_x(:)$ $P_y(:)$ P_z. In practice, however, the time constant of the ESR spectrometer limits the range of measurable relaxation rates. This can be shown, considering the effect of an RC-filter on ESR transients.

When a time-dependent voltage $S(t)$ is supplied to a RC-filter, the following relation between $S(t)$ and the charge Q on the capacitor (capacitance C) applies:

$$S(t) = R \frac{d\,Q\,(t)}{dt} + \frac{Q\,(t)}{C} ,$$

where R is the resistance. The voltage over the capacitor, given by $S^1(t) = Q(t)/C$, is the measured voltage. When $S(t)$ is given by eqn. (8a) the signal after a RC-filter can be obtained using a Laplace transformation, yielding

$$S^1(t) = \frac{S_{11}}{1 - \lambda_- \cdot \tau} (1 - e^{-\lambda_- \cdot t}) + \frac{S_{12}}{1 - \lambda_+ \cdot \tau} (1 - e^{-\lambda_+ \cdot \tau}) -$$

$$- \{ \frac{S_{11} \cdot \lambda_- \cdot \tau}{1 - \lambda_- \cdot \tau} + \frac{S_{12} \cdot \lambda_+ \cdot \tau}{1 - \lambda_+ \cdot \tau} \} (1 - e^{-t/\tau}) \qquad (12)$$

where τ is the time constant of the RC-filter. For the Varian E-6 ESR spectro-meter used in this study τ has been lowered to a value of 3.10^{-4} sec.. With this time constant and the values for λ_- and λ_+ deduced from analogue simula-tions of the transients of Chl $\underline{a}$ in MTHF, one finds $\lambda_- \cdot \tau \sim 0.2$, $\lambda_+ \cdot \tau \sim 20$ and eqn. (12) can be approximated as

$$S^1(t) = S_{11} (1 - e^{-\lambda_- \cdot t}) + S_{12} (1 - e^{-t/\tau}),$$

so that the second exponential is determined by the instrumental time con-stant and not by λ_+^i. Therefore, relaxation rates cannot be determined. Since the mathematical analysis results in seven relations for the three canonical orientations together, whereas there are eight unknown parameters (K_T, k_x/k_y, k_x/k_z, P_x/P_y, P_x/P_z, W^x, W^y and W^z) it is impossible to obtain the parameters, as long as SLR is taken to be fully anisotropic ($W^x \neq W^y \neq W^z$). As can be seen from eqn. (12), the RC-filter affects not only the decay constants, but also the pre-exponential factors. This will be particularly important when $\lambda_- \cdot \tau \ll 1$ no longer applies.

The most complete mathematical analysis of the triplet ESR transients has been given by Winscom [15]. This author did not use the approximations $W_1 = W_2$, $k_{+1} = k_{-1}$ and $P_{+1} = P_{-1}$. When the approximation $k_{+1} = k_{-1}$ and $P_{+1} = P_{-1}$ are introduced in his results, it follows that W_2 is eliminated from the kinetic equations and the result is the same as that obtained by Levanon [17]. These approximations are permitted as long as the spin functions $|+1\rangle$, $|0\rangle$ and $|-1\rangle$ are the pure high-field functions. When the ZFS parameters D and E are non-zero, the exact relation between high- and zero-field spin functions are, for example for $\vec{H}//x$ [18]

$$|+1\rangle = \frac{1}{\sqrt{2}} \left\{ (1 - \frac{D + E}{2\alpha})^{\frac{1}{2}} |\tau_y\rangle + i(1 + \frac{D + E}{2\alpha})^{\frac{1}{2}} |\tau_z\rangle \right\}$$

$$|-1\rangle = \frac{1}{\sqrt{2}} \left\{ (1 + \frac{D + E}{2\alpha})^{\frac{1}{2}} |\tau_y\rangle - i(1 - \frac{D + E}{2\alpha})^{\frac{1}{2}} |\tau_z\rangle \right\}$$

where $\alpha = [\frac{1}{4}(D + E)^2 + (g\beta H)^2]^{\frac{1}{2}}$. Using these equations one finds the following relations for k_{+1},

$$k_{+1} - k_{-1} = \frac{-(D + E)}{2g\beta H} (k_y - k_z)$$

and a comparable relation for P_{+1}. In this investigation $|D + E| < 0.05$ cm^{-1} so that $(D + E)/2g\beta H < 0.08$; thus, in first order the proposed approximations are allowed.

3.4.3 Analogue electronic simulation

The kinetics of a triplet state, consisting of three spin levels, which are populated by P_i, depopulated by k_i and coupled to each other by W, can be simulated by an electronic network, as given in fig. 4. The three capacitors (C_i) correspond to the three spin states. Each capacitor can be loaded by an independent, adjustable current source (P_i) and decay through an adjustable resistor (k_i) in the form of an RC-circuit. Furthermore, the SLR is simulated by adjustable resistors, connecting the capacitors. The differential equations, describing the time dependence of the charges on the capacitors are identical to eqns. (4a-c) for the kinetics of the triplet state. The charge differences between the capacitors correlates with the time-dependent population differences between the triplet spin states. These differences can be determined by measuring $(V_1 - V_2)$ and $(V_2 - V_3)$, where V_i
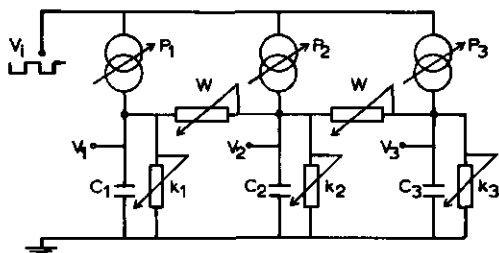
46

is the voltage across the capacitor C_i.

Until now, the capacitance of the capacitors is not considered. When the three spin levels should have equal energy, the capacitors should have to be equal. Because of the small energy separations between the spin levels, the capacitors have to be slightly different to introduce the Boltzman factors. Since we are interested in the charge on the capacitors, measured voltages have to be corrected for the difference in capacitance of the C's. In practice the Boltzman factors are very small (~ 0.005) and it is not feasible to select capacitors within such narrow limits of tolerance that this small difference can be accounted for. The voltage correction, however, can be adjusted so that, under circumstances that an ESR spectrum without spin-polarization will be found ($\delta W \gg K_T$), the voltage difference $V_1 - V_2 = V_2 - V_3$ and equals ~ 0.005 {$1/3(V_1 + V_2 + V_3)$}. Although the full effect of the Boltzman factor on the transient can only be simulated, when sufficiently accurate capacitors are used, the approximation described above has no large effects on the transients, since there is only an appreciable effect of the Boltzman factor when the population differences between the spin levels is in the order of this factor.

To derive the kinetic triplet state parameters from the high-field transients, the transients are simulated by the above described electronic network, the spin level $|+1 \rangle$ corresponding to level (1), $|0 \rangle$ to (2) and $|-1 \rangle$ to (3). Since the experimental transients are measured through a RC-filter, the simulated transients also pass a RC-filter before they are visualized on a scope. Varying P's, k's and W in the electronic network, optimum agreement is sought between experimental and simulated transients. For this purpose, both transients are visualized on the screen of a HP 5480B signal averager.

47

For each of the transients there are many sets of values for k's, P's and W simulating the observed transient. The number of possibilities are restricted, however, by the following conditions:

a) For each of the canonical orientations $k_1(k_{+1}) = k_3(k_{-1})$ and $P_1(P_{+1}) = P_3(P_{-1})$, whereas the transients for the $|+1\rangle \leftrightarrow |0\rangle$ as well as for the $|0\rangle \leftrightarrow |-1\rangle$ transitions have to be simulated with a *single* set of parameters.

b) The populating - and depopulating parameters for the three canonical orientations are related to each other as discussed in section 3.2.3.

When these two conditions are taken into account, for all compounds discussed in this study only a limited range of values for all kinetic parameters is found; in all cases the variation in k's and P's was considerable smaller than for the relaxation rates.

3.5   REFERENCES

1. M.P. Tsvirko, K.N. Solovev, A.T. Gradyushko, S.S. Dvornikov, Opt. Spectrosc., 38, 705 (1975).
2. G.R. Seely, in "The chlorophylls", eds. L.P. Vernon, G.R. Seely, New York, 1966.
3. H. Eyring, J. Walter, G.E. Kimball, Quantum Chemistry, New York, 1944.
4. J.C. Slater, Quantum theory of atomic structure, Vol. II, London, 1960.
5. S.P. McGlynn, T. Azumi, M. Kinoshita, Molecular spectroscopy of the triplet state, Englewoods Cliffs N.J., 1969.
6. D.S. McClure, J.Chem.Phys., 17, 665 (1949).
7. F. Metz, S. Friedrich, G. Hohlneicher, Chem.Phys.Lett., 16, 353 (1972).
8. D.A. Antheunis, J. Schmidt, J.H. van der Waals, Mol.Phys., 27, 1521 (1974); D.A. Antheunis, thesis, University of Leiden, 1974.
9. F. Metz, Chem.Phys.Lett., 22, 186 (1973).
10. J.P. Wolfe, Chem.Phys.Lett., 10, 212 (1971).
11. M. Schwoerer, U. Konzelman, D. Klipper, Chem.Phys.Lett., 13, 272 (1972).
12. D.A. Antheunis, thesis, University of Leiden, 1974.
13. U. Eliav, H. Levanon, Chem.Phys.Lett., 36, 377 (1975).
14. M. Schwoerer, H. Sixl, Z.Naturforsch., 24a, 952 (1969).
15. C.J. Winscom, Z.Naturforsch., 30a, 571 (1975).
16. J. Schmidt, D.A. Antheunis, J.H. van der Waals, Mol.Phys., 22, 1 (1971).
17. H. Levanon, S. Vega, J.Chem.Phys., 61, 2265 (1974).
18. J.H. van der Waals, M.S. de Groot, in "The triplet state", ed. A.B. Zahlan, Cambridge, 1967.

4 The electronic structure of chlorophylls and model systems

4.1 INTRODUCTION

Whereas in Chapters 2 and 3 the methods and techniques, used in this investigation, have been introduced, in this Chapter we will consider the subject of study: the electronic structure of photosynthetic pigments. Recent X-ray studies [1] have produced accurate information about the positions of the nuclei in the pigment. About the electron distribution, however, which is very important for the function of the pigments in photosynthesis, much less is known. The electronic structure of chlorophylls and some model compounds has been studied by spectroscopic methods as well as by quantum chemical calculations. Extensive information about the results of such studies is available in the form of reviews [2]. This Chapter gives only an introduction to the main features of the electronic structure of porphyrin-like compounds, treated in more detail in Chapters 5, 9, and 10.

4.2 SPECTROSCOPIC CHARACTERIZATION

The visible-near U.V. absorption spectrum of a porphyrin-like compound contains two main absorption regions: the Q-bands (500 - 900 nm) and the B- or Soret bands (350 - 450 nm), corresponding to the transitions $S_1 \leftarrow S_0$ and $S_2 \leftarrow S_0$, respectively. In metal porphyrins the excited singlet states S_1 and S_2 are both orbitally degenerate and single Q(0-0)- and B(0-0)-bands occur. For free base porphyrins, as well as for dihydro- and tetrahydro-porphyrins, the degeneracy is lifted and the absorption bands are split. Whereas the splitting between Q_x and Q_y (the two components of the Q-band) is relatively large, a very small or no splitting of the Soret band is found for most systems [3].

For free base- and metallo-porphyrins the extinction coefficient of the Q(0-0) bands is much smaller than for the B(0-0) bands (for Cu-porphin 9.3×10^3 vs 330×10^3 $1.mol^{-1}.cm^{-1}$ [4]); the vibronic components of the Q-bands have the same or larger intensity than Q(0-0). When one or two

pyrrole rings are hydrogenated, the extinction coefficients of the Q(0-0) bands and the Soret band are of the same order of magnitude [3]

A striking feature, found from optical studies is the fact that absorption spectra exhibit only small changes when side groups are introduced on the tetrapyrrole macrocycle. Even hydrogenation of one or two pyrrole rings leaves the spectra basically unchanged [5]. From these observations, it can be concluded that the chromophoric group, which is responsible for the spectroscopic properties of porphyrin-like compounds, is only slightly perturbed by introduction of side groups or reduction of pyrrole rings. Bearing this in mind, we will limit our discussion about the quantum chemical calculations of porphyrin-like systems to an introduction to two simple models.

4.3 THEORETICAL CALCULATIONS

4.3.1 *Free electron model*

Applying the free electron (F.E.) model to the π-electrons of free base porphin, Simpson [6] assumed that 18 electrons move along a ring. From the 26 π-electrons, eight are supposed to be more or less localized: four on N-atoms bearing the free base hydrogens and four forming localized $C_\beta - C_\beta$ double bonds in two opposite pyrrole rings (for basic structure and nomenclature C-atoms, see fig. 1, Chapter 5). For metallo-porphyrins, the 18 electrons are assumed to move along the 16-membered inner ring, whereas the other eight π-electrons form four localized $C_\beta - C_\beta$ bonds [7].

The four lowest excited states in the free electron description are in first order degenerate. These four states can be divided in two sets: S_1 with $L_z = \pm 9$ (L_z is the orbital angular momentum) and S_2 with $L_z = \pm 1$. When electron-electron interactions are taken into account, S_1 will have lower energy than S_2 because of Hund's rule [6]. The optical selection rule $\Delta L_z = \pm 1$ predicts that the transition $S_1 \leftarrow S_0$ is forbidden and $S_2 \leftarrow S_0$ is allowed. Three points should be noted: (i) the F.E. theory qualitatively explains the observed spectra; (ii) the restriction to 18 electrons on the 16 membered ring is in agreement with the observed insensitivity w.r.t. changes in molecular structure at the outer ring; (iii) whereas up to now the value $L_z = 9$ has not been reported for any porphin, relatively high values of L_z are found for S_1: $L_z = 5.0$ for Zn-porphin [8], $L_z = 7.9$ for cytochrome c [9].

4.3.2 The 4-orbital model

A general approach to obtain the electronic wavefunctions for
molecules, is forming molecular orbitals as a linear combination of atomic
orbitals [10]. This approach (LCAO) is used in the simple cyclic
polyene model [11], as well as in Hückel [12] and PPP calculations [13].
As shown by Gouterman [14], the spectroscopic properties and the effect of
side group substitution on these properties, can be treated using the two
highest occupied MO's (HOMO's) and the two lowest unoccupied MO's (LUMO's)
only (in D_{4h} porphin a_{1u}, a_{2u} and e_{gx}, e_{gy}, respectively). In the 4-orbital
model, the excited states S_1 and S_2, calculated using configuration inter-
action (CI), are supposed to consist of the pure excited states, obtained by
one-electron promotions between the two HOMO's and two LUMO's. A further
restriction of CI results from symmetry considerations. Only states with the
same polarization can be mixed: $|a_{1u}\ e_{gy}\rangle_x$ with $|a_{2u}\ e_{gx}\rangle_x$ and $|a_{1u}\ e_{gy}\rangle_y$
with $|a_{2u}\ e_{gx}\rangle_y$ ($|a_{1u}\ e_{gx}\rangle$ denotes the excited state obtained by a one-
electron promotion from a_{1u} to e_{gx}; the subscript indicates the polarization
of the related transition). In Appendix A and Chapters 5, 9 and 10, the
effects of changes in molecular structure on the energy levels of the two
HOMO's and two LUMO's are discussed.

The energies and electron distribution of the four MO's
are deduced from calculations using all $2p_z$ AO's of the C- and N-atoms of the
ring, whereas all 26 π-electrons are taken into account [14]. As will be
discussed in the next section, extensive calculations show that the restriction
to the 4-orbital model is allowed, because of the relative isolation of the
two HOMO's and two LUMO's w.r.t. the other MO's and that the π-electron de-
localization is mainly restricted to the 16-membered ring [15].

4.3.3 More extensive calculations

Many calculations on the electronic structure of porphyrin-
like systems have been reported. Using CI-SCF-PPP methods, Weiss et al. [13]
have calculated the energies, charge distribution and bond orders of a series
of molecules related to porphin. Two features should be noted: (i) Restric-
tion of CI to the 4-orbital pure excited states results in lowest excited
state energies, only slightly different from those obtained with full CI;
(ii) the π-electron bond order of the C_α - C_β bond is relatively small, indi-
cating isolation of the C_β - C_β bond π-electrons w.r.t. the 16 membered inner

ring π-electrons. The CI-SCF-PPP method has also been applied to chlorophyll
[16] . From these calculations it can be concluded that the 4-orbital model
provides a good description for the Q-band in the chlorophylls; for the Soret
band more refined calculations appear to be necessary.

Whereas in the aforementioned PPP calculations only the
π-electrons are considered, in the iterative extended Hückel (IEH) method
[17] , the peel electron theory [18] and the all valence electron CNDO
calculations n, σ and metal-ion electrons are also taken into account.
Whereas the IEH method predicts the presence of a nitrogen lone pair MO be-
tween the π-electron MO's a_{2u} and e_g in free base porphin, the peel electron
theory and CNDO/S calculations result in an ordering of energy levels for the
two HOMO's and two LUMO's comparable to those proposed in the 4-orbital model;
this is true for porphin, as well as for dihydro- and tetrahydroporphin [19] .
These calculations show again that the two HOMO's and two LUMO's are clearly
separated from all other MO's. As shown by Maggioria et al. [19] , especially
the S_1 state can be fairly well described in the 4-orbital model: more than
95 % of this state originates from the 4-orbital pure excited states.

Recent ab-initio calculations [20] also confirm the
assumptions made in the 4-orbital model. We are therefore on safe ground to
use the 4-orbital model as a basis for the interpretation of the results of
this study.

4.4   REFERENCES

1. H.C. Chow, R. Serlin, C.E. Strouse, J.Am.Chem.Soc., 97, 7230 (1975).
2. Bioenergetics of Photosynthesis, ed. Govindjee, New York, 1975.
3. J.E. Falk, Porphyrins and Metalloporphyrins, Amsterdam, 1964.
4. U. Eisner, R.P. Linstead, J.Chem.Soc., 1955, 3749.
5. M. Gouterman, J.Chem.Phys., 30, 1139 (1959).
6. W.T. Simpson, J.Chem.Phys., 17, 1218 (1949).
7. J.R. Platt, in "Radiation Biology", ed. A. Hollaender, New York, 1956.
8. G.W. Canters, G. Jansen, M. Noort, J.H. van der Waals, J.Phys.Chem., 80,
   2253, (1976).
9. J.C. Sutherland, M.P. Klein, J.Chem.Phys., 57, 76 (1972).
10. H. Eyring, J. Walter, G.E. Kimball, Quantum Chemistry, New York, 1944.
11. W. Moffit, J.Chem.Phys., 22, 320 (1954).
12. H.C. Longuet-Higgins, C.W. Rector, J.R. Platt, J.Chem.Phys., 18, 1174
    (1950).

13. C. Weiss, H. Kobayashi, M. Gouterman, J.Mol.Spectrosc., 16, 415 (1965).

14. M. Gouterman, J.Mol.Spectrosc., 6, 138 (1961).

15. K. Tomono, K. Nishimato, Bull.Chem.Soc.Japan, 49, 1179 (1976).

16. C. Weiss, J.Mol.Spectrosc., 44, 37 (1972).

17. M. Gouterman, in "Excited states of matter", ed. C.W. Shoppee, 1973.

18. M. Sundbom, Acta Chem.Scand., 27, 1317 (1968).

19. G.M. Maggioria, L.J. Weimann, Int.J.Quantum Chem., Quantum Biology Symp. 1, 179 (1974).

20. D. Spangler, R. McKinney, R.E. Christoffersen, G.M. Maggioria, L.L. Shipman, Chem.Phys.Lett., 36, 427 (1975).

5 A spectroscopic study of Mg-tetrabenzoporphin
I. Excited singlet state properties

Joop F. Kleibeuker, Tjeerd J. Schaafsma

5.1 INTRODUCTION

The participation of pigments containing the porphin ring system in a number of important biological processes has provoked the study of these compounds for quite some time [1,2]; fig. 1a represents the basic porphin structure. (Throughout this paper "porphin" indicates the porphin macrocycle with a formal charge of -2; if it is not explicitly state otherwise, no interaction of a central metal-ion or two protons with the ring is included). In photosynthetic pigments, such as chlorophyll a and b and bacteriochlorophylls, one and two pyrrole rings are saturated, respectively [1], whereas a Mg-ion is coordinatively bound to the four nitrogen atoms; the chlorin structure given in fig. 1b forms the basis of chlorophyll a and b.

The benzoporphins are non-naturally occurring porphyrins with one or more benzoïd groups condensed with the pyrrole rings as shown for tetrabenzoporphin (TBP) in fig. 1c. We will show that the perturbation of a porphin ring by hydrogenation of one or more pyrrole rings essentially has the same effects as the introduction of benzoïd groups. As Weiss [3] indicated, one may expect the same configuration interaction (CI) pattern for dihydroporphin and TBP. This is one of the reasons why MgTBP, which is a relatively stable compound, can be considered as an attractive model for chlorophyll [4].

The absorption spectra of porphyrins contain two transitions in the visible region: one at $\sim$ 400 nm (Soret or B-band) and one at $\sim$ 600 nm (Q-band) [1]. For TBP and dihydroporphins the intensity ratio $I_{Q(0-0)}/I_{B(0-0)}$ is considerably larger than for porphyrins with unreduced pyrrole rings and without benzoïd groups [1].

As shown by Storm et al.[5], for a series of porphyrins, the position of the Soret band depends on the coordination number of Mg. Evans et al.[6] reported a change of the position of the Q_x band in bacteriochlorophyll and chlorophyll a upon adding pyridine to a toluene solution, which
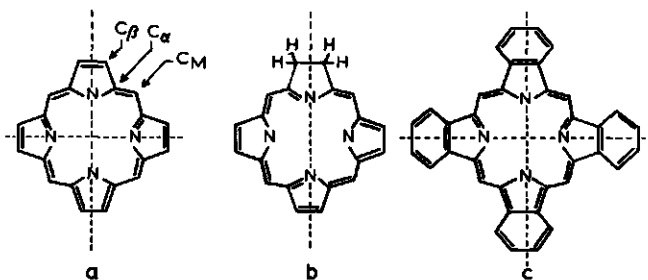
Fig.1 Molecular structures of porphin (a), dihydroporphin (b) and
    tetrabenzoporphin (c).

these authors attributed to the coordination of an extra ligand to the central Mg-ion. The coordination properties of MgTBP are found to be similar to those of chlorophylls rather than to those of other Mg-porphyrins. Qualitative considerations, based on the 4-orbital model of Gouterman [7] can explain the spectroscopic resemblance between hydroporphins and benzoporphins, as well as the difference between Mg-porphyrins and MgTBP with respect to the stability constants of their bi-ligated complexes.

This study is aimed to answer three questions:

1. How good a model compound is MgTBP for chlorphyll?
2. Are splittings, observed in the excited singlet states and the lowest triplet states of metallo-porphyrins in solid solution, caused by the presence of differently coordinated species or by the lifting of the degeneracies of energy levels of one and the same molecule?
3. Is it possible to correlate the excited state molecular structure with the observed, but unusual, S_2 fluorescence and the U.V. absorptions of MgTBP?

The following abbreviations will be used in this paper: (Mg)TBP is (Magnesium)tetrabenzoporphin, MTHF is 2- methyltetrahydrofuran, tol/pyr is a mixture of toluene and pyridine (9:1), Chl a/b is chlorophyll a/b, Bchl is bacteriochlorophyll a.

5.2 EXPERIMENTAL

MgTBP used in this study was a gift from Dr. J. C. Goedheer. A purity-check was made by its absorption spectrum and thin layer chromatography. The compound was found to be sufficiently free from impurities for use without further purification. A small amount of an unknown impurity, also reported by Bayema et al.[8], absorbing at 455 nm and emitting at 650 nm,

55

did not interfere with our measurements. All solvents (ethanol, 2-methyl-
tetrahydrofuran (MTHF), pyridine, toluene and methanol) were of high purity
(pro analysis) grade. As judged from spectroscopic analysis, MgTBP solutions
were stable for many weeks upon storage at $-18^{o}C$; no degradation was found
during measurements.

Absorption spectra were measured using a Cary-14 spectrometer,
whereas a Perkin-Elmer MPF 2a, as well as two home-built fluorimeters were
used for fluorescence measurements; phosphorescence spectra were determined
using home-built instruments.

5.3   LIGATION OF THE MAGNESIUM ION

Empirically, it has been found that the coordination number
of Mg^{2+} in porphin-like complexes is 5 or 6 [5], i.e. at least one extra
ligand is coordinatively bound to the central metal ion, apart from its four
coordination bonds to the porphyrin nitrogens. In a complexing medium like
pyridine, a biligated species, with six-coordinated Mg^{2+} is easily formed.
For a series of porphyrins, with pyridine as ligands, Storm et al.[5] found
the equilibrium constant K to vary between 0.07 and 0.5 $1.mol^{-1}$ for the
equilibrium $PL + L \rightleftarrows PL_2$, where P = magnesium porphyrin, L = ligand. Such
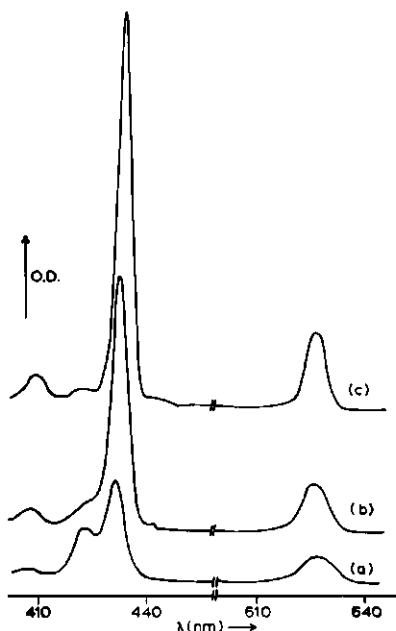

Fig.2 Absorption spectra of MgTBP
in ethanol at 293 K (a), 223 K (b)
and 123 K (c). The spectra are not
corrected for conc. changes due to
changes of specific volume of the
solution with temperature.

data can be obtained because the shape and/or position of the Soret-band depend on the number of ligands and - to a less extent - on the strength of the metal-ligand interaction.

In acetone [4] and ethanol (fig.2a) the Soret-band for MgTBP at 293 K exhibits a splitting into two clearly separated bands, whereas in tol/pyr a single narrow band is observed; in MTHF and in methanol a broadening occurs on the short wavelength side of the main band.

We have carried out titration experiments on the equilibrium

$$MgTBP.Py + Py \rightleftharpoons MgTBP.(Py)_2 \qquad (1)$$

(Py = pyridine) in the following way: a small amount of MgTBP-pyridine complex, obtained by evaporating a solution of MgTBP in tol/pyr, was dissolved in toluene. By this procedure, a minimum ratio [Py]/[MgTBP] in the
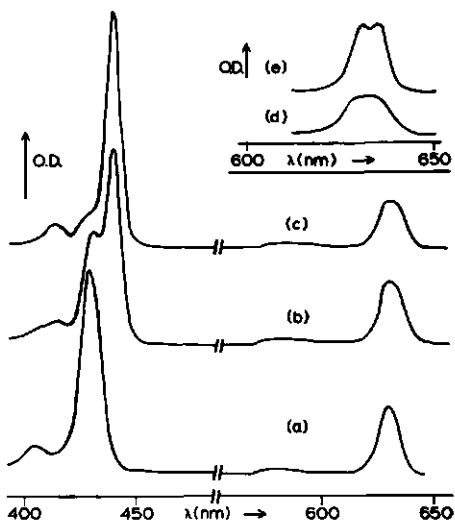
Fig. 3 Absorption spectra of MgTBP ($\sim 2 \times 10^{-5}$M) in toluene pyridine mixtures:
(a) MgTBP-pyridine complex in pure toluene, T = 293 K (see text)
(b) as (a), but with 8×10^{-3}M pyridine;
(c) as (a) but with 0.23 M pyridine; insert:
(d) MgTBP in tol/pyr (9:1) at 293 K
(e) MgTBP in tol/pyr (9:1) at 123 K. Note different wavelength scale of insert.

toluene solution is obtained, before starting the titration experiment. The room temperature absorption spectrum of this solution contains an unsplit Soret band at 429 nm (fig.3a); addition of pyridine causes a second band centered at 440 nm to appear (fig. 3b). Progressive titration of the solution reduced the intensity of the 429 nm band with a simultaneous increase of the intensity of the 440 nm band. Attributing the 429 nm and 440 nm bands to MgTBP.Py and MgTBP.(Py)$_2$, respectively, the titration data can be analyzed in terms of the equilibrium (1), yielding K = 45 $\pm$ 10 l·mol^{-1}. The value of K for MgTBP is much larger than those for other Mg-porphyrins

Table 1. Relation between refractive index n and the position of the Q (0-0)
band (λ_Q) in the absorption spectrum of MgTBP

Solvent	n	λ_Q (nm)
Methanol	1.33	625$\pm$1
Ethanol	1.36	627$\pm$1
MTHF	1.41	627$\pm$1
Toluene	1.50	630$\pm$1
Pyridine	1.51	632$\pm$1

[5], but of the same order as for chlorophylls [6]. Addition of pyridine has
no effect on the position of the Q-band; its shape, however, changes from
roughly Gaussian to flat-topped (fig. 3d).

As is shown in table 2, the Soret band shifts with temperature for
all solvents, which have been studied. The broadening on the short wavelength
side of the Soret band in MTHF solution as well as the 422 nm band observed
at room temperature for the ethanol solution, disappears at lower tempera-
ture (see fig. 2c). The latter effect is a result of the temperature
dependence of the equilibrium between MgTBP.Py and MgTBP.(Py)$_2$. For ethanol
solutions, the 422 nm and 431 nm bands are assigned to mono- and biligated
species, respectively. The temperature dependent shift of the Soret band of
biligated species results from an increase in the metal-ligand interaction
strength (see section 5.5.1). The position of the Q-band is temperature
independent. From the ratio of overlapping absorption bands of mono- and bi-
ligated MgTBP in ethanol the equilibrium constant K is found to be $\sim$ 0.1 l.mol^{-1},
and thus is much smaller than for pyridine ligation. We attribute the
difference between the equilibrium constants for biligation with pyridine
and ethanol to different basicities of N and O containing ligands. Besides,
the inequality of the biligation equilibrium constants for ethanol and
methanol (from the single Soret band in the absorption spectrum of MgTBP in
methanol it can be concluded that MgTBP is mostly biligated in this solvent
at 293 K) can be ascribed to the difference in steric hindrance between both
ligands and the porphyrin molecule [9, 10]: methanol has better acces to the
Mg^{2+}-ion than the bulkier ethanol.

As Evans et al. [6] have shown, the position of the Q-band of Bchl
is strongly dependent on the coordination number of the Mg-ion. Furthermore,
an increasing ratio between bi- and monoligated species can be predicted to

result in an effective red shift of the intensity maximum of this composite absorption Q_x band. From Bchl spectra (see Weiss [3]) in different solvents it can be concluded that λ_Q increases for the series diethylether-acetone--ethanol-pyridine, implying a corresponding increase in ligand-binding strength. Employing the intensity ratio of the two Soret bands of MgTBP in these solvents [4] we derived the order diethylether < acetone ∿ ethanol < pyridine for their ligand binding strength, in good agreement with the results obtained for Bchl.

5.4 EXCITED STATE PROPERTIES OF MgTBP

The position of the Q-band in the absorption spectra of MgTBP in a series of solvents can be related to the refractive index of the solvents [11] (Table 1). The absence of any shift in the $S_1 \leftarrow S_0$ transition when the monoligated MgTBP complex is converted into the biligated species as found in titration experiments with pyridine (fig. 3), indicates that the Q-band for both species coincides.This is confirmed by the absence of any temperature dependence of the position of these bands (fig. 2, Table 2).

As is shown in fig. 3d, the Q-band of MgTBP in tol/pyr has a flat-topped absorption profile, which indicates the presence of an unresolved splitting, which is indeed partially resolved at 123 K. In the temperature range studied (293 K - 123 K) the splitting, $\Delta = 120\pm20$ cm^{-1}, and intensity ratio R of both components are constant (fig. 3e); a small vibronic band at 610 nm has the same splitting. For solutions in ethanol and MTHF, only at lower temperatures there is an indication of a splitting. For these solvents, the splitting is smaller and is not detectable at 293 K, because of severe line broadening. From spectra taken at lowest temperatures (123 K for ethanol and 93 K for MTHF) we estimated the splitting $\Delta = 60\pm20$ cm^{-1}, whereas the intensity ratio R ∿ 1.

At 4.2 K the fluorescence spectra are characterized by sharp single 0-0 bands. For MgTBP in tol/pyr at 293 K we observed a weak shoulder separated from the main Q transition by ∿ 130 cm^{-1}, on the short wavelength side of the 0-0 band. The fluorescence excitation spectrum of MgTBP in tol/ pyr at 77 K shows a comparable splitting ($\Delta = 110\pm20$ cm^{-1}) for the different components of the Q-band, in agreement with the splitting previously found in the absorption spectra.

Whereas no resolved splitting is observed in the Soret band of any of the solutions, which we studied, the Soret bandwidth is larger for the

Table 2. Temperature dependence of the position of Q-bands and B-bands in absorption spectra of MgTBP in various solvents.

solvent	band[b]	wavelength (nm) at T(K):				Shift[a]
		293	223	173	123	
ethanol	BI	422				
	BII	431	432	433	434	+
	Q	627	626	626	626	0
tol/pyr	BII	441	442	443	445	+
	QI	633	630	630	631	0
	QII		636	636	636	0
MTHF	BII	431	433	435	437	+
	Q	627	627	627	627	0

[a]Shift denotes the sign of shift for decreasing temperature

[b]For designations B_I, B_{II}, Q_I, and Q_{II}, see text.

tol/pyr solutions than for the MTHF and ethanol solutions at 123 K, 290 ± 20 cm^{-1} and 230 ± 20 cm^{-1}, respectively. At 293 K the bandwidth is the same for all solutions, 370 ± 30 cm^{-1}. We explain these results by an unresolved splitting of the Soret band, that is larger for the tol/pyr than for the MTHF and ethanol solutions, in agreement with the result for the Q-band.

In fig. 4 we present the S_2-fluorescence of a 10^{-6} M solution of MgTBP in tol/pyr at 293 K. This fluorescence spectrum shows the same vibrational progression as found for the Soret and Q-bands in absorption. The excitation spectrum of this fluorescence fully agrees with the Soret region of the absorption spectrum and the S_1-fluorescence excitation spectrum.

Fig. 4 $S_2 \leftarrow S_0$ absorption spectrum (——) and $S_2 \rightarrow S_0$ emission spectrum (---) of a 2×10^{-6} M solution of MgTBP in tol/pyr at 293 K.
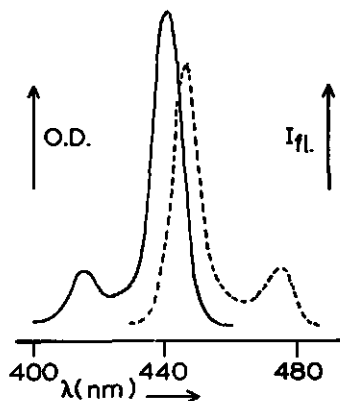
The relative quantum efficiency of the S_2-fluorescence with respect to the S_1-fluorescence, measured with excitation in the B(0-1) band is ~ 0.01. Whereas the Q-band has only a small Stokes-shift of $\lesssim 50$ cm^{-1}, the S_2-fluorescence is red-shifted by ~ 200 cm^{-1} with respect to the absorption maximum. S_2-fluorescence has been reported for ZnTBP in n-octane at 293 K by Bayema et al. [8] and for ZnTBP and CdTBP in various solvents by Zalesskii [12], whereas the recent results of Fielding [13] do not confirm this conclusion.

5.5 DISCUSSION

5.5.1 *Effects of ligation on electronic distribution*

During the last two decades many theoretical studies about the electronic structure of porphyrins have been published [1, 7, 14-17]. In the following discussion we will interpret our results using a simple qualitative model and compare these results with published SCF-MO calculations.

As found by Kobayashi [18], the inner 16-membered ring of metallo-porphyrins can be supposed to form the main π-electron conjugation path; Kuhn [19] argued that this is especially true for metallo-TBP's, because of the presence of the benzoîdgroups. This viewpoint has been confirmed by recent calculations carried out by Tomono et al. [20].

For the study of the two lowest excited states the four orbital model, as proposed by Gouterman [7], is a good approximation. Only the two
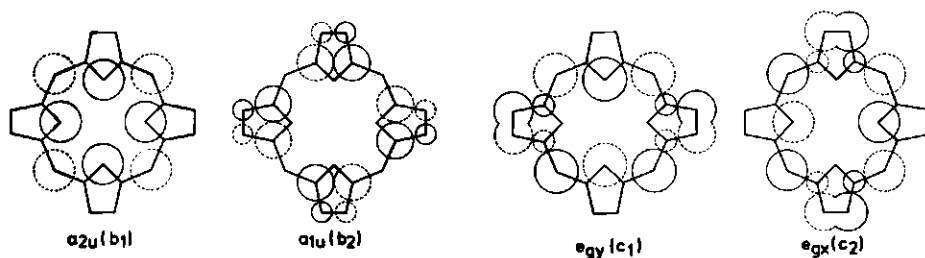

Fig. 5 Electron distribution of the two HOMO's (a_{2u} and a_{1u}) and two LUMO's (e_{gy} and e_{gx}) of D_{4h} porphin following Goutermans 4-orbital model. The size of the circles is proportional to the atomic orbital coefficients; dotted or closed circles indicate their sign.
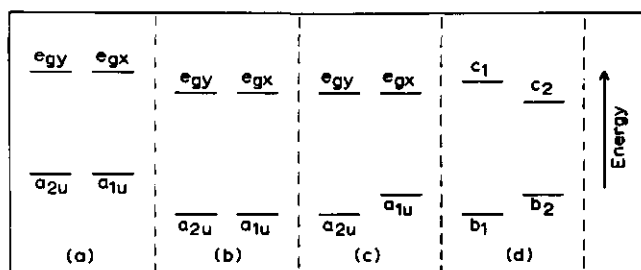
Fig. 6 Energy diagram of the two HOMO's (a_{2u} and a_{1u}) and the LUMO's (e_{gx} and e_{gy}) in a 16-membered polyene ring (a), porphin (b), TBP (c), and di-hydroporphin (d) (b_1 and b_2 resp. c_1 and c_2) [1, 7]. The diagrams only indicate relevant energy differences and shifts and do not represent absolute energies.

highest occupied and the two lowest unoccupied molecular orbitals (in the following abbreviated as HOMO and LUMO), a_{1u}, a_{2u} and e_{gx}, e_{gy} in a system with D_{4h} symmetry, are considered in this model. Following Gouterman [7], orbital designations for D_{4h} and lower symmetry are correlated by $a_{2u} \leftrightarrow b_1$, $a_{1u} \leftrightarrow b_2$, $e_{gy} \leftrightarrow c_1$, $e_{gx} \leftrightarrow c_2$. The a_{1u} orbital has highest electron-density on C_α atoms (fig. 5), whereas the a_{2u} orbital has the highest density on N-atoms and methine carbons (C_M).

For a 16-membered polyene macrocycle with D_{4h} symmetry, consisting of 16 C—H fragments, the orbitals a_{1u} and a_{2u} as well as e_{gx} and e_{gy} are pairwise degenerate (fig. 6a) [1]. The introduction of four N-atoms in por-phin will stabilize the a_{2u} orbital, because of the high electron-density of this molecular orbital at the N-positions. The branching at the C_α-positions, present in porphin, however, stabilizes the a_{1u} orbital, which has highest electron-density on C_α. Neither substitution of N-atoms, nor C_α-branching will remove the degeneracy of the e_{gx} and e_{gy} orbitals in the porphin skeleton with D_{4h} symmetry. In D_{4h} porphin the two orbitals a_{1u} and a_{2u} are found to be almost degenerate (fig. 6b) [7], thus the zero order excited states $e_g \leftarrow a_{1u}$ ($|e_g\, a_{1u}\rangle$) and $e_g \leftarrow a_{2u}$ ($|e_g\, a_{2u}\rangle$) are degenerate resulting in con-figuration interaction (CI), which mixes states with the same polarization in equal amounts. It should be noted that the optical transitions $e_{gy} \leftarrow a_{2u}$ and $e_{gx} \leftarrow a_{1u}$ are both y-polarized, whereas the transitions $e_{gy} \leftarrow a_{1u}$ and $e_{gx} \leftarrow a_{2u}$ are x-polarized. CI causes the degeneracy of the excited states S_1 and S_2 to be removed and results in a low $S_1 \leftarrow S_0$ radiative transition proba-bility, because of cancelling of transition moments; for $S_2 \leftarrow S_0$ the transition probability is enhanced due to addition of moments [7]. This agrees with the

experimental spectra for e.g. Mg-porphin [21] with a very weak Q(0-0) and a strong B(0-0) transition.

Reduction of branching of the π-electron system at C_α will destabilize the a_{1u} orbital (fig. 6c) with respect to porphin. Then, equally polarized transitions for $e_g \leftarrow a_{1u}$ and $e_g \leftarrow a_{2u}$ are non-degenerate, such that the amount of CI is decreased, resulting in non-zero $S_1 \leftarrow S_0$ transition probability. A C_α-branching reduction can be realized in two ways:

a) reduction of the pyrrole rings by hydrogenation of the C_β - C_β bonds;

b) participation of the C_β - C_β bonds in conjugation paths other than the 16-membered porphin inner ring.

The dihydroporphin ring system and the opposite-tetrahydroporphin system, obtained after hydrogenation of one or two pyrrole rings, are the basic structures for Chl $\underline{a}$, $\underline{b}$ and Bchl, respectively. The reduction of 1-3 pyrrole rings result in a loss of D_{4h} symmetry and a lifting of the e_{gx} - e_{gy} degeneracy (fig. 6d). This, in turn, leads to a different amount of CI for the y-polarized states ($c_1 \leftarrow b_1$, $c_2 \leftarrow b_2$) and the x-polarized states ($c_2 \leftarrow b_1$, $c_1 \leftarrow b_2$) [7].

In the benzoporphins one or more C_β - C_β bonds participate in the π-electron conjugation paths of a benzoïdgroup. Introduction of less than four benzoïdgroups lifts the degeneracy of the orbitals e_{gx} and e_{gy}, similar to the situation in hydroporphins. Comparing the pure excited states of the benzoporphins, as calculated by McHugh [16] , with those of the hydroporphins, which we deduced from the orbital energies found by Gouterman [22] , it is clear that the perturbations in the two series are of the same nature (fig. 7);
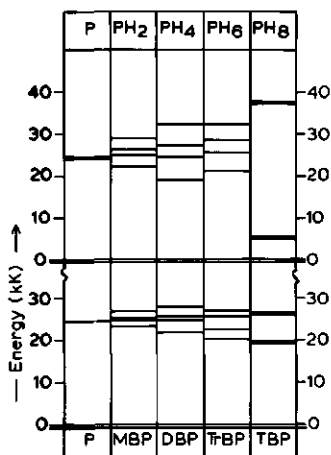
Fig. 7 Energies of the pure excited states $|a_{1,2u} \, e_{gx,y})$ of porphin (P), dihydroporphin (PH$_2$), opposite-tetrahydroporphin (PH$_4$) hexahydroporphin (PH$_6$) and octahydroporphin (PH$_8$) as calculated by Gouterman [22] and the energies of these states for porphin, monobenzoporphin (MBP), opposite-dibenzoporphin (DBP), tribenzoporphin (TrBP) and tetrabenzoporphin (TBP) as calculated by McHugh [16]. For porphin four energy levels coincide, for PH$_8$ and TBP the energy levels coincide pairwise.

63

for the hydroporphins the effects are larger than for the benzoporphins.

Study of the electronic structure of porphins, dihydroporphins and benzoporphins is necessary to decide whether MgTBP is a suitable model compound for protochlorophyll, as proposed by Goedheer [4], or for chlorophyll. (Protochlorophyll is identical to the corresponding chlorophyll except for the lacking of a hydrogenated pyrrole ring.). As we just have shown, the introduction of benzoïdgroups has a very similar effect on the electronic structure as hydrogenation of C_β - C_β bonds. Although dihydroporphin has no 4-fold symmetry as TBP has, fig. 7 demonstrates that the distance between the y-polarized pure states $|c_1b_1\rangle$ and $|c_2b_2\rangle$ is roughly the same for these two compounds, which results in a comparable amount of CI, as noticed already by Weiss [3]. As a result, the intensity ratio I [$Q_y(0,0)$]/I[$B_y(0,0)$] is expected to be roughly the same for dihydro- and tetrabenzoporphins, which is found for e.g. Zn-dihydroporphin and ZnTBP [22]. For the x-polarized transitions of dihydroporphin, however, the pure states $|c_2b_1\rangle$ and $|c_1b_2\rangle$ are nearly degenerate as in porphin, resulting in a strong B_x and a very weak Q_x transition, due to 50/50 CI. For symmetry reasons TBP hàs equivalent x- and y-polarized excited states. The small splitting of the Q-band in bi-ligated MgTBP results from a splitting between the e_{gx} and e_{gy} orbitals. This splitting, however, is so small that we may safely assume that x and y transitions still have the same amount of CI, resulting in the same intensity for Q_x and Q_y bands.

A change in the energy levels of one of the two HOMO's in dihydroporphin has different effects on Q_x and Q_y band positions and intensities, since CI has different magnitude for both transitions; for TBP, the situation is essentially different: here, Q_x and Q_y behave identically. The effect of ligation of the central metal ion on spectral changes for chlorophyll and MgTBP provides a demonstration of the previous statement. Coordinative binding of a ligand with Mg^{2+} in these compounds reduces the electron transfer from the ring N-atoms to Mg^{2+}, causing the N-atoms to be less electro-negative. Thus the energy of the a_{2u} orbital — and to an appreciably less extent the energy of the e_g orbitals — is increased. For MgTBP, the ratio b/a in the wavefunctions

$$|B_{x,y}\rangle = a|a_{2u}\, e_g\rangle \mp b|a_{1u}\, e_g\rangle$$

$$|Q_{x,y}\rangle = a|a_{1u}\, e_g\rangle \pm b|a_{2u}\, e_g\rangle$$

is relatively small, as compared with porphin, because of restricted CI.

Therefore, increasing the energy of the a_{2u} orbital will mainly affect the Soret band and to a less extent the Q-band, in agreement with our experimental results. Since porphyrins without benzoïdgroups or saturated pyrrole rings have nearly 50/50 mixing of the pure states $|a_{2u} \, e_g \rangle$ and $|a_{1u} \, e_g \rangle$, resulting in a ratio b/a $\sim$ 1, one expects small changes of the a_{2u} orbital energy to have large effects on the position and intensity of the Q-band due to a change in CI. In agreement with this prediction, Storm et al. [5] have reported not only a red shift of the Soret band, but also appreciable intensity changes of the Q(0-0) band for several Mg-porphyrins.[*]

Illustrating the concept developed before, y-transitions for chlorophylls (having relative weak CI) are found to behave like MgTBP, whereas changes in their x-polarized transitions follow those for porphin: when Chl $\underline{a}$ and Bchl are titrated with pyridine using toluene as a solvent [6], only minor effects on the strong Q_y band were found, whereas appreciable effects on the Q_x transitions are observed, in agreement with our model.

5.5.2 *Effects of molecular structure on the equilibrium constant for biligation*

The value of the equilibrium constant for equilibrium between mono- and biligated MgTBP species is expected to depend on electronic as well as steric properties of the porphyrin ring and the ligand. As a reduction of C_α-branching will have only minor influences on the *total* π-electron-density on the N-atoms, it is not likely that the large differences between the equilibrium constants of MgTBP and chlorophyll (10-45 1/mol) vs. those of unperturbed Mg-porphyrins (0,07-0,5 1/mol) results from a difference in the effective charge on Mg^{2+}. With respect to the steric hindrance between the porphyrin ring and a ligand, MgTBP and chlorophyll appear to be more favourable for biligation on Mg^{2+} than unperturbed Mg-porphyrins.

[*]As an example of the influence of ligation on spectral characteristics, due to changes in CI we refer to a recent report by Kielman et al. [23] on temperature dependent MCD. In the light of our discussion the results reported by these author become clear: whereas the equilibrium constants for the formation of biligated Mg-porphyrin complexes is much smaller than for MgTBP [5], lowering the temperature for Mg-porphin in EPA causes a shift of the equilibrium between mono- and biligated complexes. Since Mg-porphin is in the limit of strong CI, this shift will induce a considerable change in the Q-band absorption and MCD spectra.
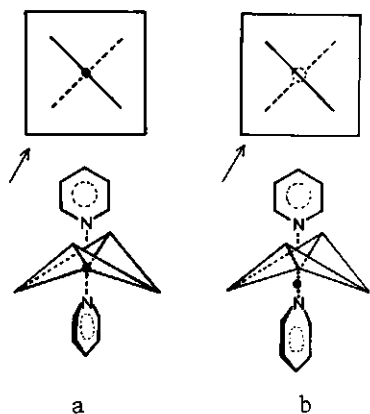
Fig. 8 Diagrams of two conformations of the MgTBP.$(Py)_2$ complex. The upper part represents the top view, the lower part a side view looking along the arrow shown below the top-view diagram. The corners of the square, representing the porphin skeleton, correspond to the position of the methine carbons; the N-atoms are positioned half-way the sides of the square.
a) Both pyridine ligands perpendicular to the porphin plane, with their planes parallel to the two perpendicular "valleys" of the ruffled porphyrin molecule. Mg^{2+} lies in the plane containing the four N-atoms.
b) As (a) but with Mg^{2+} below the plane containing the four N-atoms.

When considering the effects of steric hindrance between the por-
phin core and two axial ligands, Hoard [24] demonstrated that the ruffled
conformation, with D_{2d} symmetry, of the porphin core provides a sterical
configuration favouring biligation. In the ruffled bi-pyridine complex, both
ligands are likely to have their longest N—C axis perpendicular to the
porphin plane, whereas the normals to the pyridine planes are expected to be
approximately parallel to the diagonals connecting opposite methine carbons
in the porphin plane (see fig. 8a). Reduction of the π-electron density on
the C_α - C_β bonds as a result of the introduction of benzoïdgroups lowers
the energy barrier for deformation of the individual pyrrole rings, resulting
in a more flexible structure, than in porphyrins with normal bond-order for
the pyrrole C_α - C_β bonds. (For TBP Weiss [15] has calculated a C_α - C_β
bond order of 0.386 as compared to 0.468 for porphin). The C—C bond in
benzene (1,39 A) is somewhat larger than that of the C_β - C_β bond in unper-
turbed porphin (1,35 A). Therefore, introduction of a benzoïdgroup will
lengthen the C_β - C_β bond which easily results in a D_{2d} ruffling of the por-
phyrin skeleton by rotating the benzoïdgroups out of the molecular plane.
These predictions are confirmed by molecular models of the complex. By con-
structing such models for chlorophyll, one also learns that introduction of
a pentanon ring and hydrogenation of one or two pyrrole rings induces a de-
formation of the planar porphin ring structure, similar to the D_{2d} deformation
proposed for MgTBP. This observation is in agreement with results from X-ray
studies [25].
These findings all point into the same direction: the relative

66

large equilibrium constant for ligation of MgTBP can be explained by invoking a lowering of the resistance against deformations, necessary to give steric accessability of the central metal for a second ligand. This model can also be applied to spectral properties of the complex: as a consequence of the ruffled structure, the benzoïdgroups are rotated out of the molecular plane, thereby increasing the isolation of these groups from the porphin π-electron path. This is in agreement with the observation of benzoïd absorptions in the 48.000 - 54.000 cm^{-1} region. Also, the isolation of the porphin π-electron system w.r.t. the benzoïdgroups may offer an explanation for the relatively long triplet lifetime (τ = 230$\pm$20 msec) — as compared to $\tau \sim$ 70 msec for Mg-porphin [26] — : introduction of isolated benzoïdgroups reduces the number of C—H bonds effective in the radiationless transition $T_1 \rightarrow S_0$ [27]. In the following paper (II) we will discuss in more detail the properties of the lowest excited triplet state [28].

5.5.3 Jahn-Teller effects

The temperature independence of the intensity-ratio of the two components of the Q-band in the absorption spectrum of MgTBP in tol/pyr, as well as the absence of any splitting in low temperature fluorescence and phosphorescence are evidence of a splitting of the first excited singlet state, the ground state being unaffected. The two Q-band components cannot be accounted for by the mono- and biligated species in thermodynamic equilibrium, since a change of temperature would affect the relative intensity of both components of the Q-band, contrary to our results.

Anticipating the discussion in section 5.5.1, we note that the first and second excited states S_1 and S_2 are both orbitally degenerate. A Jahn-Teller coupling will separate the potential wells of the two components of both states along the normal coordinate Q of the Jahn-Teller active vibration, but does not remove the degeneracy as shown in fig. 9 [29]. In this diagram, the potential wells of the two degenerate excited states ψ_η and ψ_ξ have their minima at the nuclear conformations $Q = Q_0$ and $Q = -Q_0$, respectively.

In the D_{4h} porphin skeleton there are two Jahn-Teller active vibrations with b_{1g} and b_{2g} symmetry, respectively, inducing in-plane deformations. An external field, e.g. a crystal-field, with non-equal components along the two principal, mutually perpendicular axes in the molecular plane can remove the degeneracy between the two distorted conformations. For a b_{1g}
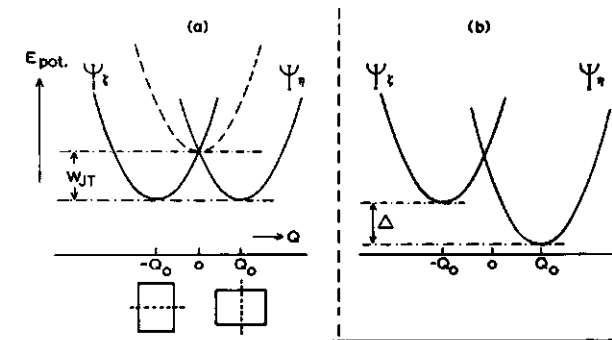
Fig. 9 Effect of Jahn-Teller instability and an anisotropic field on the potential $E_{pot}(Q)$; Q is the Jahn-Teller active normal coordinate. In (a) (------) represents $E_{pot}(Q)$ in the absence of vibronic coupling, (———) is $E_{pot}(Q)$ in the presence of vibronic coupling; at Q_0 and $-Q_0$ $E_{pot}(Q)$ has minima corresponding to distorted conformations with electronic wavefunctions ψ_η and ψ_ξ; W_{JT} is the stabilization energy of the distorted conformations w.r.t. a square shaped molecule [29]. The distorted conformations for a b_{1g} Jahn-Teller active vibration are shown. Dashed lines through the rectangle-shaped molecular conformations represent the locus of modes for ψ_η and ψ_ξ.
b) The effect of an anisotropic field on the energies of the distorted conformations; Δ represents the energy difference between the two distorted conformations [21].

distorted conformation the principal axes pass through the N-atoms, whereas for a b_{2g} distorted conformation the methine C-atoms are on the principal axes. Canters et al. [21] found the Q-band of Zn-porphin in a n-octane single crystal to be split by 109 cm^{-1}, which these authors ascribe to a Jahn-Teller instability in the presence of a crystal-field; from MCD measurements on Zn-porphin in EPA Kielman et al. [23] obtained a zero-field splitting of the lowest excited state $\Delta = 58\pm10$ cm^{-1}.

The observed splitting Δ of the visible absorption band of MgTBP in tol/pyr is remarkable in several respects. Rapidly fluctuating molecular fields in a liquid solution cannot cause such a splitting nor can a Jahn-Teller distortion involving non-degenerate vibrations [21, 30]. Even in the presence of degenerate vibrations, the vibrationless lowest excited singlet level (E_u) cannot be split [30] (higher vibrational levels do split, however, when degenerate vibrations interact with E_u electronic states).Thus, a resolved splitting, such as observed in the presence of ligands, requires a well-defined crystal-field, arising from a fixed molecular environment during a time τ, such that $\tau \gg \frac{h}{\Delta}$, where Δ is the observed splitting; from

the observed value of Δ it can be inferred that $\tau \gg 10^{-12}$ sec.

The temperature independence of the splitting of the Q-band of MgTBP in tol/pyr in a temperature range covering both the liquid and the glassy state (transition temperature $\sim$ 150 K) indicates that this splitting is caused by an anisotropic field arising from a well-defined molecular environment. The short range surroundings of the 16-membered ring, which is the chromophoric group in MgTBP (see section 5.5.1), is made up of four benzoïdrings and two axial ligands. Whereas the benzoïdrings are fixed, bound and unbound ligands can exchange in solution. In the biligated complex, the chromophoric group is well shielded from medium and long range interactions with solvent molecules. Ascribing the splitting to a porphin-ligand inter-action in the presence of a Jahn-Teller distortion, leaves us with the question: how can such interactions be different for the excited states ψ_η and ψ_ξ? Any physical model explaining our results should contain an inequivalency for the ligand-porphin interaction for the in-plane principal axes of the MgTBP molecule in order to get a site symmetry excluding degenerate states.

The complex consisting of a ruffled porphin core and two pyridine ligands, with their longest C—N axis parallel to the normal to the porphin plane and the planes of the pyridine molecules along the two perpendicular 'valleys' in the ruffled porphin core (fig. 8a), has D_{2d} symmetry so that the degeneracy between the states ψ_η and ψ_ξ is retained. Small ligand re-orientations can remove the degeneracy. However, when no well-defined external distorting forces are present, there is no reason why a single distorted conformation, necessary to obtain a single valued splitting Δ, is more stable
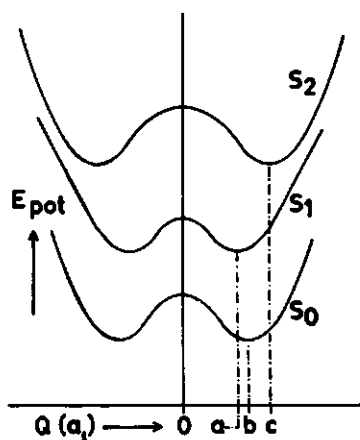
Fig. 10 Proposed cross section of the potential energy surfaces along the normal coordinate $Q(a_1)$ containing the displacement of Mg^{2+} out of the porphin plane (along the normal to the plane) for ground state S_0 and excited states S_1 and S_2 of a biligated MgTBP complex (see text); $Q = 0$ if Mg^{2+} is in the molecular plane. The minima of potential energy occur for $Q = \pm a$, $\pm b$, $\pm c$ for the states S_1, S_0, and S_2, respectively.

than all other conformations. This makes it unlikely that the splitting in solution results from such reorientations of the pyridine molecules. In addition , the comparable splitting, found for ligation with pyridine and ethanol, indicates that it is not the interaction between the ligands and the porphin core, which is responsible for the observed splitting, since for ethanol the most favourable conformation of the biligated complex has already a symmetry in which the degeneracy is removed.

An alternative distortion is the displacement of the Mg-ion out of the plane containing the four N-atoms of the ruffled porphin core. Even without axial ligands, this distortion results in a symmetry of the complex in which the degeneracy can be removed. The absence of d-orbitals and the ionic radius of Mg^{2+} support the idea that the in-plane position of the Mg-ion is not the most favourable one [24]. In the non-ligated and the biligated complex, such a displacement of Mg^{2+} will result in a double well potential (fig. 10), where the position of the minima, related to the equilibrium positions of the Mg-ion, depends on the presence of and the strength of interaction of Mg^{2+} with axial ligands. For the mono-ligated complex, the two minima will be inequivalent.

The stronger basicity of pyridine w.r.t. MTHF and ethanol will result in a larger out-of-plane displacement of Mg^{2+} in $MgTBP.(Py)_2$ than in $MgTBP.(MTHF)_2$ or $MgTBP.(ethanol)_2$. This larger displacement for $MgTBP.(Py)_2$, being related to a larger distortion of D_{2d} symmetry, correlates with a larger Q-band splitting for $MgTBP.(Py)_2$ than for $MgTBP.(MTHF)_2$ or $MgTBP.$ $(ethanol)_2$ as is experimentally observed. ($MgTBP.(Py)_2$: $\Delta = 120 \pm 10$ cm^{-1}; $MgTBP.(MTHF)_2$ and $MgTBP.(ethanol)_2$: $\Delta = 60 \pm 20$ cm^{-1}). Concluding, a displacement of Mg^{2+} out of the molecular plane can explain the splitting of the originally degenerate excited state, as well as the amount of the splitting.

We note that apart from the ruffled conformation, shown in fig. 8a, there may be other out-of-plane distorted conformations, which do not lift the degeneracy between ψ_ξ and ψ_η states, as long as Mg^{2+} is in the porphin plane. The relatively broad absorption bands, exhibiting the splitting, discussed before, do not allow a distinction between different out-of-plane conformations. In this paper, we have limited our discussion to the sterically most favourable one.

For the Soret band, corresponding to the $S_2 \leftarrow S_0$ transition, one does not necessarily expect the same splittings as for the Q-band because of the different electronic distribution in the two excited states. In H_2TBP, in which the replacement of Mg^{2+} by two protons can be considered as a strong

in-plane anisotropic field, the splitting of the Q-band is larger than that of the Soret-band: $\Delta_Q = 1350$ cm^{-1} and $\Delta_B = 800$ cm^{-1} [7]. In agreement with these free-base results, the relatively broad Soret-band of MgTBP seems to consist of two unresolved components with a splitting, which is smaller than that of the Q-band.

5.5.4 S_2-fluorescence of MgTBP

The Stokes shift can be related to the difference in geometry of the excited and ground state. As discussed previously, the chromophoric group within the complex is well shielded from solvent interactions other than ligation, implying that the dominant mechanism resulting in an observable Stokes shift should involve geometrical changes within the complex upon excitation $S_1 \leftarrow S_0$ or $S_2 \leftarrow S_0$.

Turning now to our results, we observe that S_2 exhibits a larger Stokes shift than S_1. $S_1 \leftarrow S_0$ and $S_2 \leftarrow S_0$ excitations correspond to electron promotions $e_g \leftarrow a_{1u}$ and $e_g \leftarrow a_{2u}$, respectively. Referring to fig. 5, we note that the first electron promotion results in an *increase* of π-electron-density on the porphin-nitrogens, whereas the second involves a decrease. This predicts that the magnitude of interaction between Mg^{2+} and the porphin nitrogens decreases in the order $S_1 > S_0 > S_2$. It should be stressed that this ordering pertains to the interaction between Mg^{2+} and the porphin-nitrogens, which does not necessarily imply the same relative ordering of interactions between the ligand and the porphin π-electron system. This results in different displacement of Mg^{2+} out of the porphin plane, such that its distance from that plane decreases for the series S_2, S_0 and S_1. Since the change in electronic distribution on the N-atoms is larger for $e_g \leftarrow a_{2u}$ than for $e_g \leftarrow a_{1u}$ one expects also that the geometry of the complex in the S_0 state resembles more closely that of S_1 than that of S_2. Our observations agree with these predictions, if we relate the observed Stokes shift for $S_1 \leftarrow S_0$ and $S_2 \leftarrow S_0$ transitions to a Mg-displacement. Such a situation is depicted in fig. 10 representing a vibrational cross-section of the potential energy profile of the C_{2v} complex along an a_1 normal coordinate, which involves Mg displacement perpendicular to the porphin plane. The separation of potential minima for S_0, S_1 and S_2 states reflects the qualitative conclusions which we reached before. This now could explain the unusual $S_2 \to S_0$ fluorescence: the radiative $S_2 \to S_0$ process can compete with the radiationless transition $S_2 \rightsquigarrow S_1$ because of the small Franck-Condon factor of the latter.

A similar situation may apply to the triplet manifold.

The solvent dependence of the ratio between the S_2-fluorescence and the S_1-fluorescence, reported by Zalesskii et al. [12], can be easily understood in this model. The difference in basicity of the various ligands, bound to the central metal-ion generally will affect the equilibrium displacement of the central metal-ion w.r.t. the porphin plane for the three excited states to a different degree, resulting in unequal Franck-Condon factors for the $S_2 \rightarrow S_0$ and $S_2 \rightarrow S_1$ transitions for the various ligated species.

5.6   CONCLUSIONS

1. Gouterman's four orbital model satisfactorily explains the changes in π-electron structure of porphins upon condensation with benzoïdgroups. A comparison with hydroporphins can be made in the same framework.
2. MgTBP is a good model compound for chlorophyll w.r.t. ligation and some of its spectral effects: optical transitions polarized along one of the in-plane axis of chlorophyll behave as in MgTBP, the other in-plane polarized transitions follow a porphin pattern.
3. The electronic structure of MgTBP allows a molecular conformation favouring biligation of Mg^{2+} and isolation between the π-electron systems of benzoïdgroups and the inner 16-membered porphin ring, resulting in bezoïd absorption bands.
4. The proposed structural model for MgTBP with out-of-plane displaced Mg^{2+} explains the occurrence of S_2 fluorescence and the observation of Jahn-Teller distorted S_1 and S_2 states, split by an anisotropic 'internal' field.

5.7   ACKNOWLEDGEMENT

5.8 REFERENCES

1. G.P. Gurinovich, A.N. Sevchenko, K.N. Solov'ev, Spectroscopy of chlorophyll and related compounds, NTIS, Springfield, U.S.A., 1968.
2. K.M. Smith, Porphyrins and Metalloporphyrins, Elsevier, Amsterdam, 1975.
3. C. Weiss, J.Mol.Spectros., 44, 37 (1972).
4. J.C. Goedheer, J.P.J. Siero, Photochem.Photobiol., 6, 509 (1967).
5. C.B. Storm, A.H. Corwin, R.R. Azellano, M. Martz, R. Weintraub, J.Am. Chem.Soc., 88, 2525 (1966).
6. T.A. Evans, J.J. Katz, Biochem.Biophys.Acta, 396, 414 (1975).
7. M. Gouterman, J.Mol.Spectros., 6, 138 (1961).
8. L. Bayema, M. Gouterman, C.B. Rose, J.Mol.Spectros., 39, 421 (1971).
9. B.C. McLees, W.S. Caughey, Biochemistry, 7, 643 (1968).
10. S.S. Eaton, G.R. Eaton, R.H. Holm, J.Organometal.Chem., 39, 179 (1972).
11. G.R. Seely, R.G. Jensen, Spectrochim.Acta, 21, 1835 (1965).
12. J.E. Zalesskii, V.N. Kotlo, A.N. Sevchenko, K.N. Solov'ev, S.F. Shkirman, Dokl.Akad.Nauk SSSR, 210, 312 (1973) (Sov.Phys.Dokl. 18, 320 (1973)).
13. P.E. Fielding, A.W.H. Mau, Aust.J.Chem., 29, 933 (1976).
14. J.R. Platt, 'Electronic structure and excitation of polyenes and porphyrins' in 'Radiation Biology', ed. A. Hollaender, 1956.
15. C. Weiss, H. Kobayashi, M. Gouterman, J.Mol.Spectros., 16, 415 (1965).
16. A.J. McHugh, M. Gouterman, C. Weiss, Theor.Chim.Acta, 24, 346 (1972).
17. D. Spangler, R. McKinney, R.E. Christoffersen, G.M. Maggiora, L.L. Shipman, Chem.Phys.Lett., 36, 427 (1975).
18. H. Kobayashi, Nippon Kagaku Zasshi, 83, 1167 (1962).
19. H. Kuhn, Forsch.Chem.Org.Naturstoffe, 17, 404 (1959).
20. K. Tomono, K. Nishimato, Bull.Chem.Soc. Japan, 49, 1179 (1976).
21. G.W. Canters, G. Jansen, M. Noort, J.H. van der Waals, J.Phys.Chem., 80, 2253 (1976).
22. M. Gouterman, G.H. Wagnière, L.C. Snijder, J.Mol.Spectros., 11, 108 (1963).
23. E.C.M. Kielman-van Luyt, H.P.J.M. Dekkers, G.W. Canters, Mol.Physics, 32, 899 (1976).
24. J.L. Hoard, 'Stereochemistry of porphyrins and metallo-porphyrins' in 'Porphyrins and metallo-porphyrins', ed. K.M. Smith, Amsterdam, 1975.
25. H.C. Chow, R. Serlin, C.E. Strouse, J.Am.Chem.Soc., 97, 7230 (1975).
26. G. Jansen, J.H. van der Waals, Chem.Phys.Lett., 43, 413 (1976).
27. R. Englman, J. Jortner, Mol.Physics, 18, 145 (1970).

28. J.F. Kleibeuker, R.J. Platenkamp, T.J. Schaafsma, to be published.
29. J.T. Hougen, J.Mol.Spectrosc. 13, 149 (1964).
30. G. Herzberg, Molecular spectra and molecular structure, Vol. III, Van Nostrant, New York, 1966.

6 The triplet state of MgTBP

6.1 INTRODUCTION

Since MgTBP turns out to be a good model system for chlorophylls w.r.t. some properties of the first excited singlet state, one may wonder if its triplet state properties also resemble those of the chlorophylls. This question has prompted us to measure phosphorescence and $\Delta m = 1$ triplet ESR spectra of MgTBP, and - to a limited extent - fluorescence detected magnetic resonance (FDMR) spectra at zero magnetic field |1|. For experimental conditions we refer to Chapters 5, 7, 8 and 9.

6.2 RESULTS

The (0-0) band in phosphorescence spectra of MgTBP in various solvents (MTHF, methanol, polymethylmethacrylate (PMMA) and tol/pyr) is invariably found at 800 ± 5 nm. Two features of the spectra should be noted: (i) the phosphorescence spectra have a normal Franck-Condon profile, i.e. the (0-0) band has appreciable larger intensity than higher vibronic bands, as contrasted with spectra reported for other porphyrins |2|; (ii) although no accurate quantum efficiency measurements have been carried out, the phosphorescence intensity indicates a relatively large phosphorescence yield.

The $\Delta m = 1$ triplet ESR spectrum of MgTBP in MTHF at 100 K consists of two sharp Z-peaks and broad bands in the X-Y regions, exhibiting some structure indicating the presence of X and Y peaks (see fig. 1c). To find the origin of this unusual X/Y bands, the temperature dependence, as well as the solvent dependence of the $\Delta m = 1$ triplet ESR spectrum of MgTBP has been studied in detail. For studies in the high temperature regime (100 - 300 K) the compound was incorporated in solid PMMA, whereas for T = 5 - 100 K, the measurements were carried out using MTHF, tol/pyr, methanol and ethanol solutions; fig. 1a-f represent a number of typical spectra. For all four solvents the experimental spectra are very similar. The main features of the spectra are (i) the sharp Z-peaks with an almost temperature independent width, (ii) the single X/Y peaks at 300 K, whereas at 5 K double X and
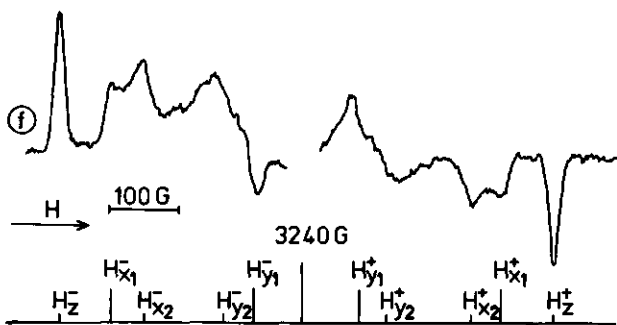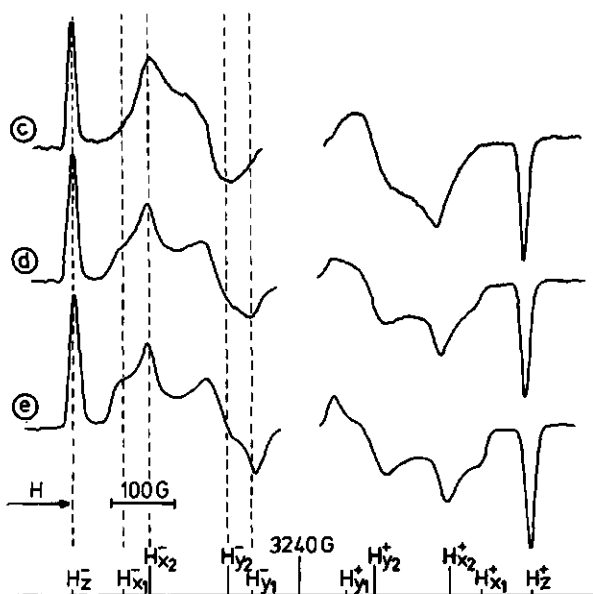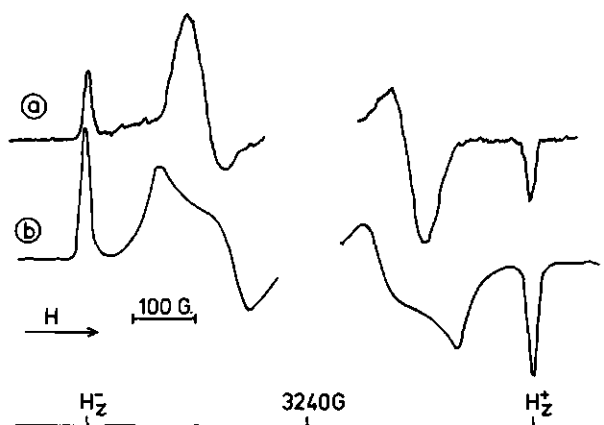
Fig. 1 Δm = 1 triplet ESR spectra of MgTBP in various solvents and at different temperatures.
(a) MgTBP in PMMA at 315 K;
(b) MgTBP in PMMA at 100 K;
(c) MgTBP in MTHF at 80 K;
(d) MgTBP in MTHF at 40 K;
(e) MgTBP in MTHF at 15 K;
(f) MgTBP in tol/pyr at 5 K;
H_z^-, H_x^- etc. mark the field positions for the various peaks. Note the two sets of X and Y peaks in (e) and (f). The samples are illuminated with red light (λ > 570 nm). Experimental conditions: microwave frequency 9.1 GHz, microwave power 5 mW (a) — 0.2 mW (f), field modulation frequency 100 KHz, modulation amplitude 10-16 Gauss.

double Y peaks are found in the X-Y regions and finally, (iii) the absence
of appreciable electron spin polarization (ESP), even at 5 K, the lowest
temperature which could be experimentally obtained. The low temperature
spectra can be thought to be a superposition of two $\Delta m = 1$ triplet ESR
spectra, characterized by the same D-value but different E-values. The ZFS
parameters obtained for the various solutions are collected in table 1. From
phosphorescence, as well as from the time dependence of the ESR signals
following a pulse of exciting light, the lifetime of the lowest excited
triplet state has been determined to be $\tau = 230 \pm 20$ msec.

Up to now we did not succeed in measuring optically detected zero-
field magnetic resonance of MgTBP at 4.2 K in MTHF, ethanol or tol/pyr
glasses, monitoring either fluorescence or phosphorescence detection. For
solutions of MgTBP in n-octane, containing a small amount of MTHF, FDMR
spectra are easily obtained, when detecting at the MgTBP (0-0) fluorescence
band at 627 nm. The observed resonances can be divided into two sets:
(i) measuring with 1 mW microwave power, resonances are found at 1220,740 and
480 MHz, corresponding to $D = 327 \times 10^{-4} cm^{-1}$ and $E = 80 \times 10^{-4} cm^{-1}$;
(ii) measuring with 10 mW microwave power, in addition to the aforementioned
resonances, transitions are observed at 1440 and 602 MHz, most probably
corresponding to $D = 344 \times 10^{-4} cm^{-1}$ and $E = 160 \times 10^{-4} cm^{-1}$.
Detecting, however, at 647 nm (fluorescence of an unidentified impurity |3|),
microwave resonances occur at 1108 and 740 MHz, corresponding to a triplet
state with $D = 308 \times 10^{-4} cm^{-1}$ and $E = 61 \times 10^{-4} cm^{-1}$.

6.3 DISCUSSION

The unusual shape of the MgTBP $\Delta m = 1$ triplet ESR spectrum and its
temperature dependence is not found for photosynthetic pigments (Chapter 7-10).
Furthermore, in view of the relatively long lifetime and the absence of

Table 1 Zero-field splitting parameters of MgTBP in different matrices.
E_1 and E_2 refer to the two sets of X and Y peaks.

Solvent	$D \times 10^4 cm^{-1}$	$E_1 \times 10^4 cm^{-1}$	$E_2 \times 10^4 cm^{-1}$
tol/pyr	334 ± 2	65 ± 2	38 ± 2
MTHF	341 ± 2	69 ± 2	37 ± 2
ethanol	341 ± 2	71 ± 2	37 ± 2
methanol	339 ± 2	72 ± 2	38 ± 2
PMMA	334 ± 3	–	–

appreciable ESP, even at temperatures where this phenomenon is usually observed, we may conclude that MgTBP does not represent a good model system for chlorophyll w.r.t. triplet state studies. The origin of the unusual and interesting $\Delta m = 1$ triplet ESR spectra, as well as their temperature dependence will be discussed elsewhere, since it is outside the scope of this thesis. In the following we will only consider the effects of ligands, bound to Mg^{2+} and of the benzoïdgroups on the ZFS parameters.

Only one set of ZFS parameters obtained from FDMR is in satisfactory agreement with the ESR results: FDMR yields $D = 327 \times 10^{-4} cm^{-1}$, $E = 80 \times 10^{-4} cm^{-1}$, whereas from ESR at 5 K we obtain $D = 334 - 340 \times 10^{-4} cm^{-1}$ and $E_1 = 65 - 72 \times 10^{-4} cm^{-1}$. In n-octane, containing a small amount of MTHF, mono- and biligated MgTBP (MgTBP.L and MgTBP.L_2) are expected to be present. As reported in Chapter 5, we found from optical studies that the S_1 energy level is equal for both complexes, so we attribute the two sets of ZFS parameters detected at the 627 nm (0-0) fluorescence band to the mono- and biligated compound. Since MgTBP in polar solvents at $T \leq 100$ K is expected to be completely biligated, the correspondence between ESR, measured using polar solvents, and FDMR results indicates that for MgTBP.L_2 $D = 327 \times 10^{-4} cm^{-1}$ and $E = 80 \times 10^{-4} cm^{-1}$, whereas for MgTBP.L $D = 344 \times 10^{-4} cm^{-1}$ and $E = 160 \times 10^{-4} cm^{-1}$. Up to now we have no explanation for the strong increase of E for MgTBP.L w.r.t. MgTBP.L_2. The larger D-value in MgTBP.L can be attributed to a larger effective electronegativity of Mg^{2+} in MgTBP.L, because of the presence of only one instead of two electron donating ligands. Then, the larger electron attraction of Mg^{2+} in MgTBP.L vs. MgTBP.L_2 results in a decrease of the extent of the π-electron delocalization and consequently in a larger D-value of the monoligated compound (see Chapter 2). Recently comparable effects have been found for Chl a [4].

The D-value for MgTBP.L is only slightly smaller than that reported for Mg-porphin - lacking benzoïdgroups - in n-octane, containing a small amount of ethanol ($D = 350 \times 10^{-4} cm^{-1}$) [5]. If the unpaired electrons in MgTBP would be delocalized over the porphin ring *and* the four benzoïdgroups, one would predict the D-value for MgTBP.L to be smaller than for monoligated Mg-porphin. The similarity of the D-values for both compounds indicates - in agreement with the results obtained from optical studies - that the dominant π-electron conjugation path in TBP is located on the 16 membered ring, which is electronically isolated from the benzoïdgroups.

6.4 REFERENCES

1. S.J. van der Bent, A. de Jager, T.J. Schaafsma, Rev.Sci.Instrum., 47, 117 (1976).
2. M.P. Tsvirko, K.N. Solovev, A.T. Gradyushko, S.S. Dvornikov, Opt. Spectrosc., 38, 400 (1975).
3. L. Bayema, M. Gouterman, C.B. Rose, J.Mol.Spectrosc., 39, 421 (1971).
4. R.P.H. Kooyman, T.J. Schaafsma, J.F. Kleibeuker, Photochem. Photobiol., to be published.
5. G. Jansen, J.H. van der Waals, Chem.Phys.Lett., 43, 413 (1976).

7 Spin polarization in the lowest triplet state of chlorophyll

Joop F. KLEIBEUKER and Tjeerd J. SCHAAFSMA

Laboratory of Molecular Physics, Agricultural University,
Wageningen, The Netherlands

Chlorophyll-b in glassy solution has a spin-polarized lowest triplet state at and above 77 K. The magnitude of the effect is different for MTHF and ethanol as solvents, in contrast to what is found for the porphin free base. Chlorophyll-a does not exhibit spin-polarization under identical conditions as for chlorophyll-b. Zero-field parameters are found to be:

chlorophyll-a (MTHF) $D = (281 \pm 6) \times 10^{-4}$ cm^{-1}; $E = (39 \pm 3) \times 10^{-4}$ cm^{-1};

chlorophyll-b (MTHF) $D = (289 \pm 4) \times 10^{-4}$ cm^{-1}; $E = (49 \pm 3) \times 10^{-4}$ cm^{-1}.

From ESR signal kinetics it follows that for chlorophyll-b, population and depopulation mainly involve the spin level $|y\rangle$, describing a spin moving in a plane perpendicular to the molecular plane:

$$P_y > P_x > P_z; \quad k_x = 240 \pm 40 \text{ s}^{-1}; \quad k_y = 600 \pm 120 \text{ s}^{-1}; \quad k_z \leqslant 75 \text{ s}^{-1},$$

where P_i and k_i denote populating and decay rates. Thus, the kinetic scheme for the chlorophyll triplet is different from that of porphyrins with heavier metal ions, but very similar to that of the porphin free base. The spin–lattice relaxation time is found to be anisotropic and shorter than the decay rates of individual spin levels. Nevertheless, spin polarization can be observed, essentially because the ESR signal amplitude depends on population *differences*.

1. Introduction

Upon illumination of photosynthetic pigments both in vitro and in vivo, significant steady-state levels of triplets can be formed [1–3]. Furthermore, it has been found that triplet state kinetics affect the populations of the ground and excited singlet states of chlorophyll [4] and of the porphin free base [5]. On the other hand, the triplet lifetime of chlorophyll at room temperature is in the millisecond region [1], thus exceeding the period which is significant for the photosynthetic energy conversion. Therefore, it is still a matter of debate as to whether the lowest triplet state of chlorophyll is part of the energy transfer pathway in photosynthesis [3,6], and more kinetic studies are needed to settle this question.

Also from the molecular point of view, the triplet state of chlorophyll is of interest, since it belongs to the class of porphyrins, for which well-developed theories on electronic structure [7] as well as a large amount of spectral data [1,8,9] are available. Even if the triplet state is not an essential intermediate in biological energy conversion, it provides an attractive probe to study primary processes in photosynthetic model compounds and in the in vivo unit. For example, Dutton and Leigh [3] have recently demonstrated that the presence of triplets is closely connected to the primary photochemistry in the photosynthetic reaction centre of rhodopseudomonas spheroides.

In this letter we present kinetic data on the lowest triplet state of chlorophyll-a and b, together with that of the porphin free base, obtained from the steady-state and transient behaviour of their low temperature ESR spectra.

2. Experimental

ESR spectra of the porphin free base, chlorophyll-a and b, dissolved in dry and oxygen-free 2-methyl-

tetrahydrofuran (MTHF) and ethanol were taken with a slightly modified Varian E-6 spectrometer, equipped with a low power bridge. Porphin free base (Calbiochem) chlorophyll-a and b (Fluka) were checked for purity by TLC and visible spectrum [1,8,10]. All operations were carried out in evacuated, grease-free glassware. Samples were irradiated both continuously and chopped with filtered light from a 200 W mercury arc (Osram HBO-200).

ESR signals were amplified and averaged by using a boxcar integrator or PSD (Brookdeal) and a HP 5480 signal analyzer, which also served for background subtraction.

3. Spin polarization with continuous illumination

In zero magnetic field, the lowest electronic triplet state of chlorophyll, assumed to have $\pi\pi^*$ character in polar solvents [11], is split into three non-degenerate spin levels $|x\rangle$, $|y\rangle$, $|z\rangle$; the z axis is taken perpendicular to the molecular plane, defined by x and y. As usual for $\pi\pi^*$ states, E_x, $E_y > E_z$. Fig. 1 defines the populating rates $P_{0,\pm 1}$, the total decay rates $k_{0,\pm 1}$ and spin—lattice relaxation rates w for the spin levels $|0\rangle$ and $|\pm 1\rangle$ [12—14]. Boltzmann factors $\exp[(E_m - E_{m'})/kT]$, with $m, m' = 0, \pm 1$, are approximated by $\{1 + \delta(m - m')\}$ where $\delta \equiv h\nu/kT$ and ν is the microwave frequency. Steady state ESR signal ampli-
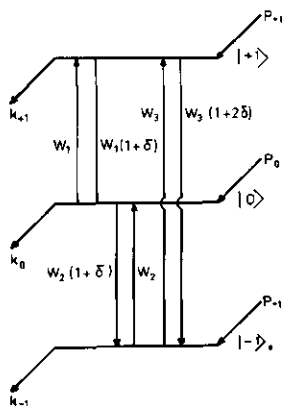

Fig. 1. Kinetic scheme for triplet magnetic sublevels $|0\rangle$ and $|\pm 1\rangle$ at high field. For definition of symbols, see text.

tudes S for each of the six $\Delta m = \pm 1$ transitions at $H_z^- < H_x^- < H_y^- < H_y^+ < H_x^+ < H_z^+$ (superscripts + and − referring to high and low field regions of the spectrum) can be calculated by solving the rate equations for the populations N_0 and $N_{\pm 1}$.

Since spin relaxation rates may be anisotropic, we use different rates w_1^i, w_2^i and w_3^i for H along any of the molecular axes $i = x$, y or z. Following Sixl and Schwoerer [13], we assume $w_1^i = w_2^i = w^i$ and $N_{-1}(t) = (1 + 2\delta)N_1(t)$ resulting in the elimination of w_3^i from the rate equations. Noting that for $i = x$, y the signal amplitudes S_i^+ and S_i^- at resonance field values H_i^+ and H_i^- are proportional to the population differences $N_0 - N_1$ and $N_{-1} - N_0$, respectively, the steady state spin polarization as defined by a *polarization ratio*

$$R_i \equiv (S_i^+ - S_i^-)/(S_i^+ + S_i^-) \tag{1}$$

can be expressed as

$$R_i = \frac{P_0 k_1 - P_1 k_0 - P_1 k_0 \delta}{\delta w^i(P_0 + 2P_1) + P_1 k_0}. \tag{2}$$

(For $H|z$, S_i^+ and S_i^- are interchanged.) In deriving eq. (2), terms in δ^2 have been neglected with respect to δ, since at 77 K, $\delta \approx 5 \times 10^{-3}$.

The experimental ESR spectrum provides three values of R_i, one for each pair of transitions at H_i^+ and H_i^- ($i = x, y, z$).

In the absence of relaxation $w^i = 0$ and $R_i \to \infty$, whereas with $w \to \infty$ no spin polarization is observed. With $w^i \gg k_0, k_1$ and $\delta \ll 1$, (2) is further simplified to

$$R_i = (k_1 p_0 - k_0 p_1)/w^i \delta , \tag{3}$$

where fractional population rates p_0 and p_1 are defined by $p_{0,\pm 1} \equiv P_{0,\pm 1}/(P_0 + 2P_1)$. Note that polarization is observed if $k_1 p_0 - k_0 p_1$ is of the same order of magnitude as $w^i \delta$, even if $w^i \gg k_0, k_1$.

As will be shown below, spin polarization in the porphin free base and chlorophyll-b arises because both the populating and decay rates are different for the three zero-field spin states $|i\rangle$, resulting in $p_0 \neq p_1$ ($= p_{-1}$) and $k_0 \neq k_1$ ($= k_{-1}$) for $H|| x, y,$ or z. Since one may neglect the radiative contribution to the total decay rates, the kinetics of the high-field spin components are entirely governed by radiationless processes. Then, the populating and decay mechanism are rather similar in nature, as has been shown by theory and experiments [15] on aromatic and aza-aromatic molecules. Quantitatively, this means that the dif-

Fig. 2. Triplet ESR spectrum of the porphin free base in MTHF (4×10^{-5} M) at 77 K indicating the presence of spin polarization. Microwave power 0.05 mW, modulation amplitude 16 G, modulation frequency 100 kHz. Spectrum recorded with continuous illumination.

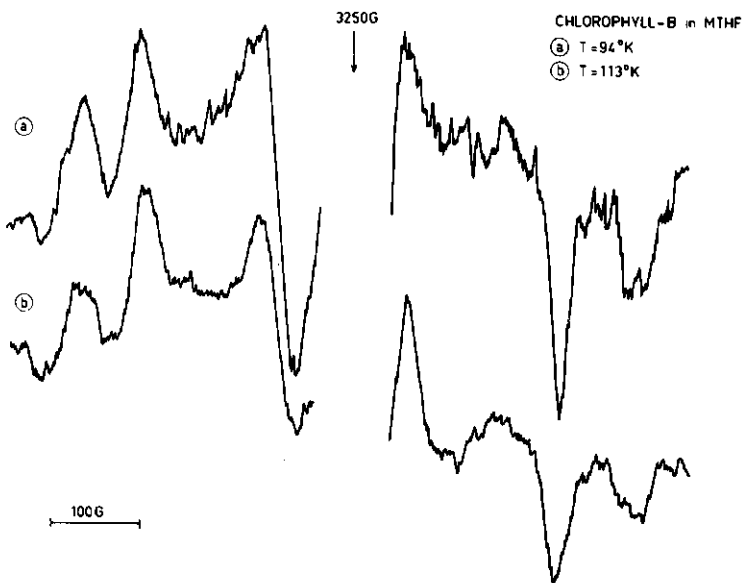Fig. 3. Triplet ESR spectra of chlorophyll-b in MTHF (2×10^{-4} M) at two different temperatures recorded with continuous illumination; the central radical signal is omitted. Microwave power is: 0.5 mW (a) and 5 mW (b), microwave frequency 9099 MHz, modulation amplitude 16 G, modulation frequency 100 kHz. In this region the shape of the observed spectrum is independent of microwave power.

ference between p_0/p_1 and k_0/k_1 is rather small for each of the canonical field directions. Therefore, the difference $k_1p_0 - k_0p_1$ can only have appreciable magnitude with respect to $w^i\delta$ for short-lived triplets, i.e., when k_0 and k_1 are large.

In most solvents at ≈ 77 K the spin system is only partially polarized due to fast relaxation and one observes no emissive transitions, but an asymmetric intensity distribution as in figs. 2 and 3. The component out of a pair of transitions (e.g., H_x^+ and H_x^-) with *lowest* intensity will appear as *emissive* if relaxation is sufficiently slowed down.

The spectra of figs. 2 and 3 give the following polarization ratios:
porphin free base (77 K, MTHF)

$R_x = +0.30(\pm 0.05)$, $R_y = -0.50(\pm 0.06)$. $R_z \approx 0$;

chlorophyll-b (94 K, MTHF)

$R_x = +0.26(\pm 0.03)$, $R_y = -0.59(\pm 0.06)$, $R_z \approx 0$.

Chlorophyll-a does not show spin polarization under the same conditions as chlorophyll-b.

Applying eq. (3), these results imply that both for the porphin free base and chlorophyll-b, transitions at H_x^- and H_y^+ are emissive and those at H_x^+ and H_y^- are absorptive in the absence of relaxation. Anticipating further results from transient ESR responses, following below, we find $p_y > p_x > p_z$. Combining this result with the steady state behaviour of transitions at H_x^+ and H_y^-, we conclude that the spin-component $|y\rangle$ decays faster than $|x\rangle$ and/or $|z\rangle$. This is very different from the kinetic scheme observed for Zn-porphin [16], where $|z\rangle$ is the dominant level for populating and decay. It follows from (3) that for isotropic relaxation ($w^x = w^y = w^z$)

$$R_x + R_y - R_z = 0 . \tag{4}$$

Spin relaxation must be anisotropic, since eq. (4) does not hold experimentally.

Table 1 summarizes the zero-field parameters for the three compounds of interest dissolved in MTHF and ethanol. Results agree with existing data obtained from high-field $\Delta m = 2$ ESR spectra [11,17,18] and with zero-field transitions observed for the porphin free base [5]. Note that D and E of the porphin free base are insensitive to a change in solvent, whereas chlorophyll-b changes its E value by $\approx 30\%$. Chlorophyll-a has a lower E value than its partner -b, in

Table 1

Zero-field parameters of the porphin free base and chlorophyll-a and b. D values were calculated from the separation of the outer peaks; E values from the average of the separation between x and y positions in the low and high field portions of the spectrum. All measurements were carried out at 77 K, except for chlorophyll-a, where $T = 95$ K. The variations in D and E in this temperature range are within the measuring error

Compound	Solvent	D $(10^{-4}$ cm$^{-1})$	$E(10^{-4}$ cm$^{-1})$
porphin	ethanol	437 ± 7	66 ± 5
	MTHF	436 ± 6	65 ± 3
chlorophyll-b	ethanol	287 ± 5	36 ± 4
	MTHF	289 ± 4	49 ± 3
chlorophyll-a	MTHF	281 ± 6	39 ± 3

agreement with previous conclusions from $\Delta m = 2$ spectra [17].

The amount of spin polarization R_i remains constant upon a change of solvent in the case of the porphin free base, in contrast with chlorophyll-b, where R_i is lower in ethanol than in MTHF. Although more data are needed to substantiate such a conclusion, it is conceivable that the lowering of both E and R_i upon a change in solvent have a common origin, if it is assumed that the amount of inequivalence of the molecular x and y axes, reflected by the magnitude of E, also affects spin relaxation, and thus R_i. A fast spin relaxation, accompanied by a low E value, could also explain the absence of spin polarization in chlorophyll-a, which is surprising in view of its triplet lifetime being shorter than that of the -b compound.

A change in solvent viscosity has a different effect on R_i and E, as is shown by fig. 3: a small temperature increase does not affect D or E, but spin polarization is nearly wiped out. Even if no spin polarization is observed, i.e., the $\Delta m = 1$ ESR spectrum has a symmetric intensity distribution around the center field, anisotropic spin relaxation can affect the relative intensities of the three pairs of transitions in a different way as is apparent in triplet ESR spectra of some metalloporphyrins [19].

4. Transient spin polarization

With standard ESR detection, quantitative information on the kinetic scheme of fig. 1 cannot be ob-

tained in a simple manner. Therefore, following Lhoste [20] and Levanon and Weissmann [21,22], we have employed a chopped light source and phase-sensitive detection with reference to the chopping frequency. It appears to be useful to study both the time dependence of each of the $\Delta m = \pm 1$ transitions, as well as the shape of the spectrum after a certain time has elapsed after the exciting light has been switched on or off, using a boxcar integrator [23]; such a spectrum is called a gated spectrum. Treatment of our results goes along the same lines as in previous studies on slower systems by Sixl and Schwoerer [13,14] and Clarke [24]. Solving the differential equations leads to a sum of exponentials for the time dependence of the various signal amplitudes. If the relaxation rates are of comparable magnitude or larger than the decay rates, signals S_i^+ and S_i^- have unequal amplitude [13]. For $H \| x$, y and z this is what we observe.

Fig. 4 represents the observed time dependence for the signal amplitudes S_x^+, S_y^+ and S_z^+; with a time reso-
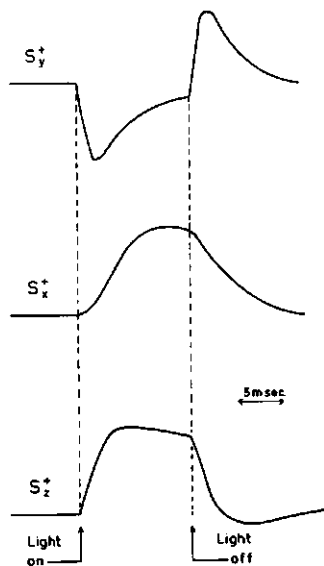

Fig. 4. Observed time dependence of S_x^+, S_y^+, S_z^+ (see text) of chlorophyll-b in MTHF. Response time spectrometer 0.3 ms; for S_y^+ a negative signal is absorption, for S_x^+ and S_z^+ a positive signal is absorption.

lution which is probably limited by the 0.3 ms RC-time of the spectrometer. After switching *off* the exciting light, the S_y^+ signal *changes sign* from absorption (A) to emission (E) and then decays to zero. The same phenomenon, but less pronounced, is found for S_z^+. This means that for $H \| y$ $k_0 > k_1$. When switching on the exciting light, signal S_i^+ initially grows proportional to $P_i - \frac{1}{2}(P_j + P_k)$ ($i, j, k = x, y$ or z). Thus

$$S(H) = \lim_{\Delta t \to 0} \int_0^{\Delta t} S(t) \, dt$$

represents a spectrum in statu nascendi with normalized signal amplitudes reflecting the *difference* in the populating rates p_0 and $p_{\pm 1}$.

A convenient experimental method to obtain a spectrum in statu nascendi is to measure a gated spectrum with the gate-open-period of the boxcar integrator directly after the switching on of the exciting light. For chlorophyll-b such a gated spectrum is shown in fig. 5. Note the large amplitude of the S_y^+ signal resulting from $p_y > p_x, p_z$. By evaluating the initial normalized slopes of the transients $S_x^+(t)$, $S_y^+(t)$ and $S_z^+(t)$, a first estimate of the populating rates can be obtained:

$$p_x : p_y : p_z \approx 3 : > 6 : \leqslant 2 .$$

The opposite behaviour of a transition with continuous or pulsed excitation can now be understood. In the former case the S_y^+ transition, for instance, would be *emissive* in the absence of relaxation, even when the *onset* of the same transition is *absorptive*. This is due to the fact that, although $p_0 > p_1$, $p_0/k_0 < p_1/k_1$.

After switching off the exciting light, $S_i(t)$ eventually decays with a rate $\frac{1}{3}\sum_i k_i$, found to be 300 ± 30 s^{-1}. Because S_y^+ and S_x^- have "emissive" character during continuous excitation,

$$k_y > 490 \text{ s}^{-1}, k_z, k_x .$$

For spin polarization to be observable, the spin–lattice relaxation time $T_1 = (3w)^{-1}$ should be in the region $(k_0 - k_1)^{-1}\delta < T_1 < (k_x + k_y + k_z)^{-1}$ [13] or

$$5 \, \mu s < T_1 < 1 \text{ ms} .$$

Using phase-sensitive detection with reference to the chopping frequency, generally leads to distorted ESR spectra, because transients of different shape are integrated for $H \| x, y, z$. Some transitions may even be ab-
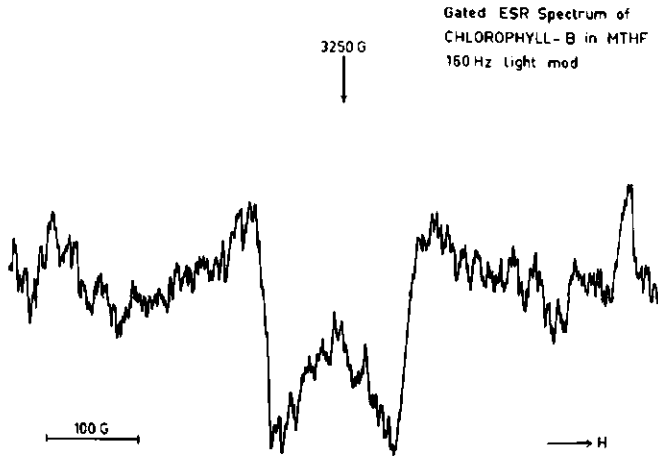
3250 G

100 G

⟶ H

Fig. 5. Gated ESR spectrum of chlorophyll-b in MTHF. Response time ESR spectrometer 0.3 ms; gatewidth: 1 ms; delay with respect to leading edge of light pulse: 1 μs. Response time gated amplifier: 10 s. Chopping frequency: 160 Hz.

sent from the spectrum, as is observed for the chlorophyll-b S_x^+ and S_x^- transitions at 160 Hz chopping frequency.

Finally, kinetic constants p_i, k_i and w^i can be obtained by electronic simulation of the ESR transients. As $w^i \gg k_i, p_i$, all transients decay to equilibrium with exponentials containing the averages $\frac{1}{3}\sum_i P_i$ and $\frac{1}{3}\sum_i k_i$ [13], and in this respect do not provide data on the individual spin components. However, the signs and relative amplitudes of $S_i^+(t)$ and $S_i^-(t)$ both for continuous illumination and at a short time after the leading and trailing edges of the applied light pulse are determined by k_i, p_i, and w^i. Fig. 6 represents a superposition of the experimental and simulated transient $S_y^-(t)$. Using the same values of k_i and p_i for the five remaining transients leads to close agreement with experimental results, if w is taken to be different for each of the three pairs of transitions $S_x^\pm$, $S_y^\pm$ and $S_z^\pm$. We find that

$$p_x : p_y : p_z$$

$$= 0.30(\pm 0.02) : 0.60(\pm 0.04) : 0.09(\pm 0.04) \, ;$$

$$k_x : k_y : k_z = 3.1(\pm 0.5) : 7.8(\pm 1.5) : \leqslant 1.$$

The value of $\frac{1}{3}\sum_i k_i$, determined from the simulation experiment, is $320 \pm 50 \text{ s}^{-1}$ in agreement with the
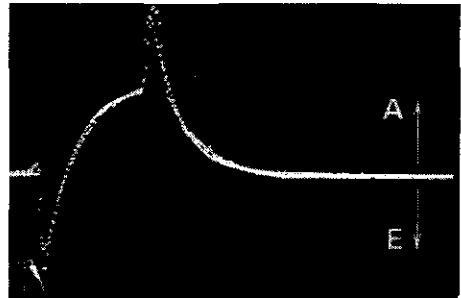
Fig. 6. Superposition of simulated and observed transient S_y^- of chlorophyll-b in MTHF at a chopping frequency of 15 Hz, ESR response time 0.3 ms. Accumulation of ≈ 1000 transients. Time base: 5 ms/div.; A = absorption; E = emission.

ESR value of 300 s^{-1}. We combined the last number with the ratio $k_x : k_y : k_z$ from the simulation experiment, yielding

$$k_x = 240 \pm 40 \text{ s}^{-1}, \ k_y = 600 \pm 120 \text{ s}^{-1}, \ k_z \leqslant 75 \text{ s}^{-1},$$

in agreement with previous conclusions from the steady state spin polarization. In actual simulation, the error limits are smaller than quoted above, since the choice of k_i and p_i must be consistent with the

85

magnitude of the steady state polarization. Spin—lattice relaxation rates are found to be of the order of 10^4 s^{-1}. Furthermore $w^x \approx w^y < w^z$, in qualitative agreement with the results obtained from (3) using experimental values for k_i and p_i. Probably, the absence of spin polarization for $H \| z$ is due to the very small value of $k_1 p_0 - k_0 p_1$ in (3) and not to fast relaxation.

Simulation was carried out with a fictitious Boltzmann difference $\delta = 0.1$. Since the shape of the transient is largely determined by $w^i \delta$, if $w^i \gg k_i, p_i$, this does not affect the results, as long as $w^i \delta$ is kept unchanged with respect to the actual ESR experiment, and $\delta \ll 1$.

Our results show good agreement with data recently obtained by Clarke [4], using optically detected magnetic resonance in zero magnetic field, and are qualitatively similar to experimental results on the porphin free base under conditions of slow relaxation [25].

Summarizing, we conclude that the kinetic behaviour of the lowest triplet state of chlorophyll-b, as derived from steady state and transient spin-polarization, is characterized by the presence of a fast decaying in-plane spin component which also has the largest populating rate. In this respect, chlorophyll-b resembles the porphin free base rather than porphyrin with heavier metal ions.

Both the presence of a different side group as in chlorophyll-a and a change of solvent affect the zero-field parameter E, as well as the observed amount of spin polarization, which also depends on the direction of the magnetic field with respect to the molecular frame, due to anisotropic spin—lattice relaxation rates.

Acknowledgement

References

[1] G.P. Gurinovich, A.N. Sevchenko and K.N. Solovyov, Spectroscopy of chlorophyll and related compounds (Science and Engineering Publishing House, Minsk, 1968) [English transl. Natl. Techn. Inform. Service, Springfield] ch. 7.

[2] A.T. Gradyushko, A.N. Sevchenko, K.N. Solovyov and M.P. Tsvirko, Photochem. Photobiol. 11 (1968) 387.

[3] P.L. Dutton, J.S. Leigh and D.W. Reed, Biochem. Biophys. Acta 292 (1973) 654.

[4] R.H. Clarke, Abstracts Intern. Conf. Excited States of Biological Molecules, Lisbon (1974), Contribution nr. C6.

[5] W.G. van Dorp, T.J. Schaafsma, M. Soma and J.H. van der Waals, Chem. Phys. Letters 21 (1973) 221.

[6] A.K. Chibisov, Dokl. Akad. Nauk USSR 205 (1972) 142.

[7] M. Gouterman, in: Excited states of matter, ed. C.W. Shoppee, Grad. Studies Texas Tech. Univ. 2:1-174, 1973, and references therein.

[8] L.P. Vernon and G.R. Seely, eds., The chlorophylls (Academic Press, New York, 1966).

[9] J.E. Falk, Porphyrins and metalloporphyrins (Elsevier, Amsterdam, 1964).

[10] U. Eisner and R.P. Linstead, J. Chem. Soc. (1955) 3749.

[11] J.M. Lhoste, Compt. Rend. Acad. Sci. (Paris) D (1968) 1059.

[12] J.H. van der Waals and M.S. de Groot, in: The triplet state, ed. A.B. Zahlan (Cambridge Univ. Press, London, 1967) p. 125.

[13] H. Sixl and M. Schwoerer, Z. Naturforsch. 24a (1969) 952; 25a (1970) 1383.

[14] M. Schwoerer, in: Proc. XVII Congress Ampère, ed. V. Hovi (North-Holland, Amsterdam, 1973) p. 143.

[15] D. Antheunis, Thesis, Leyden (1974).

[16] I.Y. Chan, W.G. van Dorp, T.J. Schaafsma and J.H. van der Waals, Mol. Phys. 22 (1971) 741, 753.

[17] G.T. Rikhireva, L.A. Sibel'dina, Z.P. Gribova, B.S. Marinov, L.P. Kayushin and A.A. Krasnovskii, Dokl. Akad. Nauk USSR (Biophysical Section) 181 (1968) 103.

[18] G.T. Rikhireva, Z.P. Gribova, L.P. Kayushin, A.V. Umrikhina and A.A. Krasnovskii, Dokl. Akad. Nauk USSR 159 (1964) 196.

[19] J.M. Lhoste, C. Hélène and M. Ptak, in: The triplet state, ed. A.B. Zahlan (Cambridge Univ. Press, London, 1967) p. 487;
J.F. Kleibeuker and T.J. Schaafsma, unpublished results.

[20] J.M. Lhoste, Stud. Biophys. Berlin 12 (1968) 135.

[21] H. Levanon and S.I. Weissman, J. Am. Chem. Soc. 93 (1971) 4309.

[22] H. Levanon and S.I. Weissman, Israel J. Chem. 10 (1972) 1.

[23] M. Plato and K. Möbius, Messtechnik 8 (1972) 224.

[24] R.H. Clarke, Chem. Phys. Letters 6 (1970) 413.

[25] M. Soma, private communication.

8   Optically induced electron spin polarization in the triplet state of chlorophyll and its model compounds

Joop F. KLEIBEUKER, Roelof J. PLATENKAMP and Tjeerd J. SCHAAFSMA

Laboratory of Molecular Physics, Agricultural University, Wageningen, The Netherlands

Optically induced electron spin polarization (OEP) is reported for the triplet state of chlorophyll-a and -b in an organic glass at 15 K and for tetraphenyl porphyrin (TPP) and -chlorin (TPC) free base in a solid polymer up to $\approx$ 200 K. Such polarization results in emissive transitions in the $\Delta m = \pm 1$ ESR spectrum during continuous illumination of these compounds. From the experimental results it is concluded that both chlorophylls have dominant steady-state population in the top zero-field level, associated with an arbitrary in-plane molecular axis. The amount of spin-polarization is strongly affected by the rigidity of the medium as is demonstrated by the observation of emissive transitions in the $\Delta m = 1$ triplet spectra of TPP and TPC up to $\approx$ 200 K.

1. Introduction

At low temperature, and in the presence of a high magnetic field, optically induced electron spin polarization (OEP) has been observed in the photo-excited molecular lowest triplet state [1]. By noting that high-field spin states T_0^μ ($\mu = \pm 1, 0$) contain zero-field spin states T_0^λ ($\lambda = x, y, z$) (referred to the principal axis system of the zero-field splitting tensor $\{x, y, z\}$) having different spin–orbit coupling with (excited) singlet states (S_n) [2], populating and depopulating rates $S_n \rightarrow T_0^\mu$ and $T_0^\mu \rightarrow S_0$ are expected to be different for $\mu = \pm 1$ and 0 [3]. Previously, it has been reported that OEP results in an asymmetric absorption pattern in the $\Delta m = 1$ triplet ESR spectrum of photosynthetic pigments at 95 K; immediately after applying an exciting light pulse, some of the $\Delta m = 1$ transitions were observed to have emissive character [4]. Transitions with apparent emissive character are obtained when the exciting light is modulated and the resulting ESR spectrum is recorded using phase-sensitive detection with the light-modulation as a reference signal [5–8].

Under favourable conditions, such as low temperature (< 4.2 K) or using a lattice with weak electron–phonon coupling – e.g. a Shpolskii-matrix [9] – relaxation between spin states T_0^μ can be made sufficiently slow, such that emissive $\Delta m = 1$ transitions also can be observed during *continuous* optical excitation.

The observation of "anomalous" emissive $\Delta m = 1$ transitions of the triplet state of bacterial photosynthetic reaction centers during continuous illumination, by Leigh and Dutton [10–13], has considerably stimulated interest in OEP as a means for obtaining information on the mechanism of in vivo energy transfer.

This paper reports emissive transitions in the spin-polarized triplet ESR spectrum of chlorophyll a and b in an organic glass at 15 K and of two model compounds, tetraphenylporphyrin free base (TPP) and tetraphenylchlorin free base (TPC) [‡] dissolved in a solid polymer, at relatively high temperature. Our experiments demonstrate that spin relaxation in the lowest triplet state of these compounds is strongly affected by the rigidity of the medium. From the interpretation of the polarization pattern in the low temperature $\Delta m = 1$ spectra of both chlorophylls under *continuous* illumination we obtain an ordering of steady-state populations of the zero-field spin levels, different from that published recently by Katz et al. [7, 8], based on OEP patterns of *light-modulated* $\Delta m = 1$ spectra.

[‡] Systematic name: tetraphenyldihydroporphyrin free base.

2. Experimental

Chlorophyll a and b were prepared and purified following methods of Strain et al. [14]; 2-methyl-tetrahydrofuran (MTHF) was purified by vacuum distillation from a sodium mirror. ESR measurements at 15–33 K were carried out on a Varian E-9 spectrometer equipped with an Air-Products variable temperature helium flow system. Other experimental conditions were the same as in ref. [4].

Populating and depopulating rate constants were evaluated from ESR transients following a light pulse, using an electronic analog simulation [15].

3. Results

Figs. 1a and 1c represent $\Delta m = \pm 1$ (first derivative) triplet ESR spectra of chlorophyll-a and -b in MTHF glass at 15 K. Emissive transitions are labelled by E,

Fig. 1. X-band $\Delta m = \pm 1$ triplet ESR spectra of chlorophyll-a in MTHF at (a) 15 K; (b) 95 K and of chlorophyll-b in MTHF at (c) 15 K and (d) 95 K. Field positions are labelled assuming the energies of the zero-field spin states to be ordered as $E(T_0^x) > E(T_0^y) > E(T_0^z)$ as is usual for $\pi\pi^*$ states; x and y are two arbitrary directions in the molecular plane, z is the out-of-plane axis.
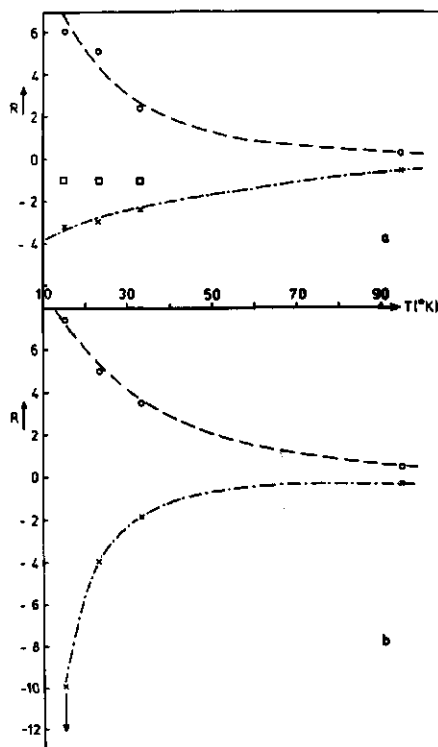
Fig. 2. Temperature dependence of OEP as measured by $R_i(T)$ for (a) chlorophyll-a and (b) chlorophyll-b both in MTHF. $\circ$: R_x; $\times$: R_y; $\square$: R_z.

those with enhanced absorption by A; their absolute sign follows from the phase of a free radical signal in the spectral center. Both spectra are rather similar, except for the absence of a transition at H_z^- for chlorophyll b (probably since it is on the verge of turning from absorptive to emissive) and a different intensity-ratio S_y^+/S_y^-.

At 15 K both compounds have a triplet ESR spectrum with an EEA/EAA pattern; from figs. 1b and 1d it can be concluded that at $\approx$ 100 K there is still no thermal equilibrium among the triplet spin levels, although no emissive transitions are observed (in contrast, bacteriochlorophyll-a in MTHF at 100 K has emissive X^- and Y^+ transitions [15]).

The magnitude of spin-polarization can be expressed as the ratio [4]

$$R_i = (S_i^+ - S_i^-)/(S_i^+ + S_i^-),$$

where $S_i^\pm$ measures signal intensity at a pair of canonical field positions $H_i^\pm$ for $i = x, y$ and H_z^+ for $i = z$; S_i is taken to be positive when the transition is absorptive and negative when it is emissive. If $|R_i| > 1$, emissive transitions are observed. Fig. 2 shows the change of R_y versus temperature for chlorophyll-a and -b in MTHF to be markedly different. Table 1 collects the effects of a change of solvent on the magnitude of R_x and R_y for both chlorophylls.

The effect of solvent viscosity on triplet spin–lattice relaxation has been studied for TPP and TPC, free base, which are structurally related to chlorophyll, and for which triplet state kinetics have been determined [16].

Intramolecular motion and molecular reorientation, such as rotation and libration, can induce transitions between triplet spin states by modulation of the nonsecular part of the dipolar interaction.

The contribution of molecular reorientation to the spin–lattice relaxation, evident from the rapid disappearance of OEP around the softening point of

MTHF at $\approx$ 120 K, can be suppressed by using solid polymethylmethacrylate (PMMA) as a solvent for TPP and TPC. Fig. 3 represents TPC $\Delta m = 1$ triplet spectra at 95 and 173 K; fig. 4 shows similar spectra for TPP at 103 and 213 K. For both compounds, transitions at different canonical orientations exhibit different changes with temperature: e.g. for TPC (fig. 3) the signal amplitude of the emissive Y^+ transition only slightly decreases with increasing temperature, whereas the Z^+ transition turns from emissive into (weakly) absorptive.

TPP in the same matrix exhibits considerable spin-polarization, even at 213 K, where Y^+ and Y^- intensities are strongly asymmetric and the X^- transition is still weakly emissive. At 103 K the triplet spectrum of TPP in PMMA contains strong emissive transitions at H_y^+ and H_x^-, in contrast with what has been reported for this compound in ethanol glass in the same temperature range [17].
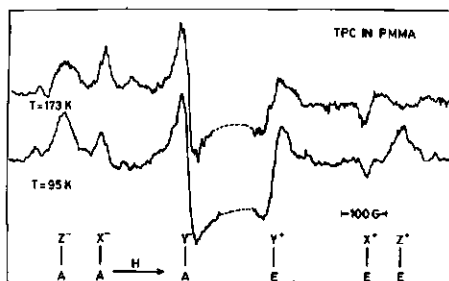
Fig. 3. X-band $\Delta m = \pm 1$ triplet ESR spectra of tetraphenylchlorin free base in solid PMMA at 95 and 173 K.
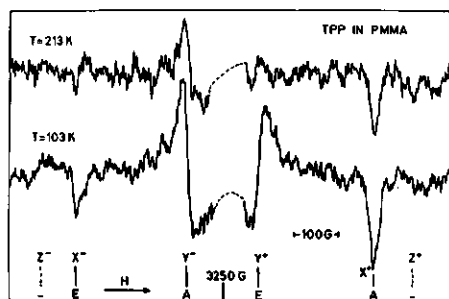
Fig. 4. X-band $\Delta m \pm 1$ triplet ESR spectra of tetraphenylporphyrin free base in solid PMMA at 103 and 213 K.

Table 1
Solvent dependence chlorophyll a/b OEP at 95 K

Compound	Solvent	R_x	R_y	R_z
chlorophyll-a	MTHF	0.45	−0.25	≈ 0
chlorophyll-a	ethanol	0.09	−0.29	≈ 0
chlorophyll-b	MTHF	0.30	−0.47	≈ 0
chlorophyll-b	ethanol	0.30	−0.07	≈ 0

4. Discussion

The EEA/EAA intensity pattern observed for both chlorophylls is characteristic for a $\Delta m = 1$ triplet spectrum of randomly oriented molecules with negligible spin—lattice relaxation, when the zero-field steady-state populations are related by $N_x > N_y, N_z$ [8,18]. The same ordering of populations has been found at widely different temperatures and using various solvents [4,18–20]. Thus, we conclude that both chlorophylls have highest steady state triplet population in the *top zero-field level*, associated with an arbitrary in-plane molecular axis. This is different from the EEE/AAA pattern found by Katz et al. [7,8] using light-modulated ESR spectra from which these authors concluded that $N_x, N_y > N_z$. At first sight this discrepancy does not appear to be alarming, since both schemes lead to dominant in-plane population. It touches, however, on a more serious problem related to the interpretation of $\Delta m = 1$ triplet spectra using light-modulation versus continuous illumination. When analyzing the light-modulated spectra parallel to a procedure published by Winscom [21] and assuming the absence of spin—lattice relaxation, the amplitudes of a pair of transitions at canonical field positions after phase-sensitive detection are given by

$$S_i^\pm \approx \mp \, [p_1 \omega/(k_1^2 + \omega^2) - p_0 \omega/(k_0^2 + \omega^2)] \sin \psi$$
$$\pm \, [p_1 k_1/(k_1^2 + \omega^2) - p_0 k_0/(k_0^2 + \omega^2)] \cos \psi \,, \tag{1}$$

where p_0, p_1 and k_0, k_1 are relative population- and depopulation rates of T_0^0 and $T_0^{\pm 1}$, respectively; ω is the light-modulation frequency and ψ defines the phase difference between the periodic wave form of the exciting light and the phase sensitive detector.

A change of sing (A ↔ E) of each component of a pair of transitions at canonical field positions, occurs when $S_i^\pm = 0$ at $\psi = \psi_0$, given by

$$\text{tg } \psi_0 = \frac{p_0 k_0/(k_0^2 + \omega^2) - p_1 k_1/(k_1^2 + \omega^2)}{p_0 \omega/(k_0^2 + \omega^2) - p_1 \omega/(k_1^2 + \omega^2)} \,. \tag{2}$$

Generally, the value of ψ_0, where $S_i^\pm$ reverses sign, is different for $i = x, y, z$. Thus, in principle, all possible intensity patterns (twelve in total) can be generated by varying ψ. Therefore OEP patterns obtained from light-modulated triplet ESR spectra cannot be related to population ratios for the triplet spin-levels in zero-field, unless the effect of phase-reversals is properly

taken into account or when $\omega \ll k_0, k_1$. The latter condition applies to measurements on bacterial reaction centers [8,13,22] and therefore both light-modulated and CW excited spectra are nearly identical, yielding a $\Delta m = 1$ intensity pattern AEE/AAE which can be shown to be incompatible with an intersystem crossing process involving isolated molecules [8].

In spinach-chloroplasts, the situation is less clear, since the light-modulated spectra [23] do not agree with cw excited spectra [13]. For continuous optical excitation ($\omega = 0$), no phase-reversal of any pair $S_i^\pm$ can occur, as follows from eq. (2). Then, eq. (1) reduces to

$$S_i^\pm \approx \pm \, (p_1/k_1 - p_0/k_0) \,, \tag{3}$$

relating the EEA/EAA pattern to the $N_x > N_y, N_z$ population distribution. Electron spin polarization is sensitive to small changes in molecular structure, as is apparent from the different temperature dependence of R_x and R_y for both chlorophylls in the *same* solvent (fig. 2 and table 1). Since spin—lattice relaxation is known to be anisotropic [4,21,24], and thus depends on the orientation of the principal axes of the zero-field splitting tensor with respect to the molecular frame, this can be — at least qualitatively — understood. As is shown in table 1, there is a pronounced solvent effect on R_x for chlorophyll a, whereas in chlorophyll b R_y is mostly affected. The temperature dependence is strongest for R_x of chlorophyll b and R_y of chlorophyll a. This can arise from a different orientation of the zfs tensor axes in the molecular plane of chlorophyll a with respect to chlorophyll b.

Assuming that the temperature dependence of R_i largely depends on that of the spin-relaxation rates W_i ($i = x, y, z$) and using eq. (3) from ref. [4], we can estimate the average magnitude of W_i at 15 K to be < 500 s^{-1}. Since this is comparable to decay rates for chlorophylls, emissive $\Delta m = 1$ transitions are observable at this temperature.

The anomalous OEP reported for bacterial photosynthetic reaction centers [10–13] cannot be explained by spin—lattice relaxation effects discussed above for isolated pigment molecules, and requires a mechanism for the formation of triplets with spatially quantized spin-states, i.e. no reference to a molecular frame, such as proposed by Katz et al. [8,23,25]. An analysis of ESR transients of TPP and TPC in

PMMA following excitation by a light pulse [4, 17] indicates that relaxation rates in this medium are considerably lower than in low-melting glasses at the same temperature. This can be helpful in the study of spin polarization in aggregated or strongly ligated pigments where relaxation is fast [26].

References

[1] H. Sixl and M. Schwoerer, Z. Naturforsch. 25a (1970) 1383.
[2] J.H. van der Waals and M.S. de Groot, in: The triplet state, ed. A.B. Zahlan (Cambridge Univ. Press, London, 1967) p. 125.
[3] H. Sixl and M. Schwoerer, Chem. Phys. Letters 6 (1970) 21.
[4] J.F. Kleibeuker and T.J. Schaafsma, Chem. Phys. Letters 29 (1974) 116.
[5] J.S. Brinen, J. Chem. Phys. 49 (1968) 586.
[6] H. Levanon and S. Weissman, Israel J. Chem. 10 (1972) 1.
[7] J.R. Norris, R.A. Uphaus and J.J. Katz, Chem. Phys. Letters 31 (1975) 157.
[8] M.C. Thurnauer, J.J. Katz and J.R. Norris, Proc. Natl. Acad. Sci. US 72 (1975) 3270.
[9] E.V. Shpolskii, Soviet Phys. Uspekhi 3 (1960) 372; 5 (1962) 522; 6 (1963) 411.
[10] P.L. Dutton, J.S. Leigh and M. Seibert, Biochem. Biophys. Res. Commun. 46 (1972) 406.
[11] P.L. Dutton, J.S. Leigh and D.W. Reed, Biochim. Biophys. Acta 292 (1973) 654.
[12] C.A. Wraight, J.S. Leigh, P.L. Dutton and R.K. Clayton, Biochim. Biophys. Acta 333 (1974) 401.
[13] J.S. Leigh and P.L. Dutton, Biochim. Biophys. Acta 357 (1974) 67.
[14] H.H. Strain and W.A. Svec, in: The chlorophylls, eds. L.P. Vernon and G. Seely (Academic Press, New York, 1966) p. 22.
[15] J.F. Kleibeuker, P.A. de Jager, R.J. Platenkamp and T.J. Schaafsma, to be published.
[16] S.J. van der Bent and T.J. Schaafsma, Chem. Phys. Letters 35 (1975) 45.
[17] H. Levanon and S. Vega, J. Chem. Phys. 61 (1974) 2265.
[18] T.J. Schaafsma, J.F. Kleibeuker, R.J. Platenkamp and P. Geerse, in: Proceedings of the 12th European Congress on Molecular Spectroscopy, eds. M. Grossmann, S.G. Elkomoss and J. Ringeissen (Elsevier, Amsterdam, 1976) p. 491.
[19] R.H. Clarke and R.H. Hofeldt, J. Chem. Phys. 61 (1974) 4582.
[20] R.H. Clarke, R.E. Connor, T.J. Schaafsma, J.F. Kleibeuker and R.J. Platenkamp, J. Am. Chem. Soc. (1976), to be published.
[21] C.J. Winscom, Z. Naturforsch. 30a (1975) 571.
[22] R.H. Clarke, R.E. Connors, J.R. Norris and M.C. Thurnauer, J. Am. Chem. Soc. 97 (1975) 7178.
[23] R.A. Uphaus, J.R. Norris and J.J. Katz, Biochem. Biophys. Res. Commun. 61 (1974) 1057.
[24] U. Eliav and H. Levanon, Chem. Phys. Letters 36 (1975) 377.
[25] J.R. Norris, R.A. Uphaus, H.L. Crespi and J.J. Katz, Proc. Natl. Acad. Sci. US 68 (1971) 625.
[26] S.J. van der Bent and T.J. Schaafsma, to be published.

9 The triplet state of photosynthetic pigments
I. Pheophytins

J.F. Kleibeuker, R.J. Platenkamp, T.J. Schaafsma

9.1 INTRODUCTION

The triplet state of chlorophylls and related compounds has been studied extensively [1-6]. The discovery of triplet state bacteriochlorophyll in photo-excited photosynthetic bacteria by Leigh et al. [7] provided new interest in chlorophyll triplet states of both *in-vitro* and other *in-vivo* systems. Although the rôle of the chlorophyll triplet state in the primary steps of photosynthesis is probably of secondary importance under natural conditions, it can be used as a natural and non-pertubing probe, sensing short-range interactions of pigments with their *in-vivo* surroundings. An important interaction is ligation of the central Mg-ion, and it is therefore interesting to study the effect of the presence or absence of Mg^{2+} on the triplet state parameters.

In this paper we report the results of a study of the triplet state of pheophytins, which can be derived from the corresponding chlorophylls by replacing Mg^{2+} by two protons. Fig. 1 represents the molecular structure of these pigments. Bacteriopheophytin has been shown to be part of the photo-
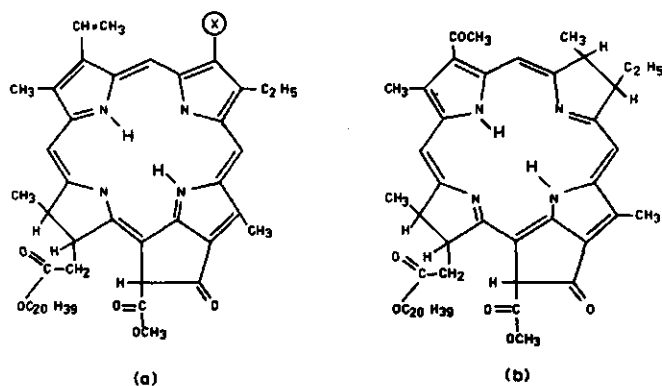
Fig. 1 a) Molecular structure of pheophytins; $X \equiv CH_3$ for Ph a, $X \equiv CHO$ for Ph b.
b) Molecular structure of bacteriopheophytin.
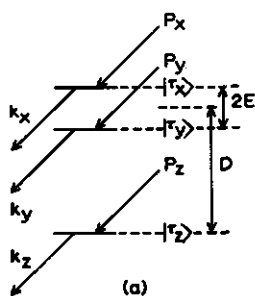
Fig. 2 Triplet state parameters in zero magnetic field. Zero-field splittings between spin levels $|\tau_x\rangle$, $|\tau_y\rangle$, and $|\tau_z\rangle$ are defined by D and E; P_x, P_y and P_z are the populating rates and k_x, k_y and k_z the depopulating rate constants of the spin levels $|\tau_x\rangle$, $|\tau_y\rangle$, and $|\tau_z\rangle$, respectively; the spin levels can be connected by spin-lattice relaxation w, which has been omitted from this figure, for reasons of clarity.

synthetic unit in bacterial reaction centers |8|; for pheophytins, derived from chlorophyll a and b, it is not clear if their presence in preparations of photosynthetic pigments from plants is natural or artificial.

Absorption spectra of the pheophytins and related chlorophylls exhibit slight differences. Krasnovskii has published phosphorescence spectra of pheophytins a and b with emission-maxima nearly coinciding with those of the corresponding chlorophylls |9|. Apart from the energy separation $\Delta E_{T_1-S_0}$ between the lowest triplet state T_1 and the ground state S_0, there are other parameters, which are of interest for a qualitative understanding of the electronic structure of that triplet state: the kinetic constants defining populating- and depopulating processes and the zero-field splitting (ZFS) parameters, defined in fig. 2.

ZFS-parameters can be obtained from ESR using continuous or modulated optical excitation of the lowest triplet state. Kinetic parameters of triplet states can be obtained by analysing the transient behaviour of the triplet ESR transitions using pulsed optical excitation |10|.

Our results clearly demonstrate a parallel between static and kinetic triplet state parameters for chlorophylls and related pheophytins. This parallel, as well as the effects of pyrrole ring reduction and substitution of carbonyl groups on the outer ring on the ZFS parameter D are explained in the framework of the 4-orbital model, so succesfully applied to porphyrins by Gouterman |11, 12|. Longuett-Higgins' concept of long- and round field molecules |13| which is, in principle, equivalent to the 4-orbital

model, will be frequently used in our discussions for reasons of clarity.

Whereas ZFS-parameters can be related to the size and shape of the π-electron cloud, a treatment of kinetic parameters requires an additional feature: the mixing of $n\pi^*$ or $\sigma\pi^*$ states into the singlet- and triplet states of interest, which are assumed to be mainly of $\pi\pi^*$ character.

Throughout this paper we use the following abbreviations for compounds and solvents: Chl a/b = chlorophyll a/b, Ph a/b = pheophytin a/b, BChl = bacteriochlorophyll a, BPh = bacteriopheophytin a, tol/pyr = toluene/pyridine mixture 9:1, and MTHF = 2-methyltetrahydrofuran.

9.2 MATERIALS AND METHODS

Pheophytins were obtained from the corresponding chlorophylls following Smith et al. |14|. Chl a and b were prepared and purified following Strain et al. |15|; Bchl was a gift from Dr. J.R. Norris. Solvents (MTHF, ethanol, toluene, pyridine) were analytical grade. All samples were degassed to 10^{-4} Torr before illumination.

ESR experiments were carried out on a Varian E-6 spectrometer; triplets were produced by illuminating the sample through a slotted window in the ESR cavity. We used a Varian VIX 150 UV Xenon lamp, which could be square-wave modulated with the aid of a home-built electronic circuit. The time dependence of the ESR signals was recorded on a HP 5480 B signal averager.

All measurements were performed at 100 K, using a N_2-variable temperature flow cryostat. Heat input, as a result of illumination was minimized by using appropriate optical filters; the temperature difference in light on and light off periods amounted to less than 1 K.

9.3 RESULTS

The triplet ESR spectrum of Ph a in tol/pyr at T = 100 K using continuous illumination (fig. 3) differs from that of Chl a |5| in two respects: firstly, as is apparent from line positions, Ph a has a larger D-value and a smaller E-value than Chl a (Table 1). The same ZFS-parameters have been found when, instead of continuous illumination, the exciting light is modulated and the ESR signal is phase-sensitive detected |5|.

Secondly, Chl a and Ph a are found to have different electron spin polarisation (ESP) patterns. In such patterns we denote by A or E the absorptive or emissive character of any of the six peaks of a $\Delta m = 1$ triplet ESR

94

Fig. 3 First derivative $\Delta m = 1$ triplet ESR spectrum of Ph a in tol/pyr at 100 K, using continuous optical excitation. H_z-, H_x- etc. mark field positions for transitions of molecules with canonical orientations H//z, H//x or H//y. Experimental conditions: microwave frequency $\nu = 9.1$ GHz; microwave power 2 mW; modulation frequency 100 kHz; modulation amplitude 16 G.

spectrum of an ensemble of random oriented molecules, measured under conditions at which spin lattice relaxation (SLR) can be neglected w.r.t. the populating and depopulating rates |5, 10|. If, however, SLR cannot be neglected the ESP pattern can be deduced from the relative intensities of peaks at the canonical field positions |2, 5|. In an incompletely relaxed spectrum, the peaks, which are emissive when SLR can be neglected, have a smaller intensity than in a completely relaxed spectrum, whereas the amplitude of intrinsically absorptive peaks is larger than in a relaxed spectrum. All chlorophyll triplet ESR spectra, obtained with continuous illumination exhibit the pattern E E A E A A |5, 16|. The polarisation pattern of pheophytin a in tol/pyr can be deduced from the triplet ESR spectrum at 100 K (fig. 3) to be A A E A E E. Note that in the spectrum, shown in Fig. 3, Y^- is

Table 1. ZFS parameters of pheophytins and corresponding chlorophylls

Solvent	Compound	$Dx10^4$ cm^{-1}	$Ex10^4$ cm^{-1}	Compound	$Dx10^4$ cm^{-1}	$Ex10^4$ cm^{-1}
MTHF	Ph a	341+3	33+3	Chl a	280+2	40+1
tol/pyr	"	340+3	30+2	"	279+2	40+1
ethanol	"	334+3	26+2	"	272+4	32+2
MTHF	Ph b	358+8	46+5	Chl b	294+3	48+1
MTHF	BPh	256+4	{54+5 / 37+5	BChl	232+4	58+3

95

emissive and X^+ has zero intensity since it is on the verge of turning from absorptive into emissive.

For MTHF and tol/pyr solutions ZFS-parameters of Ph a are very similar; the amount of spin-polarisation in MTHF is somewhat less than in tol/pyr: the Y^- transition is about to disappear, whereas X^+ is weakly absorptive. We observe a considerable change in the triplet state parameters of pheophytin, when using ethanol as a solvent. ZFS-parameters D and E are reduced (see Table 1) and the triplet ESR spectrum at T = 100 K exhibits a small amount of spin-polarization in the Y-lines only $(Y^- < Y^+)$; comparable solvent effects have been found for Chl a |2, 5|. Ph b is found to have larger ZFS-parameters than its a-analog in the same solution, and exhibit no spin polarization at T = 100 K.

By contrast, BPh in MTHF is fully spin polarized at T = 100 K as shown in Fig. 4. Evidently the spectrum shown in this figure is a super-position of two triplet ESR spectra, both fully spin polarized, and character-ized by identical D- but different E-values. Presumably, this indicates the presence of two physically distinguishable species. The ESP pattern of the two spectra A E A E A E and A A A E E E are both different from the pattern
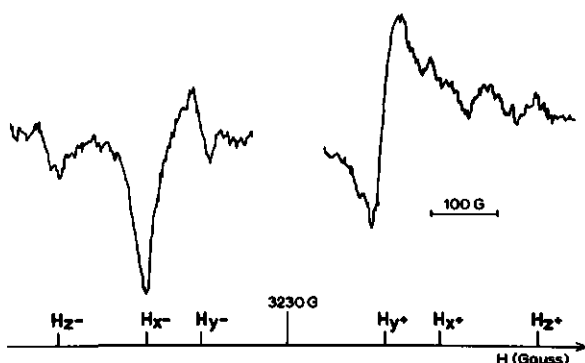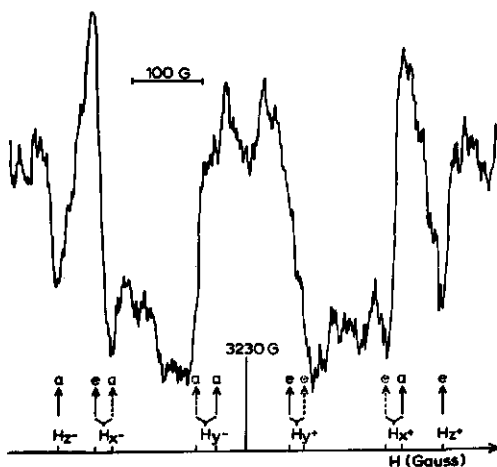

Fig. 4 First derivative $\Delta m = 1$ triplet ESR spectrum of Bph in MTHF at 100 K using continuous optical excitation. H_z, H_y etc. have the same meaning as in Fig. 3. The spectrum can be decomposed into two spectra, characterized by the same H_z+ peaks but different H_x+ and H_y+ peaks; the H_x and H_y peaks of both separate spectra are marked with (-) and (---); a and e denote absorptive and emissive character of ESR transition. Experimental conditions as in Fig. 3.

observed for Ph <u>a</u>. Using 1 kHz optical modulation and phase sensitive detection, we find the ESR spectrum of BPh in MTHF reveals the presence of only one species. Its spectrum is almost identical to that of BPh in tol/pyr as reported by Thurnauer et al. |3|.

Whereas field positions of the six $\Delta m = 1$ transitions are determined by parameters D and E, their relative intensities (including the sign) are determined by triplet state kinetics. From spin polarization patterns, observed during continuous optical excitation, the relative ordering of steady state spin level populations can be found. On the other hand, populating- and depopulating rates can be obtained for each spin level from the transient behaviour of the triplet ESR transitions after switching light on or off |2, 10|. As shown by Levanon |10| the time dependent behaviour of a triplet ESR transition contains two exponentials:

$$S(t) = A\,e^{-K_T t} + B\,e^{-(3\,W + K_T)t} \tag{1}$$

where A and B are constants determined by the relative populating- and depopulating rates for each of the three spin levels; K_T is the mean decay constant $(1/3 \sum_i k_i)$ of the three triplet spin levels and W the SLR rate constant. Since W turns out to be fast, the second exponential in (1) cannot be determined with sufficient accuracy in view of our instrumental time-resolution, thus preventing complete mathematical analysis of the transient S(T). As an additional complication, the SLR rate depends on the orientation of the magnetic field w.r.t. the molecular axes |2, 17|. Using an electronic circuit for simulation of transients |2, 16|, we obtained the relevant triplet state kinetic parameters. Of course, a single transient can be simulated in many ways. However, a unique solution yielding *one* set of kinetic parameters can usually be found, if it is required that it should be possible to simulate all 6 transients by a single set kinetic parameters and assuming at the same time that W ($| + 1 > \leftrightarrow | o >) = W (| - 1 > \leftrightarrow | o >$) irrespective of the orientation of the magnetic field w.r.t. the molecular frame. By electronic

Table 2 Relative populating rates P_i and depopulating rate constants k_i of the triplet states of Ph <u>a</u> and Ph <u>b</u> in MTHF, measured with time dependent ESR at 100 K.

Compound	sec^{-1}			%		
	k_x	k_y	k_z	P_x	P_y	P_z
Ph <u>a</u>	1040+50	1300+100	820+100	31+2	43+5	26+6
Ph <u>b</u>	590+50	870+150	420+150	30+3	48+10	23+9

simulation it is found that at T = 100K $W \gtrsim 5000$ sec^{-1}, in accordance with previous measurements on similar systems. Table 2 collects the results for Ph $\underline{a}$ and Ph $\underline{b}$ in MTHF. Due to the fast decay of BPh, our instrumental resolution limits the data on this compound to its mean decay constant K_T (see Table 3).

9.4 DISCUSSION

9.4.1 *ZFS-parameters*

For porphyrins lacking a heavy metal ion, ZFS-parameters are fully determined by the spin-spin interaction $|18|$; spin-orbit interaction can be neglected.

We note that the ZFS-parameters D and E reflect the distribution of electron density in the triplet state, since these parameters are related to the mutual distance between triplet spins:

$$D = \tfrac{3}{4} g^2 \beta^2 \; < \frac{r_{12}^2 - 3z_{12}^2}{r_{12}^5} > \qquad (2)$$

$$E = \tfrac{3}{4} g^2 \beta^2 \; < \frac{y_{12}^2 - x_{12}^2}{r_{12}^5} > \qquad (3)$$

(a)   (b)   (c)
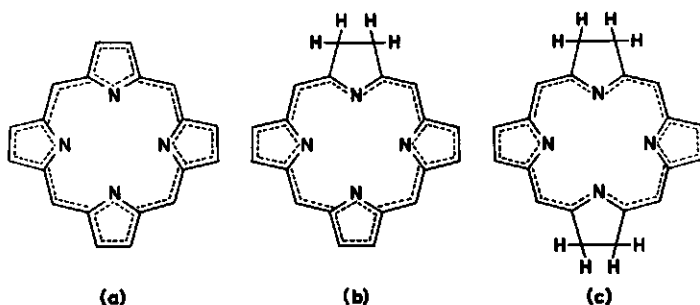
Fig. 5 Molecular structure of porphin (a), dihydroporphin (b) and opposite-tetrahydroporphin (c); central metal ion or protons are omitted. (----) denotes the π-electron conjugation path.

TABLE 3. Spectroscopic data for photosynthetic pigments and some model compounds: Energy level of the lowest excited singlet state (Q_{00}) and shifts (ΔQ_{00}) resulting from substitution of Mg^{2+} by $2H^+$, mean triplet decay constant K_T, ratio of K_T for Mg-containing and free base (f.b.) compounds (K_T^{Mg}/K_T^{H2}), participation of spin level $|\tau_z\rangle$ in the triplet decay (k_z/K_T), ZFS parameter D and the ratio of D for Mg-containing and free base compounds (D^{Mg}/D^{H2}). Data are partly taken from litterature.

Compound*	Q_{00} (cm^{-1})	ΔQ_{00}	K_T (sec^{-1})	K_T^{Mg}/K_T^{H2}	k_z/K_T	$D\times10^4$ cm^{-1}	D^{Mg}/D^{H2}	Ref.
porphin f.b.	16330	-1085	112	0.13	0.05	435	0.81	24
Mg-porphin	17415		14		>0.1	350	-	25
chlorin f.b.	15748	-645	145	-	0.17	397	-	32
Mg-chlorin	16393		-		-	-		33
Ph b	15267	-309	630	0.42	0.66	358	0.83	2, 16
Chl b	15576		270		0.15	294		
Ph a	14948	-158	1050	0.59	0.78	341	0.83	2, 16
Chl a	15106		620		0.23	280		
Bph	13351	+415	~4000	~0.6	-	256	0.91	6, 16
Bchl	12936		2100 (3000±500)		0.31	232		16

* All data refer to pigments in non hydrogen bonding sovents; systematic name for chlorin is dihydroporphin.

99

Here r_{12}, x_{12}, y_{12} and z_{12} define the mutual distance between spins and its components along three mutually perpendicular axes. For chlorophylls and related compounds, x and y are two arbitrary oriented axes in the molecular plane and z is perpendicular to that plane; g is taken to be the free electron value, β is the electronic Bohr magneton and < > denotes the expectation value calculated using the orbital part of the triplet state wave functions. For planar molecules such as porphins $<z_{12}> << <r_{12}>$ and (2) reduces to

$$D \ (:) < \ ^1/_{r_{12}^3} >, \tag{4}$$

suggesting that D measures the extent of the π-electron cloud. So, an increase of the size of the molecule is expected to decrease D.

The extent of π-electron delocalization decreases in the series porphin, dihydroporphin, tetrahydroporphin as given in fig. 5; dihydroporphin is the basic skeleton of Ph a and b, whereas the tetrahydroporphin macrocycle can be recognized in Bph. Evidently, for free base derivatives the prediction that D decreases with increasing π-electron delocalization is not born out by the data collected in table 3. A similar discrepancy is found for Mg containing compounds. However, this is not surprising, since we have ignored the perturbation of *symmetry* of the π-electron cloud - apart from a change in its *extent* - in the above mentioned series.

The effects of symmetry perturbations can be discussed using the concepts of Platt |19| and Longuett-Higgins |13|, implying that these series can be viewed as a gradual transition from a typical "round-field" molecule,
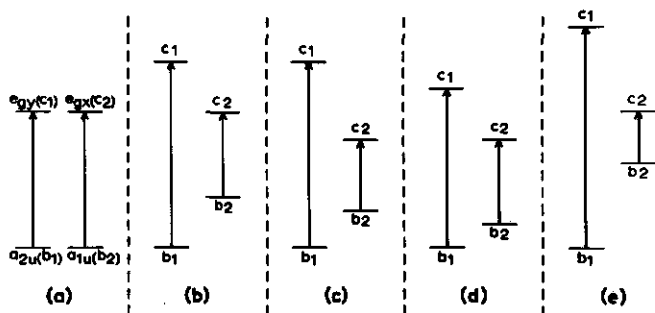
Fig. 6 Energy levels of the two HOMO's (b_1 and b_2) and two LUMO's (c_1 and c_2) of porphin (a), dihydroporphin (b), Ph a (c), Ph b (d) and opposite-tetra-hydroporphin (Bph) (e), as follows from the basic features of Gouterman's 4-orbital model. Arrows denote y-polarized transitions important for CI of the lowest excited state. Interaction with two central protons or a metal ion are ignored.

egy(c1)　　　　　egx(c2)

a2u(b1)　　　　　a1u(b2)
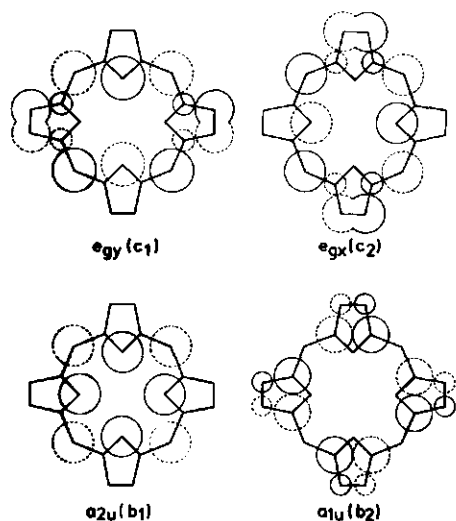
Fig. 7 Electron distribution of the two HOMO's (a_{1u} and a_{2u}) and two LUMO's (e_{gx} and e_{gy}) of D_{4h} porphin as calculated by Gouterman $|12|$. The size of the circles is proportional to the atomic orbital coefficients; dotted or closed circles indicate their sign.

such as porphin, to a typical "long-field" molecule, such as Bph. The concept "long-field"/"round-field" can also be applied to the effect of substituents, when these substituents appreciably participate in the π-electron distribution. Platt's theory predicts a red shift of the Q-band and a simultaneous increase of its oscillator strength for the series porphin → Bph, in agreement with the experimental data (see table 3).

The effects of a change in the long-field/round-field character on the ZFS parameter D in the above mentioned series is similar to that observed for planar aromatics $|20|$. In first order the parameter D depends only on the coördinates of the two unpaired electrons in the triplet state. Bearing this in mind, we will limit our discussion to the two highest occupied (HOMO) and the two lowest unoccupied (LUMO) molecular orbitals as proposed by Gouterman in the 4-orbital model $|12|$. The parallel between the 4-orbital model and the round-field/long-field concept is demonstrated by the fact that both approaches predict strong configuration interaction (CI) for the lowest excited states of porphin and weak CI for the corresponding states of Bph.

Fig. 6a represents the energy levels for the two HOMO's (a_{1u} and a_{2u}) and two LUMO's (e_{gx} and e_{gy}) for D_{4h} porphin. As discussed in appendix A, reduction of one or two pyrrole rings results in a modification of energy levels as shown in fig. 6 b, e. (Because of reduction of symmetry, the levels are denoted by b_1 (a_{2u}), b_2 (a_{1u}), c_1 (e_{gx}), and c_2 (e_{gy}) $|12|$.) The effect

of side groups - in particular carbonyl groups partaking in the π-electron delocalisation - can be understood following the same reasoning as given in appendix A. In first order, a carbonyl group will stabilize those MO's which have electron density on the position where this group is introduced; the amount of stabilization depends on the electron density on this position. Taking into account the electron distributions as calculated by Gouterman |12| (fig. 7), the effect of the ring V keto-group in Ph a w.r.t. unsubstituted dihydroporphins and the effect of the aldehyde group in Ph b w.r.t. Ph a on the energy levels can be qualitatively understood. Fig. 6 c,d shows the relative position of the energy levels for the two HOMO's and two LUMO's for Ph a and Ph b.

As shown by Gouterman |12|, a good description of the lowest excited state of porphyrin like molecules requires the inclusion of CI, which may be restricted to the four top orbitals. As discussed in appendix A, for the lowest excited states of dihydroporphins and tetrahydroporphins it suffices to consider the CI between $| c_1 b_1 >$ (pure excited state obtained by electron promotion from b_1 to c_1) and $| c_2 b_2 >$. Since the amount of CI depends on the energy difference between the interacting states, fig. 6 a-e learns that CI between these pure states decreases for the series porphin - dihydroporphin - Ph b - Ph a - Bph. It should be noted that, since we did not consider the size of the effects, the relative position of Ph b w.r.t. dihydroporphin cannot be settled on the basis of this argument alone; the experimental results, as will be discussed hereafter, point to a decrease of CI for Ph b w.r.t. dihydroporphin.

Assuming that the lowest excited singlet and triplet state approximately have the same zero-order electronic wave functions, we will show that a systematic decrease of the ZFS triplet parameter D follows from the 4-orbital model, when CI is included. Such predictions have been verified by Boorstein et al. |20| for the ZFS parameters of planar aromatics.

As demonstrated by Van der Waals et al. |21| and illustrated by Van Dorp et al. |22| for porphin free base, it is necessary to incorporate many singly excited states for sufficiently reliable calculations of ZFS-parameters. Whereas in first order mixing of the states $|a_{2u} e_{gy}>$ and $|a_{1u} e_{gx}>$ in D_{4h} porphin is prohibited for symmetry reasons |18|, second order effects can mix the states appreciably |23|. For Cu-porphin |23| and free-base porphin |18| it has been shown that there is appreciable CI in the lowest triplet state, with considerable contributions from both 4-orbital

excited states $|a_{2u} e_g>$ and $|a_{1u} e_g>$, forming together $\sim$ 90% from the mixed state. As we are primarily interested in a qualitative consideration of the effect of molecular geometry on D, we will restrict the CI to the 4-orbital model.

Within the framework of the 4-orbital model (i.e. neglecting CI with states involving higher MO's) the effect of CI on ZFS-parameters can be qualitatively predicted using

$$\psi_T = a \; |c_1 b_1>_T + (1-a^2)^{\frac{1}{2}} \; |c_2 b_2>_T \tag{5}$$

as the orbital part of the triplet wave function in eqn (2); it is readily seen that

$$D = a^2 D_1 + (1-a^2)D_2 + 2a\sqrt{(1-a^2)}D_{12} \tag{6}$$

where $D_1 \equiv <c_1 b_1|\underline{D}|c_1 b_1>$, $D_2 \equiv <c_2 b_2|\underline{D}|c_2 b_2>$, $D_{12} \equiv <c_1 b_1|\underline{D}|c_2 b_2>$ and $\underline{a}$ is the CI mixing coefficient |20|; $\underline{D}$ represents the spin-spin interaction operator. Accepting the 4-orbital approximation that the atomic orbital coefficients in the MO's are not appreciably affected by changes of molecular geometry, such that D_1, D_2 and D_{12} are constants, the change of D with molecular geometry is primarily related to the amount of CI.

For the non-charged porphin skeleton, Langhoff |18| has calculated D_1 and D_2 to be nearly equal, implying that a change in D as a result of a change in CI must be mainly due to a variation of the third term in eqn (6) only. From this equation, it is readily found that the contribution of D_{12} has a maximum when $a^2 = 1/2$, i.e. with 50/50 CI mixing, in the case that $D_1 = D_2$.

Under these conditions, eqn (6) predicts that a *decrease* in CI due to reduction of one or more pyrrole rings in the porphin skeleton results in a *decrease* of the observed D value, when the term $2a(1 - a^2)^{\frac{1}{2}} D_{12}$ has the same sign as D_1, D_2. For porphyrin systems this last condition in fulfilled |18|. This prediction is in agreement with the results collected in table 3 bearing in mind the decrease of CI for the series porphin $\rightarrow$ bacteriopheophytin mentioned before. Furthermore, as can be seen from eqn (6), the effects of changes in CI on D are largest when CI is small (a $\sim$ 0, a $\sim$ 1) and are negligible for small deviations from 50/50 mixing.

ZFS parameters for porphin free base are found to be virtually independent from the solvent. D and E values of chlorophylls |3, 5| and

pheophytins, on the contrary, are found to be smaller for ethanol as compared to MTHF as a solvent. Because the same effects are found for chlorophyll and pheophytin, we can exclude the possibility that a change of the interaction between solvent and Mg^{2+} in chlorophyll is responsible for this effect. It is plausible that hydrogen-bondings are formed between the ring V ketogroup and the solvent, only occurring in ethanol solution. Because such an interaction stabilizes extra electron density on the ring V ketogroup oxygen, the effect of this ketogroup on CI is enhanced, resulting in a further decrease of D, in agreement with the results collected in table 1.

Since the ZFS parameter E is more sensitive to *local* electron distribution and orientation of the in-plane axes of the ZFS tensor than D, no reliable analysis of the effect of CI on E seems to be possible in the framework of the 4-orbital model. For all systems, except bacteriopheophytin, we find a single E-value, independent of the method of detection. Until now we have no satisfactory explanation for the 2 E-values found for bacterio-pheophytin. Because both spectra characterized by different E-values, have full spin polarization, the corresponding transitions cannot originate from a dihydroporphin or porphin-like impurity, since for this class of compounds we do not expect full spin polarization, in view of the relatively slow triplet decay.

9.4.2. Electron spin polarization

From the electron spin polarization (ESP) pattern found for Ph a in MTHF and tol/pyr the ordering of the population of the spin levels can be deduced:

$$N_y, N_z > N_x$$

where N_y, N_x and N_z are the steady-state populations of spin levels $|\tau_y>$, $|\tau_x>$ and $|\tau_z>$ in the absence of SLR. When relaxation can be neglected the steady-state population is given by

$$N_i = P_i/k_i \tag{7}$$

where P_i is the populating rate and k_i the depopulating rate constant for spin level $|\tau_i>$. From the kinetic constants given in table 2 one derives relative spin level populations in agreement with the measured ESP pattern.

For Bph in MTHF, one finds AAA EEE (1) and AEA EAE (2) resulting in (1) $N_z > N_x$, N_y and (2) N_z, $N_x > N_y$.

It has been shown that the amount of ESP depends on the ratio of the SLR rate constant and the mean decay rate constant K_T |2|. Since the decay constants for Ph a in MTHF and tol/pyr are almost equal, the difference in ESP has to be attributed to unequal SLR rates in the two solvents. By comparison of the amounts of ESP observed for both solvents, we find that the SLR rate in MTHF is ∿ 2 times larger than in tol/pyr. The full ESP found for Bph can be understood because of its relatively fast mean decay constant K_T.

9.4.3 *The kinetic parameters*

Table 3 compiles the results obtained in the present investigation and previous reports |2, 6, 24, 25|, illustrating the effects of outer ring substitution and replacement of Mg^{2+} by two protons, on the kinetic constants. There are several striking features in these data: substitution of Mg^{2+} by two protons significantly increases the mean decay constant K_T and simultaneously increases the relative contribution of the spin-level $|\tau_z>$ in the intersystem crossing pathway. Furthermore, the ratio between kinetic constants for Ph a and b is of comparable magnitude to that between the corresponding chlorophylls. In general, there is a remarkable parallelism between the magnitude of the kinetic constants for the series porphin free-base → Bph and their Mg^{2+} containing analogs. Finally, it is to be noted that the effect of replacement of Mg^{2+} by protons on the kinetic constants decreases in the series porphin free-base → Bph.

For an understanding of the effects of Mg^{2+} substitution by two protons and perturbation by side groups on kinetic constants of the triplet state, we make use of the concepts outlined by Antheunis |26| and Metz |27|. Denoting the *non radiative* intersystem crossing (ISC) rate constants (i.e. populating and depopulating rate constants) to and from triplet spin level $|\tau_u>$ by K_u, we may use as a starting point for our discussion the statement of Antheunis |26|, that there are two factors determining the magnitude of K_u:

a) Franck-Condon (FC) overlap integrals between the iso-energetic states T_0 (v) and S_1(0) for the populating process and the states T_0(0) and S_0(v) for the decay of the lowest triplet state. These integrals are *independent* of the spin state $|\tau_u>$. (The symbol in parentheses (o,v) denotes the vibrational state.)

b) A spin-orbit coupling (SOC) factor depending on the interaction of a
particular spin state $|\tau_u\rangle$ with the relevant singlet state.

In the following we will be mainly interested in the decay mechanism,
since we have only determined absolute rate constants for decay. The FC factor
dependence of the decay rate constants k_u is represented in eqn (8).

$$k_u = \frac{2\pi}{\hbar} \; C_u^2 \; \underset{v}{\Sigma} \; |S[T_u(o); S_o(v)]|^2 \; \delta(E_{T_u(o)} - E_{S_o(v)}) \tag{8}$$

formulated by Englman and Jortner |28|. C_u is the SOC matrix element between
the electronic states and $S|T_u(o); S_o(v)|$ is the familiar FC overlap integral
between the vibration-less triplet state T_u (T_u is product function of spin
and orbital parts: $T_u = T_o \cdot |\tau_u\rangle$) and the vibrationally excited level of the
ground state S_o with energy $E_{S_o(v)}$; summation extends over the vibronic states
coupled to T_u. Eqn (8) can be worked out to give the so called *energy gap law*

$$k_u = C_u^2 \; \frac{\sqrt{2}\,\pi}{\hbar\sqrt{(\hbar \; \omega_m \Delta E)}} \; \exp(-\gamma\Delta E/\hbar\omega_m) \tag{9}$$

where ΔE is the energy separation between the electronic states T_u and S_o;
ω_m is the frequency of the vibrational mode(s), which are relevant for the
radiationless process and γ is a parameter, dependent on the relative dis-
placement of the potential energy surfaces in the two electronic states, and
which is estimated for planar aromatics to be in the range 0.50 - 1.31 |28|.
It can be shown that only the term C_u^2 is spin-state dependent |26|; this
means that the *relative* participation of the spin levels $|\tau_x\rangle$, $|\tau_y\rangle$ and $|\tau_z\rangle$
is determined by the matrix element C_u exclusively. For the mean decay
constant K_T, C_u as well as the ΔE dependent part of eqn (9) have to be taken
into account.

Eqn (9) can be rearranged in the following way,

$$\ln \{k_u \cdot (\Delta E)^{\frac{1}{2}}\} = C_1 - C_2 \cdot \Delta E \tag{10}$$

where $C_1 = \ln \{\frac{C_u^2}{\hbar} \; (\frac{2\pi}{\hbar\omega_m})^{\frac{1}{2}}\}$

and $C_2 = \gamma(\hbar\omega_m)^{-1}$.

Fig. 8 represents a plot of the data for the series Mg-porphin/Chl a, as well
as for the series porphin/Ph a, according to eqn (10). The values for ΔE
are obtained from phosphorescence data |9, 29|. As shown in this figure, the

mean decay constant, $K_T = 1/3 \sum_u k_u$, for the radiationless decay of photo-synthetic pigments and some model compounds follow the energy-gap law with $\gamma / \omega_m \sim 10^{-3}$.

Assuming that ω_m corresponds to a CH stretching vibration, such as has been proposed by Englman et al. |28| for planar aromatics, one finds $\gamma \sim 3$ with $\omega_m \sim 3000$ cm^{-1}. This value for γ is significantly larger than found for aromatic compounds and also about one order of magnitude larger than the value calculated for porphyrins following Englman's theory |28|. This discrepancy indicates that it is probably incorrect to assume that radiationless $T_1 \rightarrow S_0$ transitions in porphyrin like compounds are determined by C—H stretching vibrations only. As pointed out by Henry and Siebrand |30| it is not only the CH stretch vibration with highest frequency which has to be considered; for molecules with a small energy gap, as for porphyrins, C—C skeleton vibrations become also important for the FC factor in eqn (9),
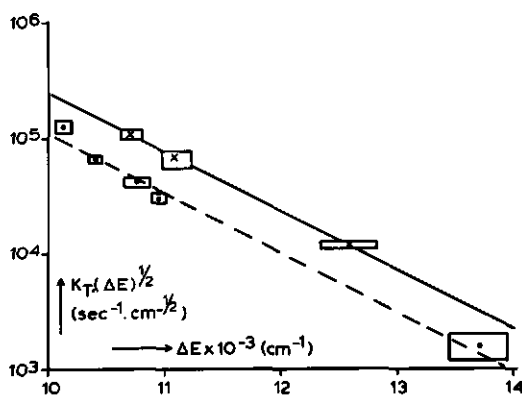
Fig. 8 Energy gap-law as given in eqn (10), defining the dependence of triplet decay constant K_T on $\Delta E \equiv E(T_o) - E(S_o)$, applied to photosynthetic pigments. Data points for the free base compounds: Ph a in MTHF (λ_{ph} = 935 $\pm$ 10 nm |9|, K_T = 1050 $\pm$ 100 sec^{-1}), Ph b in MTHF (λ_{ph} = 900 $\pm$ 10 nm |9|, K_T = 630 $\pm$ 120 sec^{-1}), porphin free-base in n-octane (λ_{ph} = 795 $\pm$ 15 nm |29|, K_T = 105 $\pm$ 5 sec^{-1} |24|) are indicated by crosses; dots mark the data for the Mg-containing compounds: Chl a in ethanol (λ_{ph} = 987 $\pm$ 7 nm) |9, 16|, K_T = 1250 $\pm$ 150 sec^{-1} |16|), Chl a in MTHF (λ_{ph} = 960 $\pm$ 5 nm |16|, K_T = 630 $\pm$ 40 sec^{-1} |16|), Chl b in ethanol (λ_{ph} = 929 $\pm$ 10 nm |16|, K_T = 410 $\pm$ 30 sec^{-1} |16|), Chl b in MTHF (λ_{ph} = 913 $\pm$ 5 nm |16|, K_T = 290 $\pm$ 30 sec^{-1} |2, 16|) and Mg-porphin in n-octane, containing ethanol (λ_{ph} = 730 $\pm$ 15 nm |29|, K_T = 14 $\pm$ 3 sec^{-1} |25|). Error limits are indicated by rectangles.

if they are related to a large displacement of the potential energy surface of the triplet state w.r.t. the ground state. The participation of C—C skeleton vibrations in the radiationless decay will influence the constant C_2 in eqn (10). When, for example, instead of $\omega_m = 3000$ cm^{-1} one assumes ω_m to be ~ 1400 cm^{-1} (frequency of C—C skeleton modes) one finds from fig. 8 $\gamma \sim 1.4$, whereas this value for ω_m, introduced in the expression for γ as given by Englman et al. |25|, gives $\gamma \sim 0.5 - 1$ dependent on the number of modes and the displacement of the potential energy surface.

In the foregoing it was supposed that the pre-exponential factor C_u^2 (eqn (9)) was constant in the series Mg-porphin/Chl a. One should realize however, that the reduction of a pyrrole ring and the introduction of carbonyl groups can affect the factor C_u^2 because of the introduction of new vibrations, inducing vibronic couplings which, as will be discussed hereafter, determine the radiationless decay. The presence of these effects is clearly demonstrated by the fact that the relative participation of the spin levels $|\tau_x>$ and $|\tau_y>$ in the ISC processes is not the same for all compounds in both series, which can only be explained by a change of the ratio $|C_x|^2/|C_y|^2$ because the FC factor in eqn (9) is spin-state independent. In view of this effect, the linear relationship, shown in fig. 8 is rather surprising, since the series Mg-porphin/Chl a cannot be considered as an ideal model for a check of the energy gap law.

One point, however, is clear: the change in K_T upon substitution of Mg^{2+} by two protons cannot be explained by a change in energy gap only. Since the Mg^{2+}/2H$^+$ substitution may change the energy levels of electronic states, as well as the number and the nature of vibrations operative in ISC, in the following we will shortly discuss the origin of the factor C_u^2 in eqn (9).

Expressing the wavefunction for the ground state S_0 and the lowest excited triplet state T_u (u = x, y, z) in a Herzberg-Teller expansion and retaining only the one-center one-electron integrals, Antheunis et al. |26| have shown that eqn (8) can be expanded as:

$$k_u(T_u \to S_0) = \frac{2\pi}{\hbar} |C_u^{(0)}|^2 \cdot F + \frac{2\pi}{\hbar} |C_u^{(1)}|^2 \cdot F + \frac{2\pi}{\hbar} |C_u^{(2)}|^2 \cdot F \qquad (11)$$

where F is the Franck-Condon (FC) factor containing the ΔE dependence resulting in the energy gap law and $C_u^{(0)}$ through $C_u^{(2)}$ represent matrix elements for vibronic spin-orbit coupling up to second order.

As all compounds, discussed in this paper, have a $\pi\pi^*$ lowest excited singlet and triplet state, the term $C_u^{(0)}$ can be shown to vanish, as long as only one center integrals are considered and any non-planarity is neglected |27|. The term $C_u^{(1)}$, however, will be non-zero especially for the spin levels $|\tau_x\rangle$ and $|\tau_y\rangle$. It can be shown |26| that $C_u^{(1)}$ contains, beside terms related to the vibronic dependence of the spin-orbit interaction, products of SOC matrix elements $\langle \mathcal{H}_{SO}\rangle$, vibronic coupling matrix elements $\langle \mathcal{H}^1\rangle$ and the inverse of the energy gap between the vibronically coupled states (ΔE^1):

$$\frac{\langle \mathcal{H}^1\rangle \; . \; \langle \mathcal{H}_{SO}\rangle}{\Delta E^1} \tag{12}$$

Retaining only one-center one-electron SOC integrals, the vibronic coupling of S_0 with singlet $\sigma\pi^*$, $\pi\sigma^*$ and $n\pi^*$ states will result only in non-zero contributions to $C_x^{(1)}$ and $C_y^{(1)}$; $C_z^{(1)}$ vanishes in this approximation. For the spin level $|\tau_z\rangle$, $C_u^{(2)}$ is the first non-zero term; its contribution to the decay constant k_u is expected to be smaller than the contribution of the term $C_u^{(1)}$, since here vibronic coupling has to involve S_0 as well as T_0.

Thus, apart from the dependence of K_T on the energy gap ΔE, as expressed by the energy-gap law, there are three possible mechanisms which can affect K_T, when the molecular structure is changed:

(a) a change in γ and/or ω_m will affect the FC factor (see eqn (9));

(b) a change of the energy-gap between $n\pi^*$, $\sigma\pi^*$ or $\pi\sigma^*$ states and $\pi\pi^*$ states affects the factors $C_u^{(1)}$ and $C_u^{(2)}$ (see eqn (12));

(c) a change in the nature or number of modes, responsible for the vibronic coupling matrix element $\langle \mathcal{H}^1\rangle$ also affects $C_u^{(1)}$ and $C_u^{(2)}$ (see eqn (12)).

Applying these concepts to porphin-like systems, we will show that effects (b) and (c) presented before, are sufficient to explain the effect of $Mg^{2+}/2H^+$ substitution on K_T. A double negatively charged porphin skeleton, without metal-ion or central protons, has four occupied non-bonding orbitals. When Mg^{2+} is introduced into the ring, the interaction with this ion will stabilize all four, originally non-bonding orbitals, since an equivalent bonding of Mg^{2+} with the four nitrogens is expected. On the other hand, when Mg^{2+} is substituted by two protons, these protons will mainly interact with two opposite nitrogens, the non-bonding orbitals of the remaining two free nitrogens being very similar to those in the double negatively charged case. Thus, the free base compounds will have lower lying $n\pi^*$ states than the Mg-containing compounds. As can be concluded from the ΔE^1 dependence of terms given in (12), the lowering of the energy of the $n\pi^*$ states in free base

compounds w.r.t. Mg-containing compounds will affect the ISC processes. Van Dorp et al. |24| have discussed such effects for porphin free base: the ISC processes for *one* of the in plane spin levels ($|\tau_x>$) increases because of an increase of $C_x^{(1)}$; for the other spin levels only the second order term $C_u^{(2)}$ is involved in these processes.

In addition to the ΔE^1 effect, considered by Van Dorp et al. |24|, the introduction of two N—H fragments as in pheophytins and porphin free-base may change the magnitude of $<\mathcal{H}^1>$ in eqn (12) and even may introduce contributions of new vibrations. Whereas the effect of the introduction of a low lying $n\pi^*$ state on each of the three triplet spin-states separately can be understood in the theoretical framework formulated by Antheunis |26|, the effect of the changed vibronic coupling matrix elements on the various spin levels is much more difficult to predict. Therefore, for the moment, we will limit our discussion to the effects of both ΔE^1 and $<\mathcal{H}^1>$ on the *mean* decay constant K_T.

As is shown in table 3 for all compounds discussed in this paper the $Mg^{2+}/2H^+$ substitution results in an increase of K_T. In contrast with porphin free-base, for Ph a and Ph b the triplet state energy is nearly the same as or slightly higher than the triplet state energy of the corresponding Mg-containing compounds |9|. So the increase of K_T has to be attributed to one of the three effects mentioned before. The parallel between the energy gap dependence of K_T found for both series as shown in fig. 8, indicates that the $Mg^{2+}/2H^+$ substitution does not affect the constant C_2 in eqn (10). Whereas it cannot be excluded that an opposite change of γ and $\hbar\omega_m$ takes place, we attribute the change of the constant C_1 in eqn (10) exclusively to a change in C_u, keeping $\hbar\omega_m$ roughly constant. Whether the change of the $n\pi^*$ energy level or the change of vibronic coupling matrix elements or both are responsible for these change in C_u cannot be decided on the basis of the available experimental results and theoretical considerations given in this study. The agreement between theoretical predictions based on Antheunis |26| work and experimental results of Van Dorp et al. |24| w.r.t. the ratio k_x/k_y, where k_x, k_y are the decay constants for $|\tau_x>$ and $|\tau_y>$, points to the importance of a lowering of the $n\pi^*$ state. On the other hand, from recent results of Völker et al. |31|, exhibiting a decrease of K_T for porphin free base after substitution of the two central protons by two deuterons ($K_T^{H}2 = 92$ sec^{-1}, $K_T^{D}2 = 46$ sec^{-1}), it can be concluded that the effect of the N—H fragments on the vibronic coupling matrices cannot be neglected.

Until now we have only considered the mean decay constant K_T.
We will now proceed with discussing the decay of the individual spin states.
Since we do not know the orientation of the in-plane axes of the ZFS tensor
w.r.t. the molecular frame, we cannot correlate the changes in the ratio
k_x/k_y with molecular structure. As discussed before, theory predicts that
lowering of $n\pi^*$ states, as well as changes in vibronic coupling matrix
elements, will mainly influence the ISC processes of $|\tau_x\rangle$ and/or $|\tau_y\rangle$ because
of a non-zero first order term $C_u^{(1)}$ for these states (cf. eqn (11)). There-
fore, one would expect a decrease of the relative participation of the spin
level $|\tau_z\rangle$, whose contribution to K_T depends on the second order term $C_u^{(2)}$
in eqn (11), in the triplet decay. The experimental results, however, show
an increase of k_z/K_T on $Mg^{2+}/2H^+$ substitution. In the following, we will give
a tentative explanation for this effect.

In the free-base compounds, two N-atoms do not participate in the
most probable conjugation path $|12|$. This results in localized π-electron
densities on these N-atoms, so that multi-center $\pi\pi^*$ SOC integrals no longer
can be neglected as in Metz' $|27|$ and Antheunis' $|26|$ work. Since these
integrals mainly attribute to k_z $|26|$, the increase of k_z/K_T can be attributed
to the introduction of such relatively localized π-orbitals and not to the
lowering of the $n\pi^*$ states or the change in the matrix elements $\langle \mathcal{H}^1 \rangle$.

Finally, we will discuss shortly the effects of pyrrole ring
reduction and side group substitution on the triplet decay mechanisms. As
shown in table 3, the ratio of decay constants for Mg-containing and free-
base compounds increases for the series Mg-porphin/porphin $\to$ BChl/BPh. This
effect can be fully explained as a result of changes in the energy gap
ΔE $(E(T_0) - E(S_0))$. As mentioned before, substitution of Mg^{2+} by $2H^+$ in porphin
results in a decrease of the triplet state energy, whereas a similar substitu-
tion in Chl/Ph causes a slight increase of ΔE $|9|$, so that the effects of the
substitution on the ΔE dependent part of eqn (9) and the C_u dependent part
on K_T reinforce each other for porphin, whereas in Chl/Ph these effects work
in the opposite direction. Because sufficiently reliable data for the triplet
energy levels of Chl $\underline{a}$/Ph $\underline{a}$ and Chl $\underline{b}$/Ph $\underline{b}$ are lacking, we cannot correlate
the increase of $K_T^{Mg}/K_T^{H_2}$ for Chl $\underline{a}$/Ph $\underline{a}$ w.r.t. Chl $\underline{b}$/Ph $\underline{b}$ with shifts in
triplet state energy levels. It should be noted, however, that the change in
singlet state energy on $Mg^{2+}/2H^+$ substitution (ΔQ_{oo}, see tabel 3) is smaller
for Chl $\underline{a}$/Ph $\underline{a}$ than for Chl $\underline{b}$/Ph $\underline{b}$. It is interesting to note that from the
increase of $K_T^{Mg}/K_T^{H_2}$ one derives a similar change in the triplet state energy
levels.

When considering the effects of pyrrole ring reduction and side group substitution, we want to point out that these changes in molecular structure will induce an inequivalence between two sets of opposite N-atoms in the chlorophylls and dihydroporphin, comparable to the effect of the introduction of two protons in the center of the ring. For example, in BChl the most probable conjugation path for π-electrons will not contain the two N-atoms of unsaturated pyrrole rings. The π-electron orbitals localized on these N-atoms can induce a relatively large contribution of the $|\tau_z>$ state to the triplet decay, as for the free-base compounds. As is shown in table 3, experimentally it is found indeed that k_z/K_T increases in the series Mg-porphin/BChl.

The redistribution of the π-electron density for the series Mg-porphin/BChl, responsible for the inequivalency of the two sets of opposite N-atoms, is also reflected in the change of the position of the Q-band (ΔQ_{oo}) and the change of the ZFS-parameters D ($D^{Mg}/D^{H}2$), when Mg^{2+} is substituted by two protons. Both ΔQ_{oo} and $D^{Mg}/D^{H}2$ decrease, as shown in table 3. This can be understood when we realize that the effect of the protons on the inequivalency between the two sets of opposite N-atoms decreases in the series Mg-porphin/BChl, because of the increasing inequivalency already present in the Mg-containing compounds. ΔQ_{oo} even changes sign, since besides the effect of induced inequivalence of the two sets of N-atoms, the electronegativity of the two protons together is larger than the electronegativity of Mg^{2+}. As pointed out already by Gouterman |11| this results in a blue-shift of the Q-band and thus in a negative contribution to ΔQ_{oo}.

Comparing the values of ΔQ_{oo} and $K_T^{Mg}/K_T^{H}2$ for Chl $\underline{a}$/Ph $\underline{a}$ and Chl $\underline{b}$/Ph $\underline{b}$, as well as k_z/K_T for Chl $\underline{a}$ and Chl $\underline{b}$, we conclude that the increase of round-field character, induced by the introduction of the aldehyde group in Chl $\underline{b}$/Ph $\underline{b}$, is probably not restricted to the four orbitals, considered in Gouterman's model. From the results in table 3 and the before mentioned theory, the π-electron distribution w.r.t. the four N-atoms is more symmetrical in Chl $\underline{b}$ than in Chl $\underline{a}$, resulting in a larger effect of the $Mg^{2+}/2H^{+}$ substitution in Chl $\underline{b}$.

9.5 CONCLUSIONS

1. The effects on the ZFS-parameter D of substitution by sidegroups or reduction of pyrrole rings, occurring in photosynthetic pigments, can be qualitatively understood by considering the configuration interaction between excited states constructed from the four orbitals in Gouterman's model |8|.

2. Steady state populations of the three spin-levels of pheophytins, during continuous optical excitation, have been found to be different from those for the related chlorophylls: the out-of-plane $|\tau_z\rangle$ spin level in pheophytins carries a *relatively* larger population than in the corresponding chlorophylls.

3. For all three spinlevels of pheophytins the radiationless decay constants are found to be larger than for the corresponding chlorophylls.

4. The difference between radiationless decay constants of pheophytins and corresponding chlorophylls cannot be explained by considering the spin-independent part of the energy-gap law, but can be understood by including the effects of $Mg^{2+}/2H^+$ substitution on vibronic coupling and the energy level of $n\pi^*$ states, relevant for this coupling.

5. A relative increase of k_z in pheophytins w.r.t. chlorophylls can be explained by a tentative model invoking localized π orbitals, giving rise to non-negligible multicenter $\pi\pi^*$ SOC integrals.

9.6 REFERENCES

1. R.H. Clarke, R.H. Hofeldt, J. Am. Chem. Soc., 61, 4582 (1974).
2. J.F. Kleibeuker, T.J. Schaafsma, Chem. Phys. Lett., 29, 116 (1974).
3. M.C. Thurnauer, J.J. Katz, J.R. Norris, Proc. Nat. Acad. Sci. USA, 72, 3270 (1975).
4. R.H. Clarke, R.E. Connors, T.J. Schaafsma, J.F. Kleibeuker, R.J. Platenkamp, J. Am. Chem. Soc., 98, 3674 (1976).
5. J.F. Kleibeuker, R.J. Platenkamp, T.J. Schaafsma, Chem. Phys. Lett., 41, 557 (1976).
6. R.H. Clarke, R.E. Connors, H.A. Frank, Biochem. Biophys. Res. Commun., 71, 671 (1976).
7. P.L. Dutton, J.S. Leigh, M. Seibert, Biochem. Biophys. Res. Commun., 46, 406 (1972).
8. D.M. Tiede, R.C. Prince, G.H. Reed, P.L. Dutton, FEBS Lett., 65, 301 (1976).

9. A.A. Krasnovskii jr., N.N. Lebedev, F.F. Litvin, Dokl. Akad. Nauk SSSR, 216, 1406 (1974).

10. H. Levanon, S. Vega, J. Chem. Phys., 61, 2265 (1974).

11. M. Gouterman, J. Chem. Phys., 30, 1139 (1959).

12. M. Gouterman, J. Mol. Spectrosc., 6, 138 (1961).

13. H.C. Longuet-Higgins, C.W. Rector, J.R. Platt, J. Chem. Phys., 18, 1174 (1950).

14. J.H.C. Smith, A. Benitz, in "Moderne Methoden der Pflanzenanalyse", vol. IV, eds. K. Paeck, M.V. Tracey, Berlin, 1955.

15. H.H. Strain, W.A. Svec, in "The chlorophylls", eds. L.P. Vernon, G. Seely, New York, 1966.

16. J.F. Kleibeuker, Thesis, Agricultural University, Wageningen, 1977.

17. U. Eliav, H. Levanon, Chem. Phys. Lett., 36, 377 (1975).

18. S.R. Langhoff, E.R. Davidson, M. Gouterman, W.R. Leenstra, A.L. Kwiram, J. Chem. Phys., 62, 169 (1975).

19. J.R. Platt, J. Chem. Phys., 18, 1168 (1950).

20. S.A. Boorstein, M. Gouterman, J. Chem. Phys., 39, 2443 (1963).

21. J.H.van der Waals, G. ter Maten, Mol. Phys., 8, 301 (1964).

22. W.G. van Dorp, M. Soma, J.A. Kooter, J.H. van der Waals, Mol. Phys., 28. 1551 (1974).

23. B. Roos, M. Sundbom , J. Mol. Spectrosc., 36, 8 (1970).

24. W.G. van Dorp, W.H. Schoemaker, M. Soma, J.H. van der Waals, Mol. Phys., 30, 1701 (1975).

25. G. Jansen, J.H. van der Waals, Chem. Phys. Lett., 43, 413 (1976).

26. D.A. Antheunis, J. Schmidt, J.H. van der Waals, Mol. Phys., 27, 1521 (1974); D.A. Antheunis, Thesis, University of Leiden, 1974.

27. F. Metz, S. Friedrich, G. Hohlneicher, Chem. Phys. Lett., 16, 353 (1972); F. Metz, Chem. Phys. Lett., 22, 186 (1973).

28. R. Englman, J. Jortner, Mol. Phys., 18, 145 (1970).

29. M.P. Tsvirko, K.N. Solovev, A.T. Gradyushko, S.S. Dvornikov, Opt. Spectrosc., 38, 400 (1975).

30. B.R. Henry, W. Siebrand, in "Organic Molecular Photophysics", ed. J.B. Birks, London, 1973.

31. S. Völker, J.H. van der Waals, Mol. Phys., 32, 1703 (1976).

32. S.J. van der Bent, T.J. Schaafsma, Chem. Phys. Lett., 35, 45 (1975).

33. U. Eisner, R.P. Linstead, J. Chem. Soc., 1955, 3749.

10 Properties of the lowest excited triplet state of chlorophyll

10.1 INTRODUCTION

In the preceding Chapters we have presented and discussed most experimental data. This Chapter contains a general outline of the properties of the triplet state of chlorophylls, based on these and some additional results.

10.2 PHOSPHORESCENCE OF CHLOROPHYLLS

Phosphorescence spectra of Chl a and b, reported by Krasnovskii [1], lead to the conclusion that the position of the lowest triplet is strongly solvent-dependent, similarly to the behaviour of other triplet state parameters (Chapter 7, 9). We have carried out similar measurements, especially for comparison of the triplet state energies of photosynthetic pigments in MTHF and ethanol. In table 1 the results for Chl a and b are collected. In ethanol the $S_0(0) \leftarrow T_0(0)$ transition occurs at a longer wavelength than in MTHF for both compounds. The presence of an aldehyde group in Chl b raises the triplet state energy, whereas it reduces the solvent shift. Up to now, we did not find any phosphorescence for Bchl below 1100 nm, the limit of our apparatus. Using the energy gap law, as plotted in fig. 8, Chapter 9, and the mean decay constant K_T of Bchl, measured by Clarke [2] ($K_T = 2100$ sec^{-1}), the phosphorescence wavelength of Bchl can be estimated to be ~ 1100 nm.

Table 1   Phosphorescence wavelength (nm) of Chl a and b

compound	solvent	
	MTHF	ethanol
Chl a	959 ± 3	987 ± 5 (985^{*})
Chl b	914 ± 3	929 ± 10 (912^{*})

*Krasnovskii [1]

Table 2 ZFS parameters of chlorophylls (T = 100 K)

compound/solvent	$D \times 10^4 \ cm^{-1}$	$E \times 10^4 \ cm^{-1}$
Chl b in MTHF	294+3	48+1
tol/pyr	293+3	51+2
ethanol	286+3	37+1
Chl a in MTHF	280+2	40+1
tol/pyr	279+2	40+2
ethanol	272+4	32+2
Bchl in MTHF	232+4	58+3
tol/pyr	227+3	55+3

10.3 ZFS PARAMETERS OF CHLOROPHYLLS

Preliminary values of ZFS parameters of Chl a and Chl b have
been presented in Chapter 7. More accurate measurements have resulted in the
values given in table 2. For both Chl a and Chl b in MTHF the ZFS parameters
are temperature-independent in the range 15 - 103 K; for the other solvents
no temperature-dependent studies have been performed. Furthermore, optical
excitation of Chl a in the Q-band, having a relatively large extinction co-
efficient, results in the same D and E values as excitation in the Soret
band. The D- and E-values for Chl a and b in ethanol and tol/pyr agree with
those given by Norris [3] ; for Bchl in tol/pyr we find a slightly higher
value than reported by this author [3] .

The decrease of the D-value in the series Chl b in MTHF -
Chl b in ethanol - Chl a in MTHF - Chl a in ethanol - Bchl in MTHF parallels
the decrease of D for the corresponding series of pheophytins. Similar to the
situation in pheophytins (see Chapter 9), this reduction of D can be related
to a decreasing triplet state CI in this series. Again, the effects of CI on
E-values are more difficult to interpret. From the definition of E, given in
Chapter 2, it can be seen that calculated E-values are strongly dependent on
the orientation of the in-plane ZFS tensor axes w.r.t. the molecular frame.
As noted in Chapter 8, in Chl a and b these axes may be oriented quite
differently. Also optical magnetoselection experiments provide evidence for
a rotation of the ZFS tensor axes in Chl b w.r.t. Chl a [4] .

Table 3 Kinetic triplet state parameters of chlorophylls; k_i represents the depopulating rate constant and P_i the relative populating rate for spin level $|\tau_i \rangle$ (i = x, y, z); $K_T \equiv 1/3 \sum_i k_i$; (eth. $\equiv$ ethanol).

compound	solvent	sec^{-1}				%		
		K_T	k_x	k_y	k_z	P_x	P_y	P_z
Chl b	MTHF	290+30	270+30	570+30	40+20	35+3	58+3	4+2
	eth.	410+30	310+30	850+30	65+20	27+3	66+3	7+3
Chl a	MTHF	630+60	620+80	1120+20	140+40	31+3	60+3	11+3
	eth.	1250+100	710+100	2710+100	370+50	25+4	65+4	10+2

10.4 TRIPLET STATE KINETICS OF CHLOROPHYLLS

Using the electronic network, described in section 3.3.3, the relative populating rates P_i and the depopulating rate constants k_i have been deduced from the ESR transients by analogue simulation (see Chapter 3). Table 3 presents the data for Chl a and b in MTHF and ethanol at 100 K.

From transient analysis using analogue simulation we could not derive accurate values for the SLR rate constants. Generally, these rate constants are likely to be different for each of the three canonical orientations, but not much is known about this SLR anisotropy. For Chl a in MTHF we found the following ranges for the SLR rate constants, which were consistent with a satisfactory simulation of the transients with P_i and k_i values given in table 3: $2200 \ sec^{-1} < W^y < 3400 \ sec^{-1}$, $3400 \ sec^{-1} < W^x < 10000 \ sec^{-1}$, $5000 \ sec^{-1} < W^z < 6600 \ sec^{-1}$, where W^i is the SLR rate constant for $\vec{H}//i$. The relative large uncertainty in W^x results from the absence of pronounced peaks in the X-transients, immediately after switching light on or off, as is found for the Y and Z transients, so that there are less features to fit the simulated curves (see fig. 3, Chapter 3). For both Chl a and Chl b the mean SLR rate constant increases roughly with a factor of two when ethanol is replaced by MTHF as a solvent. Then, eqn. (7) (Chapter 3) predicts a decrease of the ESP ratio in ethanol w.r.t. MTHF, due to increased SLR. As stated in Chapter 7, such a decrease was found for Chl b. On the other hand, Chl a exhibits a considerable amount of ESP, both in MTHF and in ethanol, which can be attributed to the strongly increased mean decay constant K_T in ethanol w.r.t. MTHF solution. However, the ESP ratio is not very suitable to

support such conclusions, since it appears to be very sensitive to small changes in kinetic parameters. As an example, the calculated ESP ratio R_y for Chl $\underline{a}$ in MTHF, using the error limits of k_i and P_i given in table 3, ranges from 72.3 x $(\delta W)^{-1}$ to -91.2 x $(\delta W)^{-1}$. Therefore, no reliable information on changes in k's, P's or W's can be obtained from ESP ratios alone.

10.5   CONCENTRATION DEPENDENCE OF TRIPLET STATE PARAMETERS

The data collected in tables 2 and 3 refer to $10^{-3} - 10^{-4}$ M chlorophyll solutions, whereas the phosphorescence data presented in table 1 are obtained with $\sim 5 \times 10^{-6}$ M solutions. In order to check concentration effects on triplet state parameters, we have measured ZFS parameters as well as Y^- and Y^+ transients of Chl $\underline{a}$ in MTHF and ethanol in the concentration range $5 \times 10^{-6} - 2 \times 10^{-3}$ M. In this range the ZFS parameters are found to be concentration-independent. Also, the transients are qualitatively the same for all concentrations; because of low S/N ratio, especially for the most diluted solutions, we could make a qualitative comparison only. In view of the polarity of the solvents and our experimental results, we conclude that our ESR and phosphorescence data refer to monomeric chlorophylls.

10.6   SOLVATION OF CHLOROPHYLLS

Titration experiments by Evans et al. [5] have shown that the Mg-ion in chlorophylls is six-coordinated for $\sim 90\%$ of the dissolved molecules in tol/pyr solutions at 293 K. Taking into account the temperature dependence of the equilibrium between the mono- and biligated complex, as discussed for MgTBP in Chapter 5, it seems reasonable to assume that at T < 100 K chlorophylls in tol/pyr are almost fully biligated.

The occurrence of biligation is clearly seen in the Q_x-band shift in the absorption spectrum of Bchl [5]. For the monoligated species this band is found at ~ 580 nm, shifting to ~ 610 nm on biligation. For Bchl in MTHF at 293 K we found the Q_x-band at ~ 590 nm, indicating that most molecules are still mono-ligated. Upon cooling this solution to 100 K this band shifts to 608 nm, which we take as evidence for the presence of almost exclusively biligated Bchl. Since all ESR experiments are carried out at this or still lower temperatures, the triplet parameters determined from these experiments are those of biligated Bchl in MTHF as well as in tol/pyr solutions.

118

For Chl $\underline{a}$ and $\underline{b}$ the effect of biligation is less clearly de-
fined. Comparing the absorption spectra of both chlorophylls in MTHF and
tol/pyr, we expect appreciably more biligation for the latter solvent, as
was found for MgTBP and Bchl. There are three main differences in spectral
behaviour of tol/pyr w.r.t. MTHF solutions:
  a) a red shift of the Soret band;
  b) a small red shift of the Q_y-band;
  c) a small but distinct, band appearing at 633 nm in the absorption spectrum
     of Chl $\underline{a}$ in tol/pyr, which was attributed to Q_x by Evans et al. [5].
All three effects are in agreement with the theoretical discussion given in
Chapter 5, indicating an appreciable amount of biligation of Chl $\underline{a}$ and $\underline{b}$ in
tol/pyr at 293 K. Again, as for Bchl, we expect that at the temperature of
our ESR experiments (T < 100 K) Chl $\underline{a}$ and $\underline{b}$ are biligated in tol/pyr. To
determine their state of ligation in MTHF and ethanol at 100 K, we have
studied the temperature-dependence of the absorption spectra of Chl $\underline{a}$ in
these solvents. As shown in table 4, lowering the temperature has roughly
the same effects as dissolving in tol/pyr. Some cautious comments have to be
made however. Apart from a red shift of the Soret band for Chl $\underline{a}$ in MTHF,
this band is split, which can be attributed to the presence of mono- and bi-
ligated Chl $\underline{a}$ in MTHF at 100 K or to a splitting of the Soret-band in B_x and
B_y components. It is generally accepted that the Soret-band at room tempera-
ture contains both transitions [6]. As discussed in Chapter 5, the effect of
ligation is expected to be different for the x and y polarized transitions,
which may result in the observed splitting. Furthermore, the triplet state
parameters for Chl $\underline{a}$ in tol/pyr and MTHF are exactly the same and we may
conclude that in MTHF Chl $\underline{a}$ is almost fully biligated like in tol/pyr. Recent
results of Kooyman et al. [7] using ODMR techniques, indicate that the ZFS
parameters for monoligated Chl $\underline{a}$ differ appreciably from those of the bili-
gated species. The possibilities of the presence of monoligated Chl $\underline{a}$ in
MTHF at 100 K, however, cannot be completely eliminated. Until now, no
$\Delta m = 1$ triplet ESR spectrum of the monoligated Chl $\underline{a}$ at 100 K was measured,
perhaps because of a very low steady state triplet state population.

        In conclusion, experimental triplet state parameters are
attributed to biligated Chl $\underline{a}$; the origin of the splitting of the Soret-band
in the absorption spectrum cannot be solved without further experiments.

        For ethanolic Chl $\underline{a}$ solutions no splitting of the Soret-band
is found in the temperature range 100-300 K. When the temperature is lowered,
the red shift of the Soret-band as well as of the Q-band, is larger in

Table 4 Wavelength (nm) of absorption bands (B I, B II, Q_x and Q_y) of Chl a ($\sim 5 \times 10^{-5}$ M) in MTHF and ethanol at different temperature (T). The two components of the Soret-band in MTHF at low temperature are denoted as B I and B II (see text); when only one band is present it is denoted as B I.

compound/solvent	T(K)	B I	B II	Q_x	Q_y
Chl a in MTHF	293	432	–	–	663
	173	436	442	(626)	666
	93	439	443	633	670
Chl a in ethanol	293	431	–	–	664
	173	444	–	643	670
	93	449	–	649	675

ethanol than in MTHF. Furthermore, a striking difference with the absorption spectra of Chl a in MTHF at 100 K is the position of the Q_x-band. Whereas in MTHF (100 K) and tol/pyr (293 K) this band is located at $\sim$ 633 nm, in ethanol (100 K) the corresponding band is found at 649 nm. Delaying the discussion about the difference between MTHF and ethanol solutions to the next section, we now consider the agreement w.r.t. the temperature dependence. The red shift of the Soret-band (430 → 450 nm) as well as the appearance of a Q_x-band at 100 K indicates the presence of mostly biligated Chl a in ethanol at this temperature, just as we found for the MTHF and tol/pyr solutions.

10.7 GENERAL DISCUSSION

Chlorophylls contain functional groups, which are suitable for many kinds of interaction with the surroundings or with other chlorophyll molecules. (see e.g. fig. 1, Chapter 1). Especially, when dimers are considered, the interactions between the two π-electron clouds has to be taken into account. These effects are of importance when dimer formation through ligation of the central Mg-ion is impossible, such as in pheophytins [8]. Using polar solvents we have avoided the formation of dimers and oligomers. Therefore the effect of π-π interactions will not be discussed in this study.

In polar solvents two kinds of pigment-solvent interactions have to be considered. Firstly, the interaction of solvent molecules with

the central metal-ion in chlorophylls; secondly, interactions with the
carbonyl side groups of the chlorophylls. There are two main differences
between these interactions: ligation of Mg^{2+} results in a net electron trans-
fer from the solvent molecule to chlorophyll, so that the strength of the
interaction depends on the basicity of the solvent molecules. The carbonyl
groups, on the other hand, are electron donating and interaction can take
place only, if acid groups are present, e.g. oxygen bound   hydrogen atoms
in ethanol or the Mg^{2+}-ion of a second chlorophyll molecule. In addition,
the ligation of Mg^{2+} is in principle an axial perturbation and will not in-
fluence the shape of the electron distribution *in* the molecular plane,
whereas e.g. hydrogen bonding with one or more carbonyl groups can have
appreciable effects on the in-plane electron distribution.

  Both effects are not only important in polar solvents but also
in in-vivo systems, where e.g. carbonyl groups of proteins can ligate Mg^{2+},
whereas (acid) hydrogens are abundantly available for interactions with car-
bonyl groups. In the following, both types of interactions will be discussed,
together with intramolecular effects having comparable influences on the π-
electron distribution.

  To study the effects of the above-mentioned interactions
separately, we have looked for methods to exclude one of the two kinds of
interaction. The hydrogen bonding with carbonyl groups is possible only, if
the solvent contains appropriate hydrogen atoms. Consequently in MTHF
and tol/pyr this interaction is absent; in ethanol, however, OH hydrogens
easily form hydrogen bonds with carbonyl groups of the photosynthetic pig-
ments. It is not possible to exclude Mg^{2+} ligation by choosing the appropriate
solvent, since carbonyl groups of other chlorophyll molecules interact with
this Mg^{2+}-ion forming dimers and oligomers [9], if the solvent is not able
to ligate with Mg^{2+}. To eliminate solvent-Mg^{2+} ligation in photosynthetic
pigments, we have substituted Mg^{2+} by $2H^+$, the result being a pheophytin.
The consequences of $Mg^{2+}/2H^+$ substitution are extensively discussed in
Chapter 9.

  The effects of ligation of Mg^{2+} on the optical properties of
Mg-containing porphyrin systems are considered in Chapter 5. On this basis
and noting the full agreement between the triplet state parameters for the
chlorophylls in MTHF and tol/pyr at 100 K, we concluded that the experimental
triplet ESR spectra refer to biligated species (see section 10.6). For MgTBP
(see Chapter 6) as well as for chlorophylls, the triplet state parameters are
nearly independent on the kind of ligands bound to the central metal ion.

For the mono-ligated complexes of MgTBP (see Chapter 6) and Chl $\underline{a}$ [7],
however, a larger ZFS parameter D is found than for the biligated species.
$(MgTBP.(MTHF)_2$: D = 326 x 10^{-4} cm^{-1}, MgTBP.(MTHF): D = 344 x 10^{-4} cm^{-1} in
n-octane at 4.2. K; Chl $\underline{a}$. L_2 : D = 280 x 10^{-4} cm^{-1}, Chl $\underline{a}$. L : D = 309 x
10^{-4} cm^{-1}, in n-octane at 4.2 K, where L is ligand (probably H_2O)).

    For all photosynthetic pigments, which we have studied, an
appreciable change of the spectroscopic parameters occurs when the pigments
are dissolved in ethanol instead of in MTHF or tol/pyr (see e.g. Chapter 7,
9). Since the model compounds porphin free base and MgTBP, lacking carbonyl
side groups, do not show comparable solvent effects (see Chapter 5, 6, 7),
we attribute these solvent effects for both chlorophylls and pheophytins to
hydrogen bonding of the carbonyl groups with ethanol.

    In Chl $\underline{a}$ three carbonyl groups are present (see fig. 1,
Chapter 1). Only the ring V keto group participates in the π-electron dis-
tribution of the tetrapyrrole macrocycle, so that hydrogen bonding with this
group can affect the π-electron properties of the macrocycle. Although hydro-
gen bonding with the other carbonyl groups may occur, we expect that these
bondings will have only minor effects on the π-electron distribution of the
ring and we have neglected these effects.

    Before applying the model developed in Chapter 9 to the effects
of hydrogen bonding, we summarize what is observed experimentally:
    a) a red shift of the Q_y absorption band [10], especially at 100 K and
a shift in the same direction of the fluorescence and phosphorescence bands
[1];
    b) a decrease of the ZFS parameter;
    c) an increase of the mean triplet decay constant K_T;
    d) a shift of the Q_x-band in the absorption spectrum of Chl $\underline{a}$, measured
at 100 K (for Ph $\underline{a}$ no effect on Q_x is observed).

    It is interesting to compare the effects of hydrogen bonding
with the ring V keto group with those of the introduction of an aldehyde
group such as in Chl $\underline{b}$. Hydrogen bonding to a carbonyl group effectively
increases the net displacement of electronic charge from the ring to this
group and therefore one expects that such bonding or the introduction of an
extra carbonyl group, conjugated with the π-electron system, will in first
order have similar effects on the π-electron properties. This, however, is
in contrast with the experimental data: w.r.t. points (a), (b), and (c) the
effect of introduction of the aldehyde group is opposite to the effect of
hydrogen-bonding of Chl $\underline{a}$; the position of the Q_x-band of Chl $\underline{b}$ at 100 K is

122

unknown. A full understanding of these data can be obtained only when the position of the perturbation on the ring is taken into account.

According to the concept of long-field/round-field character, as proposed by Platt [11] and Longuet -Higgins [12], hydrogenation of one or two opposite pyrrole rings of a porphin molecule results in an increase of the long-field character of the π-electron cloud (see e.g. fig. 5, Chapter 9). The introduction of a carbonyl group in dihydroporphin at ring III (see fig. 1, Chapter 1) will increase the long-field character of the π-electron system, when this carbonyl group participates in the π-electron distribution of the ring. The vinyl group, on pyrrole ring I, present in Chl $\underline{a}$ will further enhance the long-field character of this molecule.

Using Chl $\underline{a}$ as a starting point, we will consider the effects of hydrogen bonding of the ring V keto group and the introduction of the aldehyde group on the π-electron system. The hydrogen bonding results in a stabilization of electron density on the carbonyl-oxygen atom. Consequently, the π-electron distribution attains a slightly more long-field character. On the other hand, the introduction of the aldehyde group in ring II causes a displacement of some electron density towards this pyrrole ring, resulting in an increase of the round-field character of the π-electron cloud. So, within this crude model, hydrogen bonding and introduction of an aldehyde group are expected to have opposite effects, in agreement with the experimental data. Furthermore, the direction of the effects on the position and intensity of the Q-band is exactly as is expected from Platt's theory [11]. In Chapter 9 we mentioned that a decrease of D upon an increase of the long-field character is not restricted to the porphyrin, but also has been found for aromatic hydrocarbons [13]. Concluding, it can be stated that the long-field/round-field concept can explain qualitatively the effects of side group substitution as well as interaction of side groups with the surroundings on the properties of the lowest excited states.

Using Gouterman's 4-orbital model [14], the data can be cast into a more quantitative framework. As discussed in Chapters 4, 5, 9 and appendix A, in this model only the two HOMO's and two LUMO's are taken into account. For D_{4h} porphin the HOMO's as well as the LUMO's are supposed to be degenerate (see fig. 6, Chapter 9). As before, we limit the following discussion to the y-polarized transitions. The states of interest in the 4-orbital description, are

$$\psi_1^S = a_S |b_1 c_1\rangle_S - (1 - a_S^2)^{\frac{1}{2}} |b_2 c_2\rangle_S \qquad (1a)$$

123

$$\psi^T = a_T |b_1 c_1 \rangle_T - (1 - a_T^2)^{\frac{1}{2}} |b_2 c_2 \rangle_T \,, \tag{1b}$$

where ψ_1^S and ψ^T are the first excited singlet and triplet state, respectively; a_S and a_T are the CI coefficients for the singlet and triplet states and $|b_1 c_1 \rangle$, $|b_2 c_2 \rangle$ represent pure excited states; the subscripts S and T denote singlet and triplet character of these pure states. We assume that ψ^T and ψ_1^S correspond to the same one-electron promotions; as will be shown below, the experimental results prove this assumption to be correct.

Defining $E_0 \equiv \frac{1}{2}\{ E(|b_1 c_1 \rangle) + E(|b_2 c_2 \rangle)\}$ and $2\delta \equiv |E(|b_1 c_1 \rangle) - E(|b_2 c_2 \rangle)|$ with $E(|b_1 c_1 \rangle)$ being the energy of the pure excited state $|b_1 c_1 \rangle$ w.r.t. the ground state, the energy of S_1 is given by [14]

$$E_{S1} = E_0 - (\delta^2 + \varepsilon^2)^{\frac{1}{2}} = E_0 - \frac{\varepsilon}{2a_S (1 - a_S^2)^{\frac{1}{2}}} \tag{2}$$

where ε is the non-diagonal matrix element $\langle c_1 b_1 |\mathcal{H}| c_2 b_2 \rangle$. For D_{4h} porphin, with $\delta = 0$, CI is maximum and $a_S = 2^{-\frac{1}{2}}$. As shown by Gouterman [14], the shift of S_1, resulting from small perturbations of the porphin-ring π-electron distribution, can be accounted for by eqn. (2) with E_0 and ε constant. Although the hydrogenation of one or two pyrrole rings or the introduction of carbonyl groups is more than a small perturbation, in first order we keep E_0 and ε constant. Then, the increase of δ, resulting in an increase of a_S, causes E_{S1} to decrease, in agreement with the experimentally found red shift of the Q-band for the series Mg-porphin — Mg-dihydroporphin — Chl b — Chl a — Bchl (for energy levels, see fig. 6, Chapter 9).

The CI dependence of the ZFS parameter D is given by (see Chapter 9)

$$D = D_0 + 2a_T(1 - a_T^2)^{\frac{1}{2}} \cdot D_{12} \,, \tag{3}$$

if we suppose that the D-values for the two pure excited states both equal D_0. D_{12} is the non-diagonal term $\langle c_1 b_1 |\underline{D}| c_2 b_2 \rangle$. As discussed for the pheophytins in Chapter 9, the decrease of D for the series porphin— dihydroporphin— Ph b — Ph a — Bph can be attributed to a decrease of the CI in the triplet state. Supposing that the CI in the lowest excited singlet state and the lowest excited triplet state is equal ($a_S = a_T$), from eqn. (2) and (3) it follows,

$$D = D_0 + \frac{\varepsilon}{E_0 - E_{S1}} \cdot D_{12} \tag{4}$$

In fig. 1 D is plotted vs $(E_0 - E_{S1})^{-1}$. For E_0 the value obtained for porphin is used to eliminate as much as possible effects of CI of S_2 with other states, which is especially important for chlorophylls and pheophytins [6]. The surprisingly good fit of the data to eqn. (4), indicates that in first order CI in the lowest excited triplet state is of comparable magnitude to that in the lowest excited singlet state.

As mentioned in Chapter 9, Gouterman [15] and Langhoff et al. [16] excluded the possibility of CI for the lowest excited triplet states within the 4-orbital model for symmetry reasons. Whereas second-order effects can induce appreciable participation of both 4-orbital excited states in T_0 [17], Gouterman et al. [18] supposed that the lowest excited triplet state is a relatively pure state. This idea has received support from recent calculations by Van Dorp et al. [19] to determine the D-value as well as hyperfine splitting constants of porphin free base. The following points, however, support the idea that the CI in T_0 parallels that in S_1:

a) Phosphorescence spectra of "normal" Mg-porphyrins, with strong CI in S_1, are characterized by a 0-0 band with equal or weaker intensity than the 0-1 band [20], indicating that the transition $T_0 \rightarrow S_0$ is orbitally forbidden just as is found for the transition $S_1 \leftarrow S_0$. This orbital forbiddeness can only be accounted for by strong CI in T_0 [14]. For MgTBP, with relative weak CI in S_1 (see Chapter 5), the strong 0-0 band in phosphorescence spectra [20] points to weak CI in T_0.

b) There is a parallel between the shift of the 0-0 band of the fluorescence and the 0-0 band of the phosphorescence (fig. 2) when the molecular structure of a porphyrin system is changed, e.g. in the series Mg-porphin — Chl b — Chl a, or when interactions with solvent molecules takes place (e.g. Chl a in MTHF and ethanol).
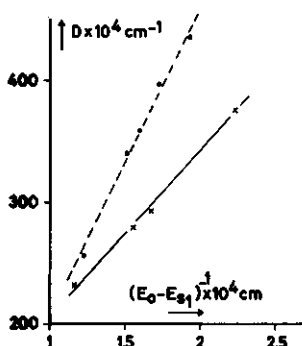

Fig. 1 Relation between energy level of lowest excited singlet state E_{S1} and ZFS parameter D following eqn. (4), for the series porphin free base, dihydroporphin free base, Ph b, Ph a, and Bph (.) and for the series Mg-porphin, Chl b, Chl a, Bchl (×). For definition of E_0 see text.
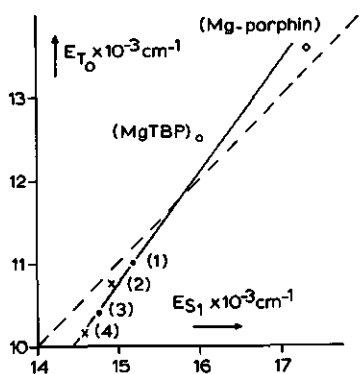
Fig. 2 Relation between energy level of the lowest excited singlet state E_{S1} and the energy level of the lowest excited triplet state E_{T0} for Mg-porphin, MgTBP, Chl b in MTHF (1), Chl b in ethanol (2), Chl a in MTHF (3), and Chl a in ethanol (4).

As mentioned before, the reduction of two opposite pyrrole rings and the introduction of two carbonyl groups, as in Bchl w.r.t. Mg-porphin, cannot be treated as a small perturbation on the energy levels only. These changes in molecular structure will affect the MO wavefunctions and consequently the parameters ε, D_0 and D_{12} in eqn. (4). Bearing this in mind, the agreement between the experimental results and eqn. (4) is quite surprising. For small changes, e.g. the introduction of the aldehyde group or hydrogen bondings with the ring V keto group, the model clearly can explain the experimental data. In addition, using this model, we can understand the relative small D-value of tetraphenyl-porphin (TPP) free base and the absence of a decrease of D when one pyrrole ring is hydrogenated [21] .

The presence of electron donating phenyl groups, bound to the methine carbons slightly destabilizes the MO b_1 w.r.t. b_2 resulting in an energy level scheme as given in fig. 3a. CI will no longer mix $|b_1 c_1 \rangle$ and
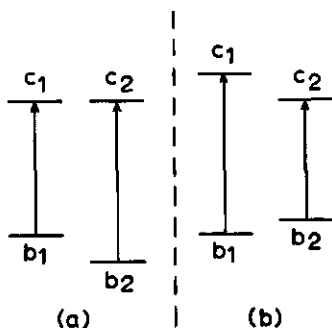

Fig. 3 Diagrams representing the relative energy levels of the two HOMO's (b_1, b_2) and the two LUMO's (c_1, c_2) of tetraphenyl-porphin free base (a) and tetraphenyl-dihydroporphin free base (b).
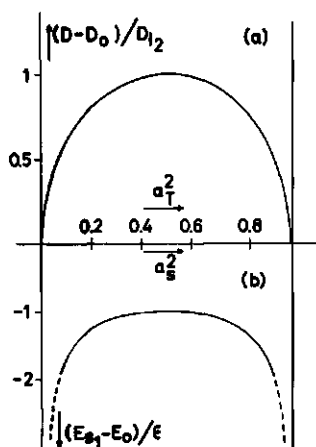
Fig. 4 Relation between ZFS parameter D and CI coefficient $|a_T|^2$ (a) and relation between lowest exited singlet state energy level E_{S1} and CI coefficient $|a_S|^2$, according to eqns.(3) and (2). The dashed part of the curve $(E_{S1}-E_0)/\varepsilon$ in (b) represents a region where the theoretical expression (2) is expected to break down. For definitions of E_0, D_0 and ε see text.

$|c_2b_2|$ in equal amount as for porphin free base. Because of the lower energy of $|c_2b_2|$, this state will contribute more than 50% to S_1 and T_1, with a_S, $a_T < 2^{-\frac{1}{2}}$ in eqns. (1a, b). Following Appendix A, the reduction of one pyrrole ring results in the energy levels of b_1, b_2, c_1 and c_2 as shown in fig. 3b. Now CI will result in a major contribution of $|c_1b_1|$, so that a_S, $a_T > 2^{-\frac{1}{2}}$. From the outline given above, it can be concluded that for TPP the reduction of one pyrrole ring results in a shift of D and E_{S1} over the top of the curves given in fig. 4a, b. Experimentally it is found that both D and E_{S1} are nearly equal in TPP and TPC free base 21, 22 , indicating that the amount of CI is the same for both compounds, but that the participation of the two pure states is different for TPP and TPC. Just as for the compounds discussed before, the amount of CI in T_0 is comparable to that in S_1.

10.8   REFERENCES

1. A.A. Krasnovskii jr., N.N. Lebedev, F.F. Litvin, Dokl. Akad. Nauk SSSR, 216, 1406 (1974).
2. R.H. Clarke, R.E. Connors, H.A. Frank, Biochem. Biophys. Res. Commun., 71, 671 (1976).
3. J.R. Norris, R.A. Uphaus, J.J. Katz, Chem. Phys. Lett., 31, 157 (1975).
4. M.C. Thurnauer, J.J. Katz, J.R. Norris, reported at the Brookhaven symposium about "Chlorophyll-proteins, reaction centers and photo-synthetic membranes", june 7-9, 1976.
5. T.A. Evans, J.J. Katz, Biochem. Biophys. Acta, 396, 414 (1975).
6. C. Weiss, J. Mol. Spectrosc., 44, 37 (1972).
7. R.P.H. Kooyman, T.J. Schaafsma, J.F. Kleibeuker, Photochem. Photobiol. to be published.

8. G.P. Gurinovich, A.N. Sevchenko, K.N. Solov'ev, Spectroscopy of chlorophyll and related compounds, NTIS, Springfield, U.S.A., 1968.

9. J.J. Katz, G.L. Closs, F.C. Pennington, M.R. Thomas, H.H. Strain, J. Am. Chem. Soc., 85, 3801 (1963).

10. G.R. Seely, R.G. Jensen, Spectrochim. Acta, 21, 1835 (1965).

11. J.R. Platt, J. Chem. Phys., 18, 1168 (1950).

12. H.C. Longuet-Higgins, C.W. Rector, J.R. Platt, J. Chem. Phys., 18, 1174 (1950).

13. S.A. Boorstein, M. Gouterman, J. Chem. Phys., 39, 2443 (1963).

14. M. Gouterman, J. Mol. Spectrosc., 6, 138 (1961).

15. R.L. Ake, M. Gouterman, Theoret. Chim. Acta, 15, 20 (1969).

16. S.R. Langhoff, E.R. Davidson, M. Gouterman, W.R. Leenstra, A.L. Kwiram, J. Chem. Phys., 62, 169 (1975).

17. B. Roos, M. Sundbom, J. Mol. Spectrosc., 36, 8 (1970).

18. M. Gouterman, D.B. Howell, J. Chem. Phys., 61, 3491 (1974).

19. W.G. van Dorp, M. Soma, J.A. Kooter, J.H. van der Waals, Mol. Phys., 28, 1551 (1974).

20. M.P. Tsvirko, K.N. Solov'ev, A.T. Gradyushko, S.S. Dvornikov, Opt. Spectrosc., 38, 400 (1975).

21. S.J. van der Bent, T.J. Schaafsma, Chem. Phys. Lett., 35, 45 (1975).

22. G. Peychal-Heiling, G.S. Wilson, Anal. Chem., 43, 550 (1971).

Appendices

EFFECTS OF PYRROLE RING HYDROGENATION ON SPECTROSCOPIC PROPERTIES IN VIEW OF
GOUTERMANS 4-ORBITAL MODEL

In porphin with D_{4h} symmetry the HOMO's a_{1u} and a_{2u} are supposed
to be accidentally degenerate, whereas the two LUMO's e_{gx} and e_{gy} have to be
degenerate by symmetry reasons (see fig. 6, Chapter 9). In lower symmetry,
a_{1u}, a_{2u}, e_{gx}, and e_{gy} are no longer appropriate symbols for the MO's and we
use the notation $b_1(a_{2u})$, $b_2(a_{1u})$, $c_1(e_{gy})$, and $c_2(e_{gx})$. Fig. 7 in Chapter 9
gives the electron distribution of the four orbitals as calculated by
Gouterman 1 . Describing the pure excited states $(e_{gy} \leftarrow a_{2u})$, $(e_{gx} \leftarrow a_{1u})$,
$(e_{gy} \leftarrow a_{1u})$, and $(e_{gx} \leftarrow a_{2u})$ by $|e_{gy}a_{2u}\rangle_y$, $|e_{gx}a_{1u}\rangle_y$, $|e_{gy}a_{1u}\rangle_x$, and $|e_{gx}a_{2u}\rangle_x$,
where the subscripts to the brackets define the polarization of the optical
transition, we note that the states $|e_{gy}a_{2u}\rangle_y$ and $|e_{gx}a_{1u}\rangle_y$, as well as
$|e_{gy}a_{1u}\rangle_x$ and $|e_{gx}a_{2u}\rangle_x$ are degenerate in D_{4h} porphin. The transition
probability for all four transitions between pure states are equal. CI mixes
transitions with equal polarization, thus $|e_{gy}a_{2u}\rangle_y$ and $|e_{gx}a_{1u}\rangle_y$, as well as
$|e_{gy}a_{1u}\rangle_x$ and $|e_{gx}a_{2u}\rangle_x$. Again for D_{4h} porphin, CI results in 50/50 mixing
and, consequently, the low energy (Q-band) transition receives zero-
transition probability, whereas the high-energy transition becomes highly
allowed.

Reducing one or two pyrrole rings, as in dihydroporphin and tetra-
hydroporphin removes the degeneracy between the e_{gx} and e_{gy} as well as between
the a_{1u} and a_{2u} MO's. The change in energy can be easily predicted: because
the a_{1u} MO has electron density on C_α atoms (and to a less extent on C_β)
(see fig. 7, Chapter 9), it will be destabilized w.r.t. the corresponding
porphin MO; the a_{2u} MO, however, is not affected by such a pyrrole reduction.
Similarly, one of the e_g MO's, say e_{gy}, is destabilized by pyrrole ring
reduction, whereas its partner e_{gx} is not affected. Thus x- and y-polarized

129

transitions do not behave in the same way anymore. For y-polarized transitions a pyrrole ring reduction results in a red shift of the Q_y-band and a simultaneous increase of the transition probability, due to the decrease of CI between $|c_1b_1\rangle_y$ and $|c_2b_2\rangle_y$. The $|c_1b_2\rangle_x$ and $|c_2b_1\rangle_x$ states remain almost degenerate, however, and CI is still large enough to result in a very small Q_x-band transition probability.

Since the reduction of a second pyrrole ring opposite to the other reduced ring reinforces the effect of the reduction of the first ring, for the series porphin-dihydroporphin- tetrahydroporphin the CI for the lowest excited state decreases, resulting from an increase of the energy gap between the pure states $|c_1b_1\rangle$ and $|c_2b_2\rangle$.

1. M. Gouterman, J. Mol. Spectrosc., 6, 138 (1961).

APPENDIX B

POSSIBLE ESP PATTERNS IN $\Delta m = 1$ TRIPLET ESR SPECTRA

The concept of the electron spin polarization (ESP) patterns has been introduced in Chapter 3. Out of the $2^3 \equiv 8$ ESP patterns, which can be constructed when zero peak intensity is excluded, the patterns A E E A A E and E A A E E A are not allowed, when only monomolecular processes are effective in the triplet state kinetics. In the following this will be proven for the pattern A E E A A E; for the other pattern the proof goes along the same lines.

If the peak H_x^- is emissive, then $N_0 > N_{-1}$ for H//x and thus,

$$\frac{P_0}{k_0} = \frac{P_x}{k_x} > \frac{P_1}{k_1} = \frac{P_y + P_z}{k_y + k_z} \quad . \tag{1}$$

Furthermore, when H_y^- is emissive, then $N_0 > N_{-1}$ for H//y, or

$$\frac{P_y}{k_y} > \frac{P_x + P_z}{k_x + k_z} \tag{2}$$

Summation of the inequalities (1) and (2) results in

$$\frac{P_x + P_y}{k_x + k_y} > \frac{P_z}{k_z}$$

or $N_{+1} > N_0$ for H//z. From this inequality it follows that H_z^- has to be

emissive and H_z^+ has to be absorptive, bearing in mind that the H_z^- peak corresponds to the transitions $|+1\rangle \leftrightarrow |0\rangle$ and H_z^+ to the transitions $|0\rangle \leftrightarrow |-1\rangle$. Consequently, when both H_x^- and H_y^- are emissive, only the ESP pattern E E E A A A is allowed.

Summary

The lowest excited triplet state T_0 of chlorophyll a, chlorophyll b, bacteriochlorophyll and corresponding pheophytins has been studied by magnetic resonance and optical spectroscopy. Zero field splitting (ZFS) parameters D and E, populating rates, and depopulating rate constants for the three triplet spin states of these pigments have been obtained. The magnitude of the triplet state parameters for the various pigments has been correlated with the differences in molecular structure, especially with the extent and shape of the π-electron cloud. In particular it has been shown that effects of molecular structure on the ZFS parameter D and on the energy of T_0 can be accounted for by Gouterman's 4-orbital model when configuration interaction (CI) in T_0 and the lowest excited singlet state S_1 is of comparable magnitude. Furthermore it has been found that the effect of substitution of the central Mg^{2+}-ion by two protons is essentially different from the effects of changes in the structure of the outer porphyrin ring.

The considerable increase of the mean triplet decay constant on substitution of Mg^{2+} by $2H^+$ cannot be accounted for by the energy-gap law. The presence of occupied non-bonding orbitals, as well as of N-H groups inducing additional promoting vibrational modes, are assumed to be responsible for the large increase of the non-radiative decay rate. There is experimental evidence that both effects are important.

The relatively stable and highly symmetric compound Mg-tetrabenzoporphin (MgTBP) has been found to be a good model compound for chlorophylls w.r.t. the effects of ligation on the lowest excited singlet states, but not for the triplet state T_0. Some special properties of MgTBP are reported and discussed, i.e. the S_2-fluorescence and the splitting of the lowest excited states S_1 and T_0 by Jahn-Teller coupling.

Samenvatting

Dit proefschrift beschrijft de resultaten van een studie aan de laagste aangeslagen toestanden van een aantal fotosynthetische pigmenten en een model verbinding, Mg-tetrabenzoporphine (MgTBP). Daarbij is in het bijzonder aandacht besteed aan de laagste aangeslagen triplet toestand T_0 van zowel chlorophyl $\underline{a}$, $\underline{b}$ (Chl $\underline{a}$, $\underline{b}$) en bacteriochlorophyl $\underline{a}$ (Bchl), als van de corresponderende pheophytines (Ph $\underline{a}$, $\underline{b}$ en Bph).

Zowel de statische parameters (nulveld splitsing parameters D en E en de energie van T_0 t.o.v. de grondtoestand S_0), als de kinetische parameters (bevolkingsnelheden P_i en verval snelheidsconstanten k_i van de drie spin componenten $|\tau_i\rangle$, i = x, y, z) van deze paramagnetische toestand T_0 zijn gemeten m.b.v. optische spectroscopie (fosforescentie) en magnetische resonantie (ESR). De effecten van veranderingen in de moleculaire structuur en van interacties van het molecuul met de omgeving op de verschillende parameters is gecorreleerd met de electronen structuur aan de hand van het zgn. "long field/round field" model en Gouterman's 4-orbital model. In beide benaderingswijzen worden alleen de π-electronen beschouwd, waarbij wordt aangenomen dat veranderingen in de moleculaire structuur, zoals reductie van een pyrrool ring en introductie van een carbonyl groep, evenals de interacties met de omgeving, kunnen worden opgevat als storingen op het π-electron systeem van de 16-ledige binnen ring van het porphine skelet, dat de basis vormt voor alle bestudeerde pigmenten.

MgTBP blijkt een goede model verbinding voor chlorophyl, voorzover het de invloed van liganden op de laagste aangeslagen toestanden betreft (Hfdst. 5). Voor de studie van de triplet toestand gaat dit niet op, daar de eigenschappen van de laagste aangeslagen triplet toestand van MgTBP sterk verschillen van die van de verschillende chlorophyl moleculen (Hfdst. 6). In hoofdstuk 5 worden tevens enkele speciale eigenschappen van het MgTBP beschreven, n.l. de S_2 fluorescentie en de opsplitsing van de laagste aangeslagen toestanden t.g.v. Jahn-Teller koppeling.

De triplet toestanden van de fotosynthetische pigmenten zijn alleen in oplossing bestudeerd. Naast de Mg-bevattende chlorophyl verbindingen, zijn

de corresponderende pheophytines onderzocht, waarin het Mg^{2+}-ion is vervangen door 2 protonen. Met betrekking tot de statische parameters is daarbij het volgende gebleken:

(a) de substitutie van Mg^{2+} door 2 H^+ doet de nulveld splitsings parameter D toenemen voor alle bestudeerde systemen, terwijl het energie niveau van T_0 voor Ph a en Ph b hoger ligt dan dat voor de corresponderende chlorophyl ver- bindingen;

(b) binnen de reeks bestudeerde chlorophyl-verbindingen en binnen de reeks bestudeerde pheophytines wordt een verband gevonden tussen de energie van S_1, de energie van T_0 en de waarde van D;

(c) het onder (b) genoemde verband kan worden geëxtrapoleerd naar de model verbindingen porphine en dihydroporphine en is ook van toepassing op de effecten van waterstofbrugvorming;

(d) het effect van de reductie van één of twee pyrrool ringen van het porphine skelet, het effect van de introductie van carbonyl groepen en van de water- stofbrugvorming met carbonyl groepen, op zowel de energie niveaus van S_1 en T_0, als op D kunnen in het 4-orbital model worden beschreven. Hierbij wordt aangenomen dat de configuratie interactie in S_1 en T_0 ongeveer gelijk is. De onderdelen a-d zijn in de hoofdstukken 9 en 10 nader uitgewerkt.

Ook de kinetiek van de triplet toestand wordt door de bovengenoemde veranderingen van de moleculaire structuur beïnvloed. Allereerst wordt dit duidelijk uit de electron spin polarisatie (ESP) van $\Delta m = 1$ triplet ESR spectra voor de verschillende pigmenten, verkregen onder continue bestraling met licht. Uit ESP kan echter geen directe eenduidige informatie over de k_i's en P_i's worden verkregen; de mate van ESP hangt sterk af van spin rooster relaxatie (Hfdst. 7 en 8). De kinetische parameters k_i en P_i zijn bepaald uit de tijdsafhankelijkheid van de ESR signalen na het aan- en uitschakelen van het excitatie licht en vergeleken voor de verschillende pigmenten. Hierbij kwam vast te staan dat:

(a) de gemiddelde verval snelheids constante K_T sterk toeneemt als het energie- verschil tussen T_0 en de grondtoestand kleiner wordt. Dit geldt, zowel binnen de reeks bestudeerde chlorophyl verbindingen als binnen de reeks pheophytines. Deze "energy-gap law" wordt nader besproken in hoofdstuk 9.

(b) de verhouding tussen de verval constanten voor de drie componenten slechts weinig verandert t.g.v. de bovengenoemde veranderingen in de moleculaire structuur.

(c) voor alle bestudeerde pigmenten de verhouding tussen de bevolkings snel- heden van de drie spin componenten ongeveer gelijk is aan de verhouding tussen

de drie verval constanten.

(d) naar analogie met wat gevonden is voor de statische parameters, de substitutie van Mg^{2+} door $2 H^+$ niet te vergelijken is met de invloed van veranderingen aan de buitenkant van de porphyrine ring. Dit kan worden toegeschreven aan de aanwezigheid van gevulde, niet-bindende banen in de pheophytines en aan de extra vibratie mogelijkheid t.g.v. de in de pheophytines aanwezige N—H groepen (Hfdst. 9).

De beschreven resultaten illustreren dat de triplet toestand een gevoelige "probe" is voor kleine veranderingen in de moleculaire structuur van de fotosynthetische pigmenten, evenals voor interacties van deze pigmenten met de omgeving. De waargenomen effecten kunnen kwalitatief met een eenvoudig model worden verklaard; dit model kan ook naar nog niet bestudeerde systemen worden geëxtrapoleerd.

Curriculum vitae

In 1965 heb ik het H.B.S.-B diploma gehaald aan het Rijks Lyceum te Meppel. Hetzelfde jaar ben ik de studie chemie aan de Rijks Universiteit te Groningen begonnen. Na het afleggen van het kandidaats examen in de Fysische Chemie in 1968, heb ik mij op de afdeling van Prof. Dr. J. Kommandeur voorbereid op het doctoraal examen. Onderwijl heb ik in het kader van het bijvak Bedrijfseconomie een stage gelopen bij de Shell Raffinaderij te Pernis.

Na het doctoraal examen, afgelegd in december 1971, en een kort dienstverband bij de Rijks Universiteit te Groningen, ben ik 1 augustus 1972 in dienst getreden bij de Landbouwhogeschool, alwaar ik te werk werd gesteld bij de in oprichting zijnde vakgroep Moleculaire Fysica.

Gedurende de eerste drie maanden ben ik werkzaam geweest bij de werkgroep Moleculen in de Aangeslagen Toestand aan de Rijks Universiteit te Leiden. Naast het onderzoek, beschreven in dit proefschrift, had ik als onderwijstaak het geven van de colleges Chemische Binding en Fysica voor Biologen.